# Performance Modelling, Validation and Operational Feasibility of a Parabolic Trough Power Plant

by

Reece Christian Barnes

*Thesis presented in partial fulfilment of the requirements for the degree of Master of Engineering (Mechatronic) in the Faculty of Engineering at Stellenbosch University*

Supervisor: Prof. F. Dinter

December 2017

The financial assistance of the National Research Foundation (NRF) towards this research is hereby acknowledged. Opinions expressed and conclusions arrived at, are those of the author and are not necessarily to be attributed to the NRF.

# Declaration

By submitting this thesis electronically, I declare that the entirety of the work contained therein is my own, original work, that I am the sole author thereof (save to the extent explicitly otherwise stated), that reproduction and publication thereof by Stellenbosch University will not infringe any third party rights and that I have not previously in its entirety or in part submitted it for obtaining any qualification.

Date: December 2017

# Abstract


## Performance Modelling, Validation and Operational Feasibility of a Parabolic Trough Power Plant

R. C. Barnes

*Department of Mechanical and Mechatronic Engineering,*
*University of Stellenbosch,*
*Private Bag X1, Matieland 7602, South Africa.*

Thesis: MEng (Mech)

December 2017

Currently, the most developed commercial Concentrating Solar Power (CSP) technology in operation is the parabolic trough power plant (PTPP) technology. This is due to more than thirty years of experience, competitive cost and high performance (Pool and Coggin, 2013). PTPP's lead the CSP market along with the central receiver (CR) technology. A study related to operational strategy is necessary and highly beneficial to increase production output and/or reduce costs. The objective of this thesis is to simulate a PTPP by making use of data supplied from a power plant currently in operation. The simulation program developed can be used as a tool for the power plant operators. It provides performance based output results that are then evaluated and interpreted in order to achieve a more desirable/optimal electricity generation. This is however, dependant on the day-to-day conditions, limitations and how the operator chooses to run the plant on any specific day. The data used in the simulation is obtained from the PTPP located in Southern Spain, namely; Andasol 3. Performance modelling of plant operation and operational feasibility is made possible by using high resolution data in the form of direct normal irradiance (DNI), energy transfer (thermal-to-electrical energy) and other power plant parameters. A validated simulation model ensures a foundation for power plant operational strategy analysis. This encourages a larger energy production, while also reducing the amount of gas used during start-up.


*Keywords: CSP, Parabolic Trough, Simulation Model, Validate, Feasibility*

# Uittreksel

## Prestasie Modellering, Bekragtiging en Operasionele Haalbaarheid van 'n Paraboliese Trog Kragsentrale

*("Performance Modelling, Validation and Operational Feasibility of a Parabolic Trough Power Plant")*

R. C. Barnes

*Departement Meganiese en Megatroniese Ingenieurswese,*
*Universiteit van Stellenbosch,*
*Privaatsak X1, Matieland 7602, Suid Afrika.*

Tesis: MIng (Meg)

Desember 2017

Tans is die mees ontwikkelde Kommersiële Konsentrasie Sonkrag (KKS) - tegnologie in werking, die paraboliese trog-tegnologie. Dit is as gevolg van meer as dertig jaar se ondervinding, mededingende koste en hoë prestasie.
'n Studie wat verband hou met operasionele strategie is nodig en hoogs voordelig om produksie-uitset te verhoog en/of koste te verminder. Die doel van hierdie proefskrif is om 'n Paraboliese Trog Kragsentrales (PTKS) te simuleer deur gebruik te maak van data wat verskaf word vanaf 'n kragsentrale wat tans in gebruik is. Die ontwikkelingsimulasie-program word dan gebruik as 'n instrument vir die kragsentrale-operateurs. Dit bied prestasiegebaseerde uitset resultate, wat dan geëvalueer en geïnterpreteer word, ten einde 'n meer wenslike/optimale elektrisiteit opwekking te bereik. Dit is egter afhanklik van die dag-tot-dag voorwaardes, beperkings en hoe die operateur verkies om die aanleg op enige spesifieke dag te bestuur. Die data wat gebruik word in die simulasie, word verkry uit die PTKS in Suid-Spanje, naamlik: Andasol 3. Prestasiemodellering van die aanlegbedrywighede en operasionele haalbaarheid word moontlik gemaak deur hoë resolusie data, energie-oordrag (hitte-tot-elektriese energie) en ander kragaanleg parameters. 'n Gekontroleerde simulasiemodel sorg vir 'n grondslag vir die bedryf van kernstrategieë. Dit moedig 'n groter energieproduksie aan, en verminder ook die hoeveelheid gas wat tydens die aanvang gebruik word.

*Keywords: KKS, Paraboliese Trog, Simulasie-program, Haalbaarheid*

# Acknowledgements

I would like to express my deepest gratitude to my supervisor, Professor Frank Dinter for all his guidance and constant support throughout the duration of my thesis. Along with helping me conduct and complete this thesis, his encouragement and expertise are sincerely appreciated.

I am indebted to the National Research Foundation (NRF) for their generous contribution and funding for this work. Also, thanks to Stellenbosch University for providing research facilities and computer equipment. Thank you to Andasol 3, who allowed me to conduct this study and provided me with the necessary data and information.

I want to extend a special word of thanks to all the members of the Solar Thermal Energy Research Group (STERG) for their contribution to renewable energy and concentrated solar power (CSP) and whose companionship and friendships I will always enjoy.

I owe my earnest appreciation to my family and friends who have not only supported me over the past few years, but have also encouraged me. A special thanks to Jarryd Barnes, Gerard Smith, Styger Kruger, Immo Kotting, Kasia Hearn and Ian Poole for their Engineering advise during the past years. Lastly, I want to acknowledge my beloved parents and gran for their unconditional love and invaluable support during my studies at Stellenbosch University.

# Dedications

*This Thesis is dedicated to the Solar Thermal Energy Research Group (STERG)*

# Contents

# List of Figures

# List of Tables

# Nomenclature

### Symbols

| | | |
|---|---|---|
| $A$ | Area | $[\mathrm{m}^2]$ |
| $Az$ | Azimuth Angle | $[^\circ]$ |
| $C_p$ | Heat Capacity | $[\mathrm{kJ/(kg \cdot K)}]$ |
| $D$ | Diameter | $[\mathrm{m}]$ |
| $DNI$ | Direct Normal Irradiance | $[\mathrm{W/m}^2]$ |
| $DS$ | Daylight Saver Modifier | $[-]$ |
| $EOT$ | Equation of Time | $[\mathrm{h}]$ |
| $f$ | Factor | $[\%]$ |
| $FLH$ | Full Load Hours | $[\mathrm{h}]$ |
| $IAM$ | Incident Angle Modifier | $[-]$ |
| $L$ | Location Longitude | $[\,]$ |
| $LC$ | Longitude Correction | $[\mathrm{h}]$ |
| $LCT$ | Local Clock Time | $[\mathrm{h}]$ |
| $m$ | Mass | $[\mathrm{kg}]$ |
| $\dot{m}$ | Mass Flow Rate | $[\mathrm{kg/s}]$ |
| $N$ | Day Number | $[\mathrm{Days}]$ |
| $P$ | Power | $[\mathrm{W}]$ |
| $\Delta P$ | Pressure Change | $[\mathrm{Pa}]$ |
| $\dot{q}$ | Heat Flux | $[\mathrm{W/m}]$ |
| $Q$ | Thermal Energy | $[\mathrm{J}]$ |
| $\dot{Q}$ | Thermal Power | $[\mathrm{W}]$ |
| $RE$ | Renolds Number | $[-]$ |
| $t$ | Time | $[\mathrm{s}]$ |
| $t_s$ | Solar Time | $[\mathrm{h}]$ |
| $\Delta t$ | Change in Time | $[\mathrm{s}]$ |
| $T$ | Temperature | $[^\circ\mathrm{C}, \mathrm{K}]$ |
| $TZM$ | Time Zone Meridian | $[^\circ]$ |
| $\bar{T}$ | Average Temperature | $[^\circ\mathrm{C}, \mathrm{K}]$ |

| | | |
|---|---|---|
| $\Delta T$ | Change in Temperature | $[^\circ C, K]$ |
| $V$ | Velocity | $[m/s]$ |

**Greek Variables**

| | | |
|---|---|---|
| $\alpha$ | Altitude Angle | $[^\circ]$ |
| $\delta$ | Declination Angle | $[^\circ]$ |
| $\rho$ | Density of Fluid | $[kg/m^3]$ |
| $\eta$ | Efficiency | $[\%]$ |
| $\lambda$ | Efficiency Modifier | $[-]$ |
| $\gamma$ | Geometry Efficiency | $[\%]$ |
| $\omega$ | Hour Angle | $[^\circ]$ |
| $\theta_i$ | Incident Angle | $[^\circ]$ |
| $\phi$ | Latitude Angle | $[^\circ]$ |
| $\tau$ | Transmissivity | $[\%]$ |
| $\theta_z$ | Zenith Angle | $[^\circ]$ |

**Subscripts**

| | |
|---|---|
| $abs$ | Absorber |
| $ap$ | Aperture |
| $bal, SCA$ | Balance of the SCA Thermal Inertia |
| $Bellow$ | Bellow |
| $Capacity, Full$ | Storage Full Capacity |
| $Cf$ | Cleanliness |
| $Col$ | Collector |
| $CyclingPumps$ | Cycling Pumps |
| $Dirt$ | Dirt |
| $DP$ | Design Point |
| $el$ | Electrical |
| $el, Gross$ | Gross Electric |
| $e, PB$ | Power Block Electrical Size |
| $H$ | High |
| $h$ | Header |
| $header, out$ | Header Out |
| $htf$ | Heat Transfer Fluid |
| $h, 0$ | Header at Time Zero |
| $i$ | Incidence Angle |
| $in, i$ | Input Value, Incremental Time Step (i) |

| | |
|---|---|
| $k$ | Day Increments |
| $L$ | Low |
| $Loop$ | Solar Collector Loop |
| $Max$ | Maximum |
| $Optical$ | Optical |
| $out, i$ | Output Value, Incremental Time Step (i) |
| $PartialOperation$ | Partial Discharge Operation |
| $PB$ | Power Block |
| $Pipe$ | Pipe Section |
| $Rec$ | Receiver |
| $rec, i$ | Receiver Tube, Incremental Time Step (i) |
| $salt$ | Molten Salt |
| $SF$ | Solar Field |
| $Stored$ | Thermal Energy Stored |
| $th, SF$ | Thermal Energy in the Solar Field |
| $s$ | Solar |
| $T, HTF$ | Heat Transfer Fluid Temperature |
| $T, ambient$ | Ambient Temperature |
| $th$ | Thermal |
| $th, HTFin$ | Thermal Energy, Heat Transfer Fluid Input |
| $th - el$ | Thermal-to-Electrical |
| $thPB, dp$ | Thermal Heat Design Point of the Power Block |
| $WetCooled$ | Wet Cooled |
| $z$ | Zenith |
| 0 | Value at Time Zero |

**Abbreviations**

| | |
|---|---|
| BIL | Beam Incident Losses |
| CR | Central Receiver |
| CRPP | Central Receiver Power Plants |
| CSP | Concentrated Solar Power |
| ECSA | Engineering Council of South Africa |
| FIT | Feed-in Tariffs |
| GL | Geometric Losses |
| HTF | Heat Transfer Fluid |
| LCOE | Levelised Cost of Electricity |
| LNG | Liquefied Natural Gas |

| | |
|---|---|
| MAPE | Mean Absolute Percentage Error |
| MATLAB | Matrix Laboratory |
| NREL | National Renewable Energy Laboratory |
| PID | Proportional, Integral and Differential |
| PTPP | Parabolic Trough Power Plant |
| PV | Photovoltaic |
| SAM | System Advisor Model |
| SCA | Solar Collector Assemblies |
| SEGS | Solar Electric Generating System |
| SM | Solar Multiple |
| STERG | Solar Thermal Energy Research Group |
| TES | Thermal Energy Storage |
| TESS | Thermal Energy Storage System |
| USD | United States Dollar |

# Chapter 1

# Introduction

The solar energy market is an ever growing environment with immense potential and is changing the way government, policy makers and the general public view the power industry. Focusing on the Concentrated Solar Power (CSP) aspect of generating utility-scale energy by harnessing energy from the sun, it is identified that there are two main methods of solar thermal collection. These methods include line-focus-collection and point-focus-collection. Line-focus-collectors generally have a concentration factor in the range of 60-80 which produces temperature in the medium to high domain (100 ℃ - 550 ℃). Point-focus-collectors are able to reach higher temperatures of up to 800 ℃ (Schiffer *et al.*, 2016). The Parabolic Trough Power Plant (PTPP) technology falls into the line-focus-collector division and due to early commercial CSP developments being the focus, the PTPP technology was the first choice for large-scale solar thermal power generation (Zervos, 2016). This technology harnesses solar radiation as shown in Figure 1.1. The yellow arrows indicate the incoming radiation from the sun.

Figure 1.1: Parabolic Trough (Energy Next Solar [Online])

It is also shown that the collectors are made up of long U-shaped mirrors that focus the direct solar radiation to a receiver tube. The collector assembly tracks the sun on a linear single-axis tracking system in order to heat the working fluid to approximately 400 ℃ (Wang, 2008). Today, the market is shared fairly evenly between the PTPP technology and the Central Receiver (CR) technology (Zervos, 2016).

Refer to Figure 1.2, the CR technology is based on a field of two-axis sun-tracking mirrors that are used to reflect the incoming solar radiation to a receiver positioned at the top of a central tower. These mirrors are known as heliostats and together with the boiler at the top of the receiver, allow approximately 80 % to 95 % of the reflected energy to be absorbed into the working fluid. This technology is mainly used for high temperature applications where the operative temperature range is between approximately 260 ℃ and 567 ℃ for a molten salt CR. The temperature range differs depending on the heat transfer temperature (HTF) used, but currently the most prominent high temperature salt is known as solar salt (Kotzé *et al.*, 2012). CR's also promote the ability to reach large power levels which range from 1 MW to the current 392 MW (Gross) plant in California known as Ivanpah (BrightSourceLimitless, 2015).

Figure 1.2: Central Receiver (Torresol Energy [Online])

Other CSP technologies such as the Linear Fresnel (Figure 1.3) and Parabolic Dish (Figure 1.4) technologies have unique performance characteristics and benefits when producing utility grade electricity, however, they lack the reliability and bankability associated with the PTPP and CR technologies. The Linear Fresnel technology is based on the parabolic trough collector design with the fundamental difference in that the collectors are made up of multiple small mirror facets as shown in Figure 1.3. These mirror facets include flat or flexibly bent mirrors, which offer a variety of configurations that are

not necessarily influenced by wind loads. The receiver pipes are fixed and the mirrors track the sun's position in order to concentrate the incoming radiation to the receiver (in most cases a secondary reflector is required). Therefore, the collectors are subsequent to low cost mirrors and components with small motors for tracking. The light construction, efficient land use and constructive simplicity adds value to the technology, while ensuring an inexpensive design. Despite all these advantages relating to Linear Fresnel, the major drawback is in the low optical efficiency and low fluid temperature which means that there is a low thermal efficiency when converting solar power to electrical power.

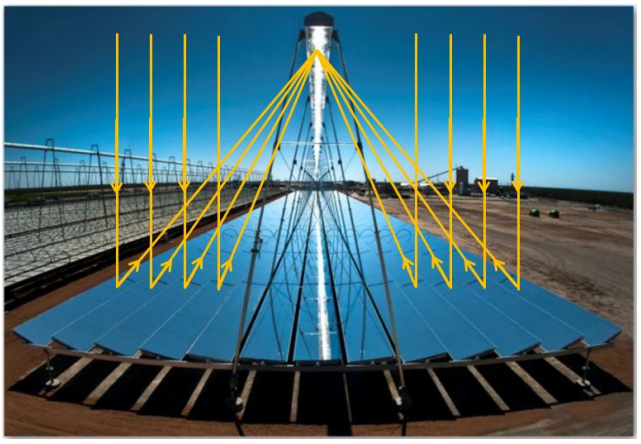

Figure 1.3: Linear Fresnel (SEIA, 2014)

The dish Stirling technology has the highest efficiency compared to any of the other CSP technologies. The technology is able to convert approximately 32 % of the incoming solar radiation to electrical power. This is far greater than the ±28 % peak efficiency achieved from the conventional parabolic trough technology.

Figure 1.4: Stirling Dish (Quasching, 2003)

An additional advantage with this technology is the modular design because of each concentrator having it's own Stirling engine. In this way an entire solar field does not have to be constructed before there is a return on investment. However, currently these benefits are over-shadowed by the fact that with the implementation of Stirling engines, electricity is produced directly and does not have the thermal storage advantage associated with other CSP technologies. This puts this technology in competition with the inexpensive, reliable and established photovoltaic (PV) technology (Deign, 2012).

Technologies that make use of a solar thermal storage systems have the potential for high levels of electricity production in countries with a large solar resource. Thus, the benefit and value added because of thermal storage systems can, in some cases out-way the standard/accepted measure used commercially when comparing electrical power generation technologies. Following this, the levelised cost of electricity (LCOE) is therefore not the only factor determining value of a power plant. The CSP technology which is focused on throughout the document and still maintains a substantial market share is the PTPP technology. This technology re-introduced thermal storage to modern renewable energy producers and has the advantage of allowing energy production for many more hours than other utility grade renewable energy produces. This includes times when it is dark, cloudy, raining, a time of highly volatile DNI or low DNI. This gives CSP technology an advantage when being compared to that of other renewable energy producers, such as wind and PV technology. PTPP and central receiver power plants (CRPP) have the potential to be dispatchable on demand, where the other solar technologies are only able to follow current demand profiles and in the case of PV this is only true during the time of day when the sun is shining (Sioshansi and Denholm, 2010).

Price, country specific policies and regulations are some of the current limitations preventing the growth of CSP and its ability to have a larger impact to the national grid. Despite this, a positive future awaits the expansion of CSP technology. This is attributed to countries expanding their current renewable energy outlook, energy integration methods and collaborations to deliver more affordable clean energy. (Tawney, 2017)

The simulation developed in this research, establishes a performance modelling tool for PTPP's. This will promote the advancement of PTPP's and encourage further developments in the field of CSP. The model is validated by a comparison to the Andasol 3 power plant. Thereafter, operational strategies are evaluated, having the potential to increase electricity production and/or reduce the operational costs. This tool will aid the plant operators in the decision making process on a day-to-day basis, regarding the performance outputs and operational strategy to be implemented in order to achieve the most desirable outcome depending on specific limitations and conditions.

## 1.1 Background and Motivation

Developing solar technologies are continuously being refined, optimised and adjusted in order to become highly competitive in a utility-scale renewable energy market. The ultimate goal of utility-scale power plants is to produce the necessary energy output which in turn generates a profitable business. Achieving this means that the performance is to be monitored, continuous maintenance is needed, reduction in losses and costs are necessary while still focusing on the tariff structure. The costs involved are most likely to include capital, operating and maintenance costs for the overall life time of the respective power plant technology (IndustriaDevelopmentCorporation, 2012).

This study is aimed to serve both grid support PTPP's as well as decentralised PTPP's. The topic *Performance Modelling, Validation and Operational Feasibility of a Parabolic Trough Power Plant*, was suggested to improve/optimise the performance at Andasol 3. The operational strategy results are also aimed at power plants that are similar in nature. The results will go beyond the scope of a single PTPP as it has the potential to promote parabolic trough operations in similarly designed power plants. A study relating to the strategy of a PTPP is captured in this research and allows for a topic of this nature to be at the forefront of parabolic trough technology. The purpose of this thesis is to design and develop a dynamic performance simulation tool that allows for operational feasibility to be analysed for the Andasol 3 PTPP. The output results from the simulation are validated with a comparison to the current Andasol 3 output data. The optimised power plant should allow for an increased electrical output and reduction in operational costs. In addition, a focus on this concentrated solar power plant's thermal-storage capacity is of interest, while identifying key aspects which produce a low LCOE. This simulation will also attempt to decrease the amount of gas used during start-up, making the power plant more environmentally friendly.

## 1.2 Research Goals and Approach

The objective of this thesis is to develop a performance based operational feasibility tool for the Andasol 3 power plant. In order to do this, a simulation of the power plant is to be developed using MATLAB, Simulink and Excel, along with supplied data measurements and readings provided by the Andasol 3 power plant. The simulation is to allow for various alternatives and adjustments giving the simulation modelling tool the ability to be used at various locations and power plants world wide. In addition, Andasol 3 is interested in a study, that investigates ways to reduce the use of gas and operational costs, while increasing electricity generation. This thesis is aimed at investigating possible alternatives and operational strategy solutions.

1. **Investigate Operational Strategy Aspects and Analyse Data**

   Analyse the Excel data supplied by the Andasol 3 power plant. Thereafter, identify and investigate key areas/aspects within the power plant, processes, operations, cycles and systems which define the power plant performance strategy. This approach of first identifying the operational strategy implemented by Andasol 3, promotes an accurate simulation model that directly relates to current plant operations and performance.

2. **Model and Simulate the Andasol 3 Power Plant**

   Make use of a set of tools which allow for the modelling of a PTPP. This simulation model should be detailed and capture all the necessary information that describes the power plant and allow for adjustments to be made. The model should define parameters, constants and coefficients which are used as inputs into a dynamic simulation tool. It should have the capacity to retain large arrays or vectors of input data as well as the capacity for look-up tables. The model is to be validated by comparing the simulation results with the Andasol 3 supplied output results.

3. **Validation of the Simulation Program**

   A process is needed to ensure that the results obtained from the developed model are valid and ultimately reliable and credible. The model is initially verified through the translation of mathematical formulae into a computer code for simulation modelling. Thereafter, the model is compared to values given by Andasol 3 in order to validate the model with actual performance data. The different operational modes implemented in the model are adapted in order to correlate with the data from current performance outputs given by the power plant. Once the model has a good correlation and small performance error percentage of below 10 % for monthly yield according to Guédez (Guédez, 2017), the model is deemed valid.

4. **Investigate the Operational Feasibility of the Power Plant**

   Once the key operational strategy aspects are identified and the simulation model is validated, the performance is evaluated and allows the operator to make performance based decisions from results generated from a simulation model. The model plots performance graphs and saves the outputs in a file which is then used to determine the most beneficial electrical output production. From this, recommendations will be made to optimise the plant. The main objective of this thesis is to enable the operators to make decisions based on reliable performance output simulations. This in turn, develops a way to operate the plant optimally, which uses the storage efficiently and maximises the electrical output of the plant.

Having a tool that simulates and evaluates various operational strategies available to operators will improve power plant performance. This can have tremendous reductions in operational costs incurred and gas used while increasing the yearly electricity production.

## 1.3 Thesis Outline

The completion and execution of this research thesis was highly dependant on the activities and milestones listed. In addition, these activities were initially assigned to a specific date, giving the author the opportunity for feedback and progress evaluation throughout the duration of the thesis.

1. **Literature Study**

   A study and overview of renewable energy on a global scale was necessary to determine the scope and application of the research. After a broad sense of renewable energy was established, the author began focusing on CSP plants, more specifically PTPP. The literature study stretches to that of the Spanish PTPP, Andasol 3 and the details of such a power plant. The Literature study also investigates the position of the parabolic trough technology in the current renewable energy market. It also address modelling tools available and the operational strategies relating to an optimised performance output.

2. **Identification of Key Operational Feasibility Aspects**

   The author focuses the research on aspects within the power plant which are key to the methodology, techniques and modelling of PTPPs. The operational strategy is identified in the data analysis and investigation related to the supplied data given by Andasol 3. For the key strategies to be implemented into the simulation model, the code is to be adjustable, flexible and dynamic. This aids the operational decisions being made and gives the opportunity for an improved electrical output production and reduced operational costs.

3. **Data Analysis**

   Analyse the data supplied by Andasol 3 and produce graphs which indicate the operational strategy currently implemented by the power plant. This is to be done over different times of the year as well as for various durations. An analysis of the daily reports logged by the plant manager is to aid in the analysis by giving reasons for specific operational strategy throughout the duration of the year. The daily reports are detailed and provide a thorough understanding as to why certain components, operational modes, maintenance and alarms are set or put in place. The

daily reports refer to the exact component that is failing and the exact issue facing the plant.

4. **Power Plant Simulation using a modelling tool**

   A simulation program is to be developed which is essentially a model of the Andasol 3 power plant. This is achieved by making use of various methodology, techniques, the previously mentioned literature, data and key operational aspects. The Andasol 3 simulation is modelled according to the following aspects:

   a) Optical and Geometric Parameters.
   b) Thermal-to-Electrical Production Cycle Losses.
   c) Solar Field Energy and Efficiency.
   d) Thermal Energy Storage System (TESS) Operation.
   e) Power Block Energy and Efficiency.
   f) Mass and Energy Balance.
   g) Overall Electrical Output Produced.
   h) Overall Operational Strategy and Modes

5. **Power Plant Operational Feasibility**

   The simulation incorporates the necessary complexities of Andasol 3, yet it is also flexible in the sense that it is able to accommodate potential adjustments and alterations hereby allowing other power plants the option of using such an operational feasibility program.

6. **Comparison of the Results**

   The simulated results are thoroughly compared to that of the actual Andasol 3 output performance data. Evaluating and analysing both the simulation model results and the Andasol 3 output data, allows the author to make a comparison and conclusion of the model which gives rise to recommendations for further implementations and operational changes for the PTPP.

7. **Documentation**

   Construct a professional document containing all the work done throughout the thesis. The report should document all research, methodology, adjustments and results that allow for a credible simulation tool. This document should comply with the Engineering Council of South Africa (ECSA) and all the outcomes given by the Mechanical and Mechatronic Engineering department of Stellenbosch University.

## 1.4 Research Limitations

The work presented in this thesis is focused on a PTPP, the simulation program was designed and developed from first principles allowing the simulation to be altered if necessary. This also gives the model the ability to be adapted for other parabolic trough power plants. With this in mind, the limitations associated with this model are that the simulation is a forward modelling approach, developed on a system level. For example, the model does not allow for an output to be set initially and after running the model, the program is not able to generate the optimum storage operation necessary to achieve that output. It rather allows the user to make adjustments and select operation modes and then run the model and view the performance under those set conditions and modes. This, therefore allows the operator to make decisions on the output results depending on the performance generated from the simulation. Another limitation is that the model does not incorporate a predictive aspect. The model does not change operation depending on a set of outlined prediction conditions. This is a subjective approach to modelling because the program developer is able to adjust those conditions associated with predicting the input values. This is able to improve the operation of the power plant simulation and is suggested as an addition to the model for further research.

# Chapter 2

# Literature Study

It is necessary to investigate the energy sector, renewable sector and more precisely the CSP environment as it introduces a more comprehensive overview of the position and importance of parabolic trough technology application in regions with large amounts of solar resource. A broad knowledge base relating to CSP and PTPP's allows for an accurate simulation program which describes the Andasol 3 power plant in detail. Also, focusing primarily on PTPP aspects, operations and strategies gives a fundamental outline for modelling of the Andasol 3 power plant and similar plants.

## 2.1 Renewable Energy and Solar Thermal Power Plants

The global energy supply today is greatly dependant on the availability of low-cost, conventional energy sources. These conventional sources of energy such as coal, natural gas and oil are slowly being depleted and are known to be limited. Conventional energy production is becoming less and less favourable due to the fact that they are one of the main causes of global warming, where the production of greenhouse gas (GHG) emissions, primarily carbon dioxide ($CO_2$), are hindering climate change and other related issues. The political sector worldwide realises the negative influence of these conventional energy production methods and processes and therefore strongly encourages renewable energy to the commercial market (McLamb, 2011). Worldwide, the development and growth of the renewable sector promotes a step forward in the direction of greener energy production solutions, ultimately reaching environmentally friendly outcomes. In the renewable energy sector, it is foreseen that sustainable energy production will greatly influence current conventional methods for producing energy. Also, because of an increase in energy consumption worldwide, it is becoming necessary to focus on the severity and impact of current approaches when generating utility-scale energy (Conti, 2016).

Extensive advances in the renewable sector, more specifically, the solar energy sector, proves to have great potential regarding energy production and electrical output at a reasonable cost. This is due to "free" energy from the sun. The sun sends enough energy to meet the world's current electricity demand 60 000 times over. This means that each year over one billion terawatt hours of energy is sent to the Earth. Harnessing this energy in a safe and efficient way is changing the way energy is viewed. This includes heating applications, small to large scale electricity production and the capacity for thermal-storage. These aspects prove that solar energy has the greatest potential over that of other renewable energy sources. Solar thermal is a term used to conceptualise solar heat usage having the potential to offer a wide variety of applications. The current solar energy implementations vary greatly, from household water-heating applications to utility grade electricity generation, which is directed to the grid or a decentralised grid. Many of these applications are essential and have convincing benefits, but the focus of this document is based on CSP, more precisely PTPP's. These power plants are the most commercially implemented concentrated solar power plants on the market today. This is due to highly developed, state-of-the-art technology providing a low-cost solution, competitive rates and high performance. This technology has also been on the market for the longest period and is currently proving to be a long term investment that allows relief for other power stations that struggle to meet the current electricity demands. (GrandViewResearch, 2017)

Comparing major differences between solar thermal energy and other renewable energy such as wind energy and photovoltaic technologies, it is recognised that a major advantage of such solar thermal power plants is their ability to store heat energy in a cost-effective manner rather than storing electrical energy. The attraction relating to this storage technology is that the solar thermal power plants can deliver power on demand. This is not limited to overcast skies or night time as in PV applications. An additional attraction includes the near continuous production of electricity during the summer time (Gladen and Mayer, 2008). In this way, the long term benefits offer exceptional potential to drive fossil fuel power plants into a near obsolete state. Fossil fuel power plants are being replaced or combined with solar thermal power plants to substantially reduce greenhouse gasses. A combined power plant is known as a hybrid power plant and is becoming ideal in particular areas where the electricity demand is not currently being met or where environmentally friendly solutions are needed. This introduces the possibility of solar thermal power plants reaching far beyond the scope of current technology. These possibilities stretch out to producing steam, cooling and heating for industrial applications, as well as desalination plants, where drinking water is a valuable commodity and is often realised as a scarce resource in particular areas.

## 2.2 Parabolic Trough Power Plant Development and Forecast

This section describes PTPP's and the developments associated with this technology. It then identifies and explains the Andasol 3 PTPP and predicts future prospects for this technology in the renewable energy sector.

### 2.2.1 Parabolic Trough Power Plant

PTPP technology is a proven technology having the benefit of being extremely reliable. Variations in the PTPP design aim to generate the most electrical power. This is achieved by eliminating heat loss throughout the electricity production process, while under the limitations and conditions presented each day. The technology comprises of three main sections, namely; solar field, thermal storage and power block. These three sections have specific tasks in the electricity generation process of the power plant. They also contribute to the two main loops in the system which are the thermal oil loop/circuit with the molten salt storage system and the steam cycle which converts the thermal energy into electricity (Wang, 2008). Figure 2.1 shows a simplified PTPP schematic, describing the closed loop cycles and main components associated with this technology.

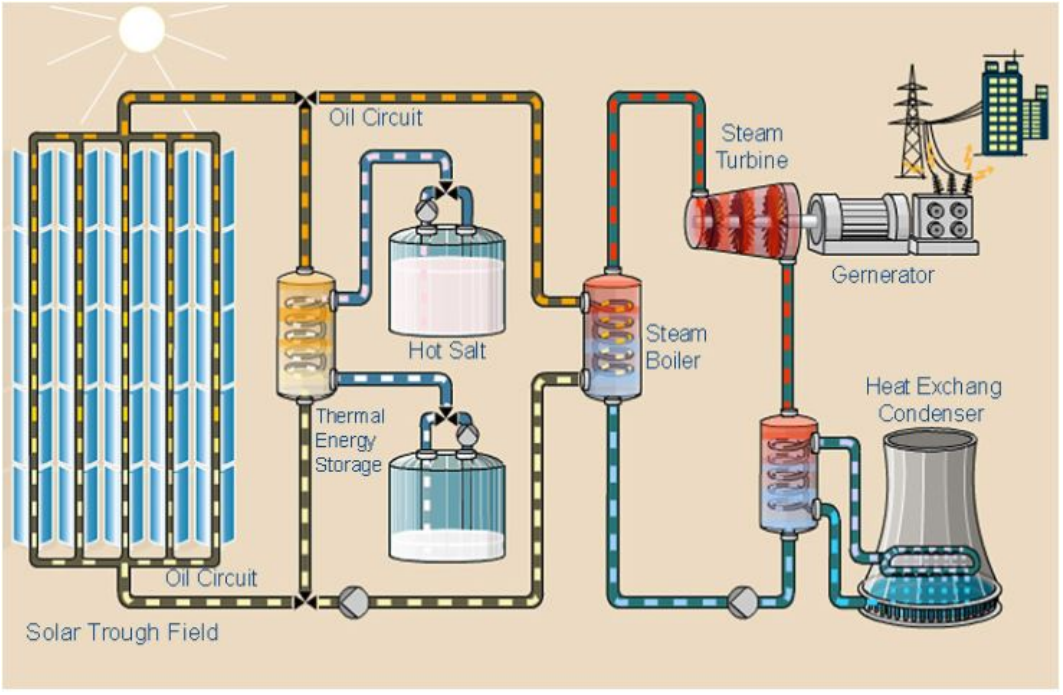


Figure 2.1: Schematic Diagram of a PTPP (Wang, 2008)

The flow of energy relating to a PTPP has a flow scheme which is depicted in Figure 2.2. Direct solar irradiation is focused/concentrated and converted into thermal energy. The thermal energy is then converted to kinetic energy through a closed loop steam cycle containing an elevated temperature and pressure driving a turbine. The final energy conversion is from the kinetic energy of the turbine transforming into electrical energy which is the final output of the power plant. (Gunther *et al.*, 2016)

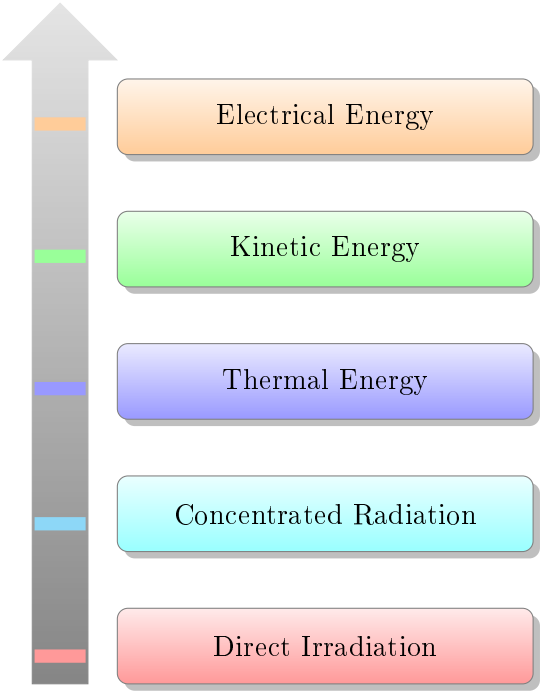


Figure 2.2: PTPP Energy Flow Schematic

The solar field consists of hundreds or thousands of solar collectors positioned in parallel rows and arranged using either a North-South axis or an East-West axis, this axis is known as the tracking axis. The orientation of the solar field is dependent on the location of the power plant. In the case of the Andasol 3 plant, a North-South axis system is implemented, where the solar collectors then follow the path of the sun from East to West in order to attain the most radiation.

A parabolic trough collector is made up of reflectors (mirrors), receiver tubes, structural framework, tracking system, connecting elements and the control system. The reflectors are manufactured from highly transparent, silver-coated glass mirrors in the shape of a parabola. The parabolic shape of the collector allows for the incident solar radiation to be concentrated onto an absorber pipe containing the HTF. Therefore, the concentration of solar radiation occurs

along a linear focal line. The receiver converts the radiation energy into thermal energy. The concentration is approximately 80 times that of the incoming solar irradiance. The HTF used in the majority of commercial operating trough plants, is a temperature-stable synthetic oil in a closed loop system. The oil is capable of reaching temperatures of 400 ℃ before the molecular structure of the oil degrades. The oil is heated in the solar field and pumped either directly to the power block, where it flows through a heat exchanger to produce steam or is redirected to flow through the thermal storage heat exchangers, where molten salt is used to store thermal energy (Pitz-Paal, 2013; Gladen and Mayer, 2008).

The power block's functionality and major components convert thermal energy into electrical energy. The steam is used to drive a steam turbine that is connected to a generator. The process entails high temperature steam and pressure which is converted into rotational movement in the turbine. Thereafter, the generator converts the rotation from the turbine into electrical energy. The steam cycle used is similar to that of conventional power plants, which involves the well established Rankine cycle. This cycle condenses the steam exiting the turbine and re-circulates the water through the closed loop power block cycle (Gladen and Mayer, 2008; SiemensAGEnergySector, 2011).

### 2.2.2 PTPP Development

The first commercial CSP plant (SEGS I), described as the Solar Electric Generating System (SEGS), was constructed in 1984 and commissioned in 1985. Soon after, 8 other CSP plants were built and completed over the next 6 years, until 1991. These power plants are situated in California and are currently operational. They operate using thermal oil as the solar field HTF and a gas burner as an energy backup. Initially, SEGS I made use of a direct thermal oil storage system, but the remaining 8 SEGS plants made use of alternative technologies due to the high costs involved. These 9 plants are considered to be the main role players in the success and development of parabolic trough operations, strategies and technology (SunLab, 1998). Some years later, in 2007, another large scale commercial trough power plant was constructed in Nevada. This only added to the current understanding and technical capabilities of this solar technology. From 2008 to 2014 a large political interest and drive had grown in this state-of-the-art technology, leading to the construction and development of the Andasol Power plants. Andasol 1, the first of three Andasol power plants, became the first commercial CSP plant built in Europe. Once the power plant was commissioned, it became the benchmark for the new generation of PTPP's globally. These three power plants each have a 7.5 hour molten salt thermal storage capacity and produce 50 $MW_{el}$. The first two Andasol power plants are very similar in nature, where Andasol 3 varies slightly in it's approach to the technologies implemented (Gunther *et al.*, 2016).

### 2.2.3 Andasol 3

The Andasol solar power plants are Europe's first commercial power plants to make use of the parabolic trough technology, refer to Figure 2.3. They are located near Guadix in Andalusia, Spain and make use of trough technology to generate a combined capacity of 150 $MW_{el}$. The location of the Andasol PTPP is indicated with the downward black arrow in Figure 2.4 (PowerTechnology: Andasol Solar Power Station, Spain[Online]).

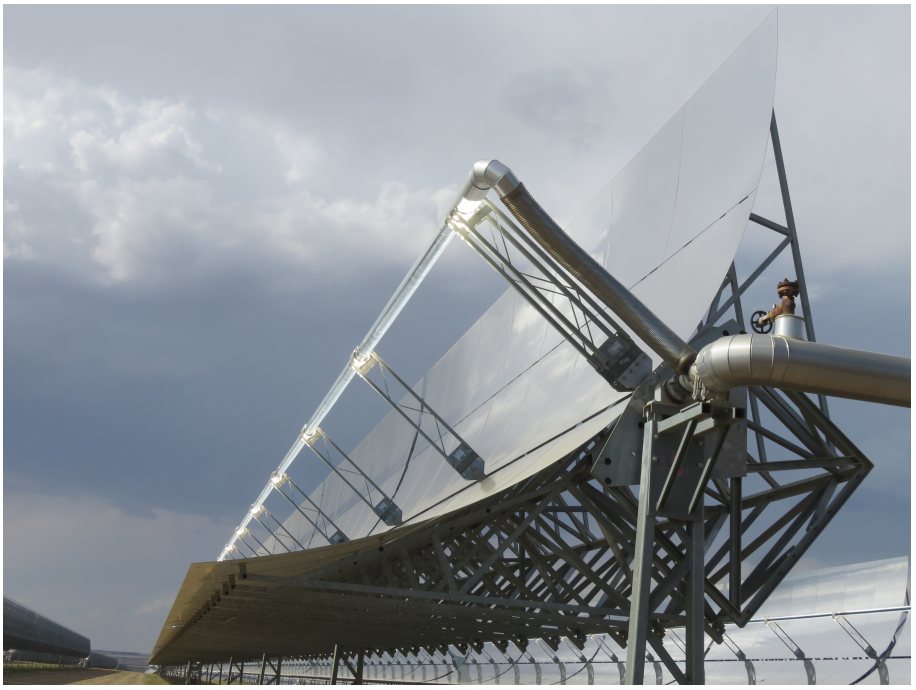

Figure 2.3: Andasol 3 Parabolic Trough

The 150 $MW_{el}$ Andasol power plant, comprises of 3 smaller power plants, which are 50 $MW_{el}$. each and are known as Andasol 1 (completed 2008), Andasol 2 (completed 2009) and Andasol 3 (completed 2011). These individual power plants make use of indirect steam generation and produce 165 GWh/year to 180 GWh/year, totalling a combined output of ±495 GWh/year for all three plants. This is due to the high altitude of 1 100m, semi-arid climate and high annual direct normal irradiance (DNI) in the region of 2 136 kWh/$m^2$ per year, refer to Figure 2.4 showing the DNI map of Spain (Solargis DNI Maps 2015 [Online]). The combined surface area of the power plants is approximately 51 hectares where a solar multiple for each Andasol power plant is approximately 2.4, allowing heat to be stored for 7.5 full load hours. During the summer time, the power plants operate for nearly 24 hours. Furthermore, each Andasol power plant is able to generate and supply environmentally friendly electricity to 200 000 people.

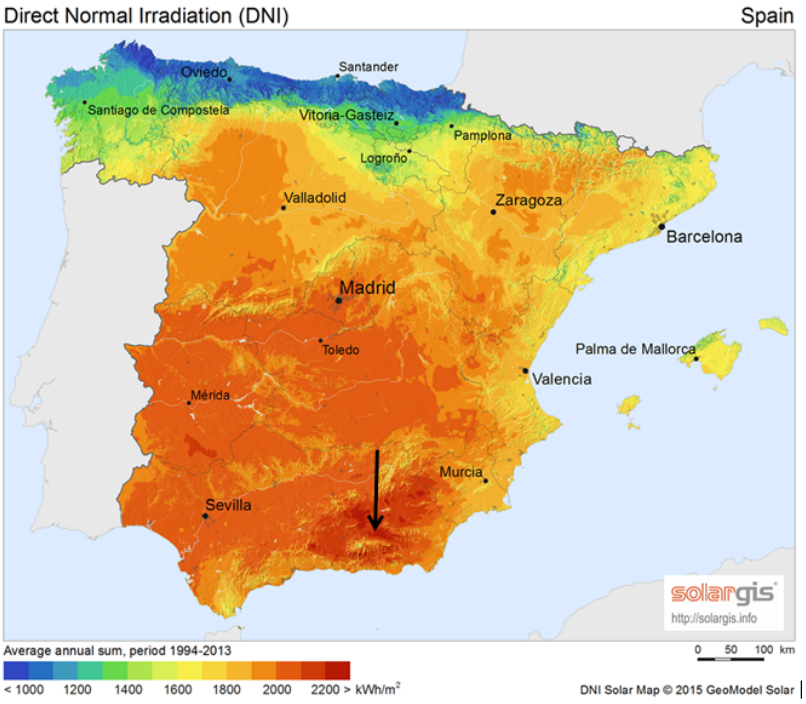


Figure 2.4: DNI Map of Spain (Solargis DNI Maps 2015 [Online])

- Power Plant Overview:
  The key technical information specific to the Andasol 3 PTPP is identified and defined in Table 2.1 (Dinter, 2014).

Table 2.1: Andasol 3 Technical Summary

| **Andasol 3 Technical Summary** | |
|---|---|
| Kind | Parabolic Trough Technology |
| Power Output | 50 $MW_{el}$ |
| Solar Field Aperture Area | 497 040 $m^2$ |
| Storage Design | 2-Tank Indirect Thermal Storage |
| Thermal Storage | 28 500t Molten Salt |
| Storage Capacity | 7.5 Full Load Hours |

- Solar Field:
  The PTPP has a solar field installed with multiple solar collector and receiver assemblies. These assemblies are made up of parallel rows which are evenly spaced to avoid losses due to shading. The solar field makes is a contributing factor to substantial power plant cost and needs to be designed with respect to incoming DNI in that region and turbine size.

- Storage System:
  The Thermal Energy Storage System (TESS) is a two-tank indirect storage system design with molten salt as the storage medium. The reason for the solar salt being used as the preferred storage medium is due to the added benefit of it being able to be stored in tanks at atmospheric pressure, this is because the molten salt has a low vapour pressure. Furthermore, it has a high volumetric heat capacity, while still being relatively inexpensive. The two-tank storage system consist of a large hot tank and large cold tank that are equal in volume. The thermal heat is stored in a molten salt mixture, comprising of 60 % Sodium Nitrate and 40 % Potassium Nitrate (Kopp, 2009). The energy that is stored and used during the night or times of overcast skies allows the electricity production to nearly double the number of operational hours per year. The fully loaded storage system is capable of holding ±1 010 MWh of heat. The molten salt thermal storage system described measures 36 m in diameter and is 14 m high (Gladen and Mayer, 2008).

- Power Block:
  The operating temperature boundaries of the thermal oil as the HTF is a major limitation for oil based PTPP's. This limits the steam conditions in the power cycle to a maximum temperature of approximately 393 ℃. The power block is where the electricity generation occurs and this is achieved through a steam cycle in the form of a Rankine cycle or modified Rankine cycle. The steam cycle considers that the nominal operating conditions for the steam turbine are in the vicinity of 100 bar pressure and the high pressure admission is 381 ℃. The reheat admission is in the vicinity of 18 bar and 381 ℃.

  A thermal engine is used in this design, which is similar to most power plants and therefore cooling is needed for the working fluid. Andasol has ample water supply as it is located near to the Sierra Nevada. The cooling aspect is important as the Andasol 3 plant vaporises approximately 784 884 $m^3$ of water per year according to the Andasol 3 data sheet (Table A.6), which is equivalent to ±2.5 l/kWh. This is a wet cooled power plant which makes use of cold water to cool the steam more effectively than an air cooled condenser, allowing for a more efficient electricity generation at the expense of high water consumption.

- Control System
  The strategies and operational decision making is put into play in the control room. The operators make adjustments and control the power plant to improve plant performance based on a number of considerations and limitations which change daily. The operations and entire power plant strategy is managed with the aid of multiple advanced thermal,

turbo-machine, power plant, actuator and valve control systems which make decisions based on logged readings. The management involves focusing on the software programs implemented and identifying factors which are influencing the operations at the plant. Each power plant has its own software implemented in order to maintain the power plant and continue producing electricity.

### 2.2.4 Cost and Rationale

PTPP's have a low power production cost relative to other solar technologies currently available. This is also a reliable technology when considering large-scale operation for long durations. In terms of renewable energies, the annual efficiency of a PTPP is regarded as being above-average. Furthermore, the energy amortisation period of the PTPP is used to measure the time the power plant needs to produce the amount of energy that was required to build the power plant itself. A PTPP has a low energy amortisation period, because solar thermal power plants have an amortisation period of approximately five months. This is low compared to alternative renewable energy power plants, such as the amortisation period required for wind power is between 4 months and 7 months and the amortisation period for photovoltaic power plants is between 2 years and 5 years.

The approximate total cost of the three Andasol power plants was €900 million to build, where Andasol 3 had a total cost of ±€315 million (NREL, 2013). According to the U.S National Renewable Energy Laboratory (NREL), about 13 % of Andasol's initial cost is from the thermal energy storage system. Furthermore, electricity is produced at a cost of €0.271 per kWh, which is almost 10 times more expensive than nuclear or coal (Gladen and Mayer, 2008).

Further developments and technological advances will reduce the costs involved CSP, making it a more attractive energy solution. The lowest CSP bids came in during May 2017 with Dubai's DEWA at 9.45 $cents/kWh. This was followed by ACWA Power who won a contract during September 2017 at just 7.3 $cents/kWh. In August 2017, SolarReserve won a solar contract at a record low of 6.1 $cents/kWh. During October 2017, they also bid in the Chilean auctions at a new world record price of under 5 $cents/kWh (CSPplaza[Online]). Solar thermal power plants are highly advantageous and distinguish themselves in that they do not require a large specific surface area in terms of the amount of output energy per square meter. Additionally, the added value due to the thermal-storage systems, allows energy production during overcast times and during the night which makes the technology highly advantageous (SEIA, 2014). The three points highlighted next will give perspective to the current CSP and more specifically PTPP's situation.

**Market Predictions:**
A study regarding CSP for the Mediterranean Region (MED-CSP) completed by the German Aerospace Center (DLR) indicates that solar-thermal power plants will have a substantial influence on overall energy production in years to come. Studies of multiple renewable energy sources, shows that by 2025, a large majority of fossil fuels will be more expensive than that of the renewable energy sources. Furthermore, by 2050, renewable energy would have replaced a vast amount of fossil fuel energy sources.

According to the DLR study, the implemented capacity of solar thermal power plants is as large as the combination of many of the other renewable energy sources; namely: biomass, wind, photovoltaic and geothermal power stations. The goal when integrating these technologies is to achieve a low-loss, but high-voltage network by making use of direct-current transmission lines. This provides an efficient way of transporting the electricity throughout the grid. The DLR concluded by stating that by the end of 2050, twenty lines in the Middle East and North Africa (MENA) could use solar power to supply electricity to approximately 15 % of Europe. This is an enticing prospect for the global market and solar thermal potential in countries all over the world, where a large amount of solar resource is received yearly. In comparison to other renewable energies, approximately double the amount of energy can be harnessed with the implementation of thermal-storage, making CSP and PTPP technology economically and environmentally viable.

Spain has been Europe's leader in solar thermal power plants and currently maintains the largest market. Through their technological advancements, solar thermal power plants have become an energy solution worldwide, promoting solar power plants on the South West of the United States, North Africa, Middle East, Asia, China and more recently South Africa. The focus of PTPP technology is set on countries with a strong drive for environmentally friendly power plants and areas where large amounts of DNI is received. These countries have climates well suited for CSP applications, where a large amount of energy provided from the sun is able to be used to produce electrical energy. PTPP's are designed to use the DNI from the sun and convert that into usable electrical energy by means of processes, closed loop cycles and methods involving energy conversion.

**Status and Development Worldwide:**
According to the renewables 2017 global status report (Zervos, 2017), nearly all countries support the development and deployment of renewable energy. This is achieved directly through policies on both a national and local level. Regulations and policies put into place, describe renewable energy targets which attract investors, encourage innovation, promote deployment and motivate flexibility in energy infrastructure. The policies make use of a feed-in

tariff (FIT) which continues to be the most widely used support regulating the power sector. In addition to the FIT's, the power sector is experiencing renewable energy project deployment support through tenders (competitive bidding or auctions). This is becoming the preferred policy tool for CSP expansion and large-scale project deployment.

Renewables contribute to three main industry sectors, namely the power sector, heating and cooling sector and transport sector. Focusing on the power sector during 2016, it is identified that solar PV represented approximately 47 % of the newly installed capacity and the majority of the remainder was accounted for by wind and hydropower which represent 34 % and 15.5 % respectively. The CSP market saw its lowest annual increase in total global capacity in 10 years, this amounted to approximately 2 %. Only 110 MW capacity come online during 2016, which brought the total year end capacity to 4.8 GW. Despite this, CSP continues on a strong growth trajectory as the 2017 year end promises a total global capacity approximately 8 times that of 2016. This market growth is far reaching, beyond the traditional and somewhat stagnant markets of the United States and Spain as many other countries facilitate the construction of large projects. South Africa was ranked as a market leader with its new additions in 2016, but struggled to maintain growth and continue construction in 2017 as the utility monopoly restricted large projects. South Africa was the second developing country to expand and focus on CSP projects after Morocco encouraged CSP market growth in 2015. Following South Africa was China who also managed to put new CSP plants online. Although the CSP market is dominated by the top companies in construction, operation and manufacturing, the market leaders were identified as Abengoa and Saudi Arabia's ACWA Power, as they owned the majority of projects under construction during 2016. ACWA Power continues to grow globally as developer, owner and operator through projects in South Africa and Morocco. Other top companies include Supcon (China); Rioglass Solar (Belgium); GE, Brightsource and Solar Reserve (all United States); and Sener, TSK, Acciona and ACS Cobra (all Spain). These companies promote and help ensure the continued drive for CSP in regions that facilitate construction. All new facilities going online are designed and commissioned with thermal energy storage (TES), as this is fundamental to the added value of providing dispatchable power to existing or new grids. Parabolic trough power plants and central receiver technologies contribute to the majority of the CSP market and recently make use of molten salts as HTF, which is becoming the preferred choice among some regions. Additional research investigates sand-like particles as an alternative to molten salt in TES systems. Studies related to increased energy storage density at lower costs for thermochemical storage systems are advancing CSP along with further studies which aim to reduce costs and potentially increase efficiency with a supercritical $CO_2$ Brayton Cycle. CSP is receiving continual policy support in developing countries with high DNI levels and economic alignment

with CSP technology benefits. These countries mainly have agendas for job creation, limited power networks, industrialisation approaches, need for energy storage, limited gas and oil reserves, promotion of local manufacturing and enhancement of engineering and skills development.

Currently, the world adds more renewable power capacity annually than it adds net capacity from all fossil fuels combined. This brings the power generating capacity contribution from renewables to approximately 30 % worldwide. This is due to renewables accounting for nearly 62 % of net additions to the global power generation capacity at the end of 2016. Investments continue to focus on solar power as the renewable energy of choice, this is however closely followed by wind power (Zervos, 2017).

**CSP Technology Forecast:**
Economic growth, technological improvements and more competitive supply chains continue to reduce the cost of solar power. Technological advances relating to cost effective collector design, high thermal capacity HTF's and efficient cycles will lead to cost reductions. Along with these aspects relating to CSP technologies, financial influences and having power on demand during the night and overcast times promotes the availability of such a technology.

According to the International Renewable Energy Agency (IRENA), there is the potential for a large cost reduction for solar power in the future. The cost of electricity for concentrated solar power technologies could fall by at least 37 % and at most 43 % by 2025. This forecast is made using 2015 as the reference. Currently, LCOE prices for CSP technologies are not as low as other renewable energies, such as wind energy and PV. However, on a global market level, the added value of a CSP plant is becoming more desirable. CSP has the ability to utilise stored thermal energy and better meet the countries demand profile. Global energy markets are influenced by pressures from competitors and financing costs, which has a direct influence on driving innovation and advancements. CSP equipment costs continue to decline, while maintenance, operation and capital costs are important factors for overall cost reduction and need to be monitored and altered in order to make these reductions.

Table 2.2 compares the projected global weighted average data for PTPP and solar towers for 2015 and 2025. The values are presented in U.S. dollars because it allows the reader to make comparisons with other data found in literature. This forecast of the two leading CSP technologies give rise to an interesting phenomenon within the solar energy space. Both these technologies have the advantage of operating during times when wind and PV technologies can no longer generate electricity. This proves to be highly valuable when focusing on utility-scale power plants (Amin, 2016).

Table 2.2: Projected Global Weighted Average Data (Amin, 2016)

| Global weighted average data | | | | | | | | | |
|---|---|---|---|---|---|---|---|---|---|
| | Investment Costs (2015 USD/kW) | | Percent Change | Capacity Factor | | Percent Change | LCOE (2015 USD/kW) | | Percent Change |
| | 2015 | 2025 | | 2015 | 2025 | | 2015 | 2025 | |
| CSP Parabolic Trough Collector | 5550 | 3700 | -33 % | 41 % | 45 % | 8.4 % | 0.15 -0.19 | 0.09 -0.12 | -37 % |
| CSP Solar Tower | 5700 | 3600 | -37 % | 46 % | 49 % | 7.6 % | 0.15 -0.19 | 0.08 -0.11 | -43 % |

According to the MENASOL 2016 conference, Nebrera stated that global CSP generation costs could potentially decrease to \$111/MWh by 2020 and further decrease to between \$77/MWh and \$89/MWh by 2025 (HELISCSP[Online]). Additionally, CSP will account for a sizeable amount of the electricity mix, particularly in regions where alternative renewable solutions are limited or there is sufficient solar resource.

In the near future and progression forward it is essential to realise that the LCOE will not demonstrate the full value of CSP plants. With this becoming reality, power authorities and policy makers should take into account the dispatch-ability and storage capacity of CSP plants as this adds additional value to the power industry. Various policy makers are able to implement multi-tier tariff structures that will promote the value of CSP and its ability to dispatch energy during times of high demand or when alternative low cost renewable energies such as PV and wind technologies are unable to.

## 2.3 Efficiencies and Losses

This section outlines and investigates the main energy losses and efficiencies associated with current PTPP's. Trough technology experiences heat losses throughout the entire solar-to-electricity process, while components only allow for a specific efficiency to be achieved, leaving only a $\pm 16$ % overall efficiency. It is therefore essential to identify these aspects that reduce the overall efficiency.

### 2.3.1 Optical Efficiencies

Optical Efficiency as described by L. Valenzuela (Valenzuela, 2012) can be divided into two main energy loss categories, namely beam incident losses (BIL) and geometric losses (GL). Refer to Figure 2.5, which shows the beam incident losses. These losses consist of the capture fracture, interception factor, transmissivity, absorptivity and reflectivity.

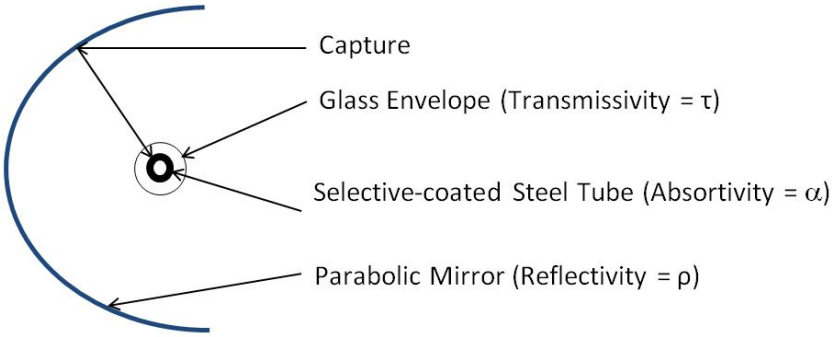


Figure 2.5: Beam Incidence Losses

The geometric loss category, refer to Figure 2.6, includes the effective collector length losses depicted in Figure 2.6a and the shading losses as shown in Figure 2.6b (Valenzuela, 2012). These loss aspects play a large role in the overall power plant efficiency and need to implemented into any power plant model describing this technology. They are therefore described next:

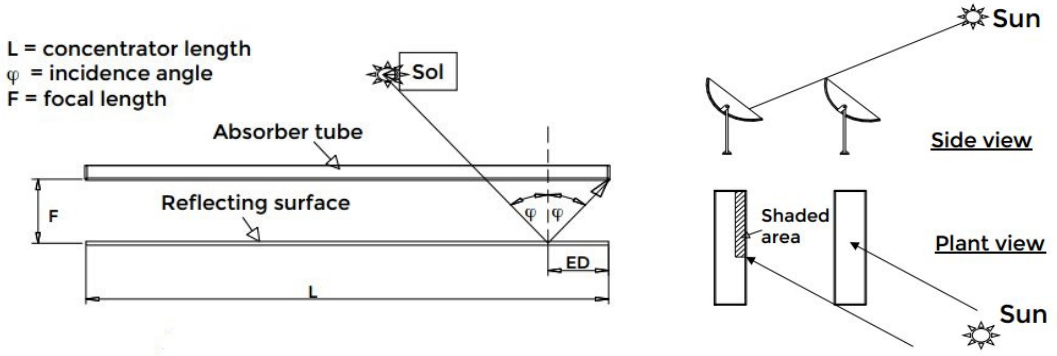


(a) Collector Length Losses (b) Shading

Figure 2.6: Geometric Losses (Valenzuela, 2012)

- **BIL - Capture Factor**

  The capture factor is a measure of both the surface shape reflecting quality and the receiver size. This is most often described in the CSP environment as *spillage*. Spillage is the fraction of reflected energy that does not come into contact with the receiver. A well shaped and sized collector and receiver assembly will drive this loss factor close to 1, approximately having a value of 0.95 or higher.

- **BIL - Glass Envelope (Transmissivity)**

  Transmittance is the fraction of solar radiation that passes through a transparent material (used as an absorber tube cover) on it's path to

the receiver or more specifically, the absorber. These transparent covers are most commonly a glass or plastic cover, which is used to reduce the convection heat losses at the absorber tube.

- **BIL - Selective-coated Steel Tube (Absortivity)**

  Absorption is the term representative of the solar energy fraction absorbed when solar radiation rays are incident upon a surface. The remainder of this energy is reflected. This property is for radiation in the solar or visible spectrum. Furthermore, the amount of energy being absorbed varies as a function of incident energy wavelength. These absorption factors are often greater than 0.98 for black surfaces, but this value decreases as the surface degrades over time and wear. The class of surfaces used in solar collectors are known as *selective surfaces* and have a higher absorptance factor in the visible spectrum than at longer wavelengths, in turn this reduces radiation loss.

- **BIL - Parabolic Mirror (Reflectivity)**

  Reflectivity relates to any aspect of the reflecting surface associated with the collector. A well designed collector is able to have a reflectivity factor of 0.94 or 0.86 when considering silver/glass mirrors or aluminium surfaces respectively. The law of reflection states that the direction of the incoming light and outgoing light have the same angle with respect to the mirror surface normal. However, when considering diffuse reflection, the incoming light is reflected in a broad range of directions. For CSP technology, only specular reflectivity is of interest because the reflected radiation must have a defined direction. It is noted that the most common parabolic mirrors today consist of silver coated glass mirrors which are extremely durable having a guaranteed life span of more than 10 years, while hardly showing a decrease in specular reflectivity.

- **GL - Loss of Effective Collector Length**

  The effective collector length losses are based on the concept known as the cosine effect. This effect is a geometric loss, which reduces the amount of solar thermal energy being reflected from the collector to the receiver, refer to Figure 2.6a. The length of reflective surface not in use is shown by the variable length (ED) and the reason for this is because of the orientation of the collectors relative to the incoming radiation from the sun. Therefore, the geometry restricts the full collector aperture area to be used. The tracking system compensates for this geometry limitation by following the sun and attempts to reflect as much solar radiation to the receiver as possible.

- **GL - Shading Losses**
  Shading losses can occur when the row spacing is too narrow and a collector limits the amount of solar radiation able to reach the collector in the next parallel row, refer to Figure 2.6b. This phenomenon can also occur during sunrise and sunset as the altitude angles are small. During this time the solar radiation is prevented from reaching all the solar collectors as they are facing either an East or West position.

### 2.3.2 Thermal Losses

The thermal losses associated with the receiver tubes are depicted in the energy balance schematic, refer to Figure 2.7. This shows the convection, conduction and radiation heat transfer related to the absorber tube and glass envelope. (Valenzuela, 2012). Figure 2.7 depicts a common receiver tube implemented in current commercial PTPP's. It incorporates a glass envelope which usually consists of an anti-reflection coating which has a high abrasion resistance and allows the transmission of more than 90 % of radiation from the sun. The glass envelope contains a vacuum interior, which prevents heat conduction/convection from the hot absorber tube to the cooler glass envelope and allows for thermal expansion. The metal absorber tube carries the HTF and is coated in a selective material that has a high solar radiation absorbance that filters out infrared rays, while having a low thermal remittance and therefore attracting visible light. The absorber diameter is small relative to the collecting reflector aperture which decreases the surface area associated with heat loss. A glass-to-metal seal is also necessary to reduce heat losses (GearSolar [Online]).

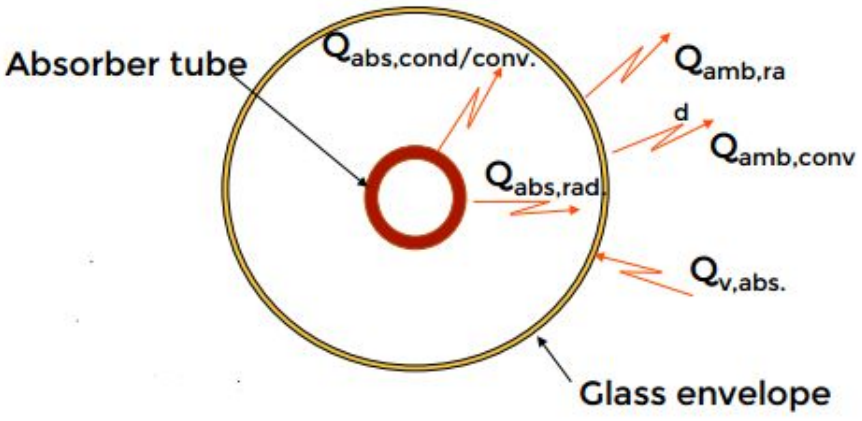


Figure 2.7: Thermal Losses (Valenzuela, 2012)

### 2.3.3 Power Block Losses

Losses found in the power block include the following aspects as described by enerMENA (Gunther *et al.*, 2016):

(a) Heat Exchanger Losses (from HTF to the water/steam)

(b) Pressure Losses

(c) Turbine Losses

(d) Thermal-to-Mechanical Losses

(e) Mechanical-to-Electrical Losses or Generator Losses

(f) Mechanical Friction Losses

The loss that carries the biggest influence in the power block is the thermal-to-mechanical loss. The Rankine cycle is a model usually used to predict the steam turbine system performance. This is an idealised thermodynamic cycle that converts heat into mechanical work while the working fluid is susceptible to a phase change. The Rankine cycle is a closed loop cycle, which makes use of externally supplied heat and a typical working fluid such as water. There are two main reasons for considering a Rankine cycle as the ideal cycle for steam plants:

1. It is a difficult challenge to build a pump that is able to handle a mixture of liquid and vapour and deliver saturated liquid. The current solution therefore condenses the vapour to liquid form to make it easier for the pump to handle.

2. In practise it is difficult to superheat steam at a constant temperature as in the Carnot cycle. The difficulty comes in when the pressure has to be dropped and in turn heat is transferred to the vapour as it undergoes expansion. Therefore a Rankine cycle is beneficial, as the vapour may be superheated at a constant pressure with little difficulty.

Curzon and Ahlborn showed that with irreversible heat transfer and all parts of an engine ideal, the engine efficiency at maximum power is described by Equation 2.1, which is also known as the Chambadal-Novikov efficiency (Askarov, D.[Online]).

$$\eta = 1 - \sqrt{\frac{T_{sink}}{T_{source}}} \tag{2.1}$$

In any thermodynamic power cycle it is important to improve overall cycle efficiencies and a common way to achieve a better steam cycle efficiency is a process known as a modified Rankine cycle is either with a reheat cycle or using a regenerative cycle. The reheating has a main practical advantage

which decreases the moisture content in the cycle as most of the heat addition occurs in the vaporization part of the heat addition process. The regenerative cycle is carried out where heat is taken from the steam between turbine stages and used to preheat water on its way from the condenser to the boiler.

## 2.4 System Losses and Efficiencies

Figure 2.8 summarises the approximate energy flow in a PTPP. The input power is described as the direct normal irradiance on the solar field aperture area. The power plant experiences on average about 25 % optical losses and 15 % thermal losses, where the power block experiences approximately 42 % losses mainly due to heat rejection in the condenser. This leaves 18 % input power that is transferred from thermal to electrical power. Parasitic energy is the electrical energy needed to operate the power plant. The parasitic energy consumption in PTPP's is considerably higher than in most other power plants. This is due to the fact that power is needed for the HTF pumps and the tracking system associated with the long collector rows in a PTPP. This amounts to about 10 % of the generated power or approximately 2 % of the input power. This leaves 16 % as the usable electrical output production.

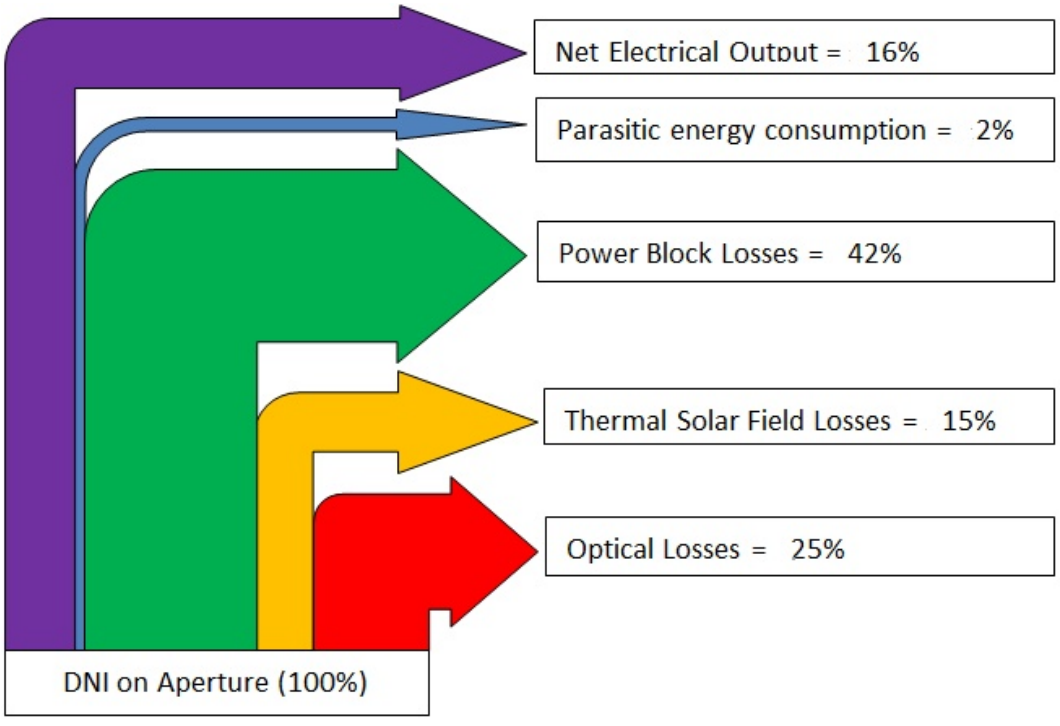


Figure 2.8: Approximate Energy Flow in a PTPP

Overall Power Plant Efficiency:
At any given moment, the total efficiency (Solar-to-Electric Efficiency) of a PTPP is defined as the ratio of electric power ($P_{el}$) to direct irradiance on the collector aperture ($G_{ap}$), multiplied with the total solar field aperture area ($A_{ap}$). This is described in Equation 2.2 (Gunther *et al.*, 2016).

$$\eta = \frac{P_{use}}{P_{in}} = \frac{P_{el}}{A_{ap}.G_{ap}} \tag{2.2}$$

This efficiency can be subdivided into the solar field efficiency and the power block efficiency (Equation 2.3).

$$\eta = (\eta_{SF})(\eta_{PB}) \tag{2.3}$$

With the addition of the TESS in a PTPP, the storage efficiency is taken into account when calculating the overall efficiency. These efficiency values change continuously unlike conventional fossil fuel power plants, because of changing operating conditions. This includes conditions such as different sun positions and other factors. This makes the efficiencies less stable than in fossil fuel power plants. It is therefore necessary to discern from peak efficiency values and average efficiency values. A peak efficiency value is in the range of 23 % to 28 %, where the average efficiency is closer to 12 % or 16 % for power plants like Nevada and Andasol 1 respectively. Focusing on the Andasol 1 power plant, there is a peak solar field efficiency of 70 % and a peak power block efficiency of 40 %, where the average efficiencies are only reaching 50 % and 30 % respectively (Gunther *et al.*, 2016) .

## 2.5 Heat Transfer Fluids (HTF)

All HTF's have to adhere to specific requirements and are also selected based on the benefits it adds to the power plant. In general HTF are evaluated based on the following aspects:

(a) The HTF must be a liquid, unless direct steam is used. This means that the fluid must have a sufficiently high evaporation temperature under a pressure which is easily manageable. The fluid should not evaporate due to high solar field temperatures.

(b) Thermal stability. The fluid should be able to handle high operation temperatures. The evaporation temperature along with the thermal stability indicate the maximum operating temperature of the HTF.

(c) Low freezing temperatures. This allows the plant to eliminate the need for such stringent freezing protection measures when temperatures in the solar field drop too low.

(d) It is useful to have a medium with a high thermal capacity as this allows high amounts of thermal energy to be transported and stored.

(e) A high heat conductivity is important for a quick heat transfer process.

(f) Low viscosity is needed to reduce the pumping energy needed to move the fluid through the various cycles or processes.

(g) Environmentally friendly and low inflammability fluid is desirable. Also, local or easily obtainable materials are preferred.

It is important to highlight all of the above mentioned aspects, while explicitly noting that some aspects are more important than others. It is of priority to have a good thermal stability and a high evaporation temperature as this determines the maximum steam cycle temperature and power block efficiency. Alternatively, low inflammability is not always considered an important selection criterion. Some of the major HTF mediums possibilities are described in Table 2.3:

Table 2.3: HTF Properties

| Medium | Max. Temp (℃) | Heat Capacity (J/kg/K) | Heat Conductivity (W/m/K) | Cost |
|---|---|---|---|---|
| Mineral Oil | 300 | 2600 | 0.12 | low |
| Synthetic Oil | 400 | 2300 | 0.11 | high |
| Silicon Oil | 400 | 2100 | 0.1 | high |
| Nitride Salt | 450 | 1500 | 0.5 | moderate |
| Nitrate Salt (Molten Salt) | 565 | 1600 | 0.5 | low |
| Carbonate Salt | 850 | 1800 | 2.0 | high |
| Sodium(liquid) | 850 | 1300 | 71.0 | moderate |

A large majority of PTPP's make use of synthetic thermo oil (theminol VP-1) as their choice of HTF. Synthetic oil meets most of the desirable aspects set out for a HTF. However, there are limitations to this medium being used, such as the maximum operating temperature is approximately 400 ℃. Beyond this temperature, thermal cracking occurs, which destroys the thermal oil. Live steam temperatures are limited to what is delivered by the solar field. The steam design point temperature is 385 ℃ with an oil temperature of 393 ℃, which limits the power block efficiency. Also, this fluid needs to be replaced on a periodic basis as the fluid ages and the chemical structure changes over long periods. This oil is also relatively expensive making up approximately 5 % of the costs for a power plant such as Andasol 3. When comparing molten salts as a storage material to that of the other mediums defined in Table 2.3, it is seen that the most important advantage is the high temperature of 565 ℃. This promotes a higher power cycle efficiency than that of the conventional VP-1 synthetic oil, which is the reason for the solar salt technology shift (Kotzé *et al.*, 2012).

## 2.6 Operational Configurations

PTPP have various operational modes and strategies to meet demand profiles and tariff structures to deliver electricity to the grid. These configurations are dependant on many aspects that change day-to-day. Although, limited to regulations and policies effecting renewable energy implementations, the parabolic trough technology is able to operate under three main operational configurations summarised by Roos (Roos, 2012; Gunther *et al.*, 2016):

**Base Load Power Plant**
A base load CSP plant is defined by a large thermal storage. This allows for the generation of electricity for long durations of time without solar energy. In turn, the turbine is small as electricity is generated on a continuous basis. This configuration operates at full load which is determined by the electricity demand from all commercial, industrial and residential sources at any given moment. In general, base load generation systems achieve their lowest average cost of energy if run continuously at full output.

**Load Following/Intermediate Power Plant**
The intermediate power plant needs a smaller thermal storage than a base load power plant. This is due to less energy having to be stored for a shorter operation time and the ability to respond to a fluctuating demand. Together with a decrease in storage size, the turbine is usually larger compared to one used in a base load power plant. This set-up is typically more expensive as it is designed for frequent flexible operations and has variable costs. All costs are also spread over less hours of the year when compared to base load generation.

**Peak Load Plant**
A peak load plant operates for only a short time to meet peak loads. These loads occur during times when generators or transmission lines are unavailable due to unforeseen outages or times of very high demands. The generators are often relatively inefficient making this configuration a short term solution with high variable costs and relatively low capital expenditure. This makes this configuration the most expensive of the three power generating configurations.

## 2.7 Modelling and Simulation Tools

Currently there are a number of simulation tools on the market which provide useful information to the designers, optimisers, power producers and investors. However, these tools/programs have limitations restricting some of the interested parties involved in the specific CSP project. This section highlights some of the popular and well developed simulation tools available and discusses the advantages and disadvantages of each.

**SAM:**
The System Advisor Model (SAM) developed by the National Renewable Energy Laboratory (NREL) is a freely available performance and financial modelling tool, which has recently allowed users access to the source code. The software has a user friendly graphic interface linked to the model and is designed to assist those active in the renewable energy industry decision making process. The financial modelling aspect is particularly well developed when considering the USA tariff system, as it includes subsidies from the government as well as tax incentives (Blair *et al.*, 2014).

**TRNSYS:**
The Solar Thermal Electricity Component (STEC) makes use of an array of the Transient System Simulation (TRNSYS) libraries and models in order to generate transient simulations. Although STEC is a free add-on, the complete simulation tool (TRNSYS) is not freely available. It is used extensively during the research and development stages of new technologies, as well as during feasibility studies regarding solar thermal power plants and similar projects. It is therefore ideal for research institutions that are willing to invest and can afford licenses (Transient System Simulation Tool , TRNSYS).

**Ebsilon Professional:**
The flexibility of this system developed by STEAG allows for virtually any thermodynamic cycle to be simulated. The software is aimed at power plant engineering and design, which includes plant dimensioning all the way through to feasibility studies of different technologies. This tool is mainly a performance based modelling program (EBSILONProfessional, 2014).

**Greenius:**
A freely available software developed at the Institute of Solar Research of the German Aerospace Center (DLR). Greenius is developed for fast and simple performance calculations for renewable energy systems based on hourly simulations. The software is primarily related to feasibility studies. The information available is typically limited when considering components, equipment and the technology being modelled. A large number of simulation runs are needed when using this software program, but comparisons are able to be made between various technologies at one specific location (Quaschning *et al.*, 2001).

**Thermoflow:**
The Thermoflow software is a comprehensive tool that includes design, simulation, cost estimation of power and co-generation. It is, however, not freely available and does not give the user access to the source code. There is a well defined user interface, where some components are represented graphically (THERMOFLOW, 2015).

**Flownex:**
Flownex is a simulation environment that enables the user to study how real world fluid driven systems behave. The tool is primarily used as a design tool, where the main attraction of this software is the ability to relay the overall effect of changing specific properties on components, which gives the user the capability to extensively examine variations in the design and optimisation of systems. It offers a fast, reliable and accurate simulation approach for a total system and subsystems in order to minimise costs that would be incurred with physical testing (Flownex[Online]).

**Matlab:**
The Matlab software is freely available to researchers at the University of Stellenbosch. It is also a mathematical modelling program that has many toolboxes. One such toolbox is the Simulink toolbox which allows for a transient response simulation. This is the preferred modelling tool for the study as it includes the Simulink toolbox, the coding is able to be written from first principles and it is freely available.

# Chapter 3

# Parabolic Trough Power Plant Modelling

As discussed in Chapter 2.7, there are highly rated modelling tools available on the market, such as the System Advisor Model (SAM) that fairly accurately models PTPP's. These modelling tools are however limited in that, typically, they are not used as operational feasibility tools for strategy and operational decision making. Some of the programs are not high resolution compatible and restrict access to source code. They are mainly used as a design tool, and it was therefore suggested that a software simulation program could help improve operations and assist the plant operators with operational decision making at Andasol 3. It is for this reason that a simulation model of Andasol 3 is constructed. The model in question will provide a space for performance analysis and operational feasibility, which has the potential for plant optimisation. This chapter is to be used as a manual that represents formulation, engineering principles, equations, coding logic, methodology, information flow, conventions and descriptions used in the Andasol 3 simulation model. The majority of these aspects are obtained from Stine and Geyer who have made a free online book available "Power From The Sun" (Stine and Geyer, 2001). Also a large contribution was attained from the technical manual for the SAM physical trough model developed by NREL (Wagner and Gilman, 2011). This chapter also takes a detailed look at the solar field, thermal storage and power block, but not before investigating high resolution data and it's effect when modelling PTPP.

## 3.1 Overall Modelling Approach

The modelling approach is a first-principle approach, where performance is unknown prior to the outcome of the model simulation. The advantage of this approach is that there is flexibility relating to system parameter values and component properties on a fundamental level. It includes transient effects

related to thermal capacity of the HTF in the field piping and the balance of the plant throughout the entire thermal-to-electrical cycle. The drawback is that there is a level of uncertainty in the final established model, which stems from equations and formula with small uncertainties. The author recognises that the document presents one possible model formulation for the Andasol 3 PTPP. However, there are many alternative and equally valid solutions and the approach selected does not necessarily represent the best possible solution. Figure 3.1 shows the overall model logic and flow.

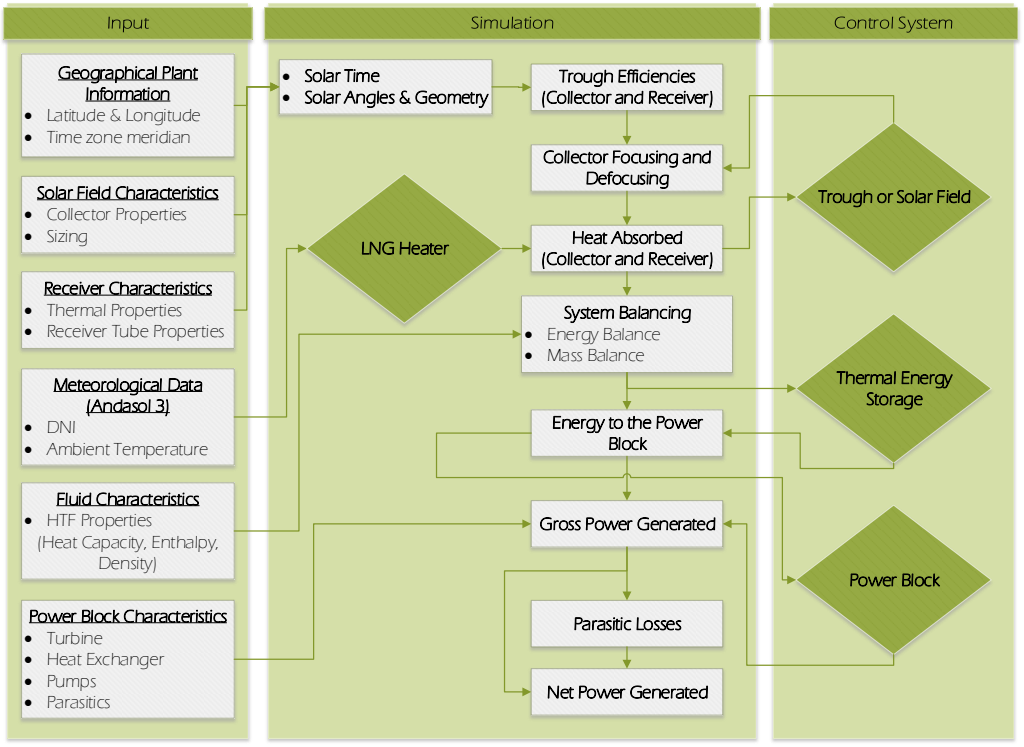


Figure 3.1: Model Flow Chart

The developed simulation model is created using MATLAB, Simulink and Excel. The MATLAB domain is the R2017a version for academic use, which has the Simulink toolbox as an additional feature. The model is constructed with a 10 second time step, where a third order explicit solver (ode3) is used. The 10 second time step was chosen in order to run a high resolution model, while still maintaining a fast overall simulation run time which gives the operator the time to still analyse the output results and make strategy decisions. The Simulink toolbox deals with the dynamic performance model and allows for components within the power plant to be managed as sub-components of the total power plant. The MATLAB script prepares the inputs, variables and parameters for the dynamic simulation solver. Once this MATLAB data is fed to Simulink for the dynamic performance simulation aspect, the model analy-

ses the values and makes calculations based on formula, logic conditions and limitations. The model has a control system, which describes the operational strategy of the solar field, storage tanks and power block. This is achieved by making use of feedback loops, control logic and flow charts. Once the simulation has finished running, an additional MATLAB script file plots graphs and files the performance results for the user to easily access.

## 3.2 High Resolution Data

High resolution data is essential for accurate simulation modelling of PTPP's. This high resolution data is obtained from various devices such as a pyrheliometer, an instrument that measures the amount of direct radiation (DNI) from the sun (Pyrheliometer [Online]). Generally, this instrument is a component of a solar resource weather station that is placed on a potential or existing CSP site location. This device is able to achieve high levels of accuracy, ideal for the purpose of CSP performance or yield based modelling. High resolution data is obtainable, but it is usually expensive. Currently, data obtained from a satellite or other historical sources is in a hourly averaged format and when comparing simulation results from ground measurements (high resolution data) to hourly resolutions data, it shows that the hourly resolution over estimates the yearly electrical yield by about 8 % (Geuder *et al.*, 2003).

Therefore, high resolution data (one, five and ten minute data) is the preferred data resolution when modelling or simulating PTPP's. The model developed allows for any resolution data to be imported and used. The user should specify the resolution in the user interface prior to the run commencing. The model currently makes use of 5 minute resolution data, obtained from the 5 measurement stations located at the Andasol 3 power plant (ground measured data). The location of these 5 measurement stations are placed at each corner of the power plant and one in the middle in order to record and average the data accurately.

## 3.3 Solar Field

Heat is collected in this segment of the power plant and consists of multiple solar collector assembly (SCA) loops. These loops are in parallel, and connected via a common cold header pipe which provides an equal cold HTF flow rate to each loop. There is a second header pipe which collects the hot HTF and returns it to either the power block for power generation or it is stored in the thermal storage system for use at a later stage. The solar field is typically divided into multiple sections containing it's own header pipes. This is done in order to maintain pumping pressure throughout the field. In addition, the

structure of a PTPP is usually of a rectangular nature. Common practice is to include the power block in the centre of the solar field, which ensures the shortest possible pipe lengths. The reason for this structuring is to reduce the thermal losses in the solar field. Regarding the distance between the parallel collector rows, the distance is approximately three times the aperture width of the parabolic collector, limiting thermal losses and encouraging a low investment cost. Figure 3.2 shows the traditional solar field layout (Wagner and Gilman, 2011). The blue lines indicate the cold header pipes, where the red lines indicate the hot header pipes.

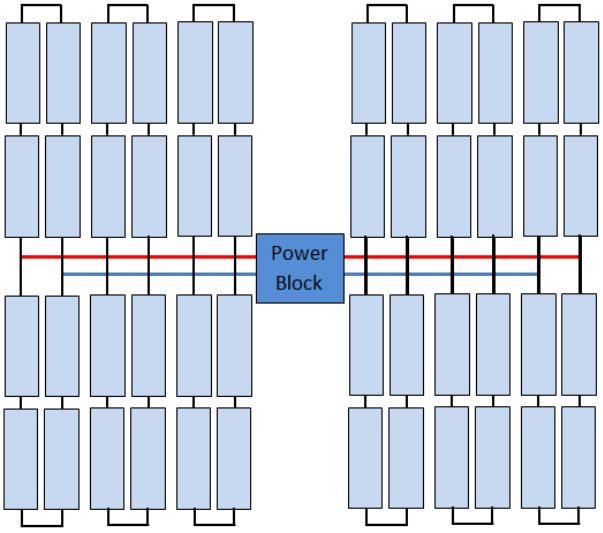


Figure 3.2: Traditional Solar Field Layout

An additional consideration when modelling the solar field is the wind speed experienced by the collectors. This is because high winds could cause damage to the collector assemblies or break the glass mirrors. Alarms are put into place that signal wind speeds exceeding specific threshold limits. These limits are different depending on the collector technology implemented. In the case of the Andasol 3 power plant, the EuroTrough design was chosen for the collectors and the wind speed alarm corresponding to this design is represented in Figure 3.4. The alarm conditions are summarised where the first two alarm conditions are for safety purposes only and the final wind alarm (strong wind alarm) is where the solar field moves into it's stow position. The values represented next correspond to a sun angle of 0°(dawn), which is the stow position. Refer to Figure 3.3.

1. Wind warning: 16 m/s
2. High wind alarm: 18 m/s
3. Strong wind alarm: 20 m/s

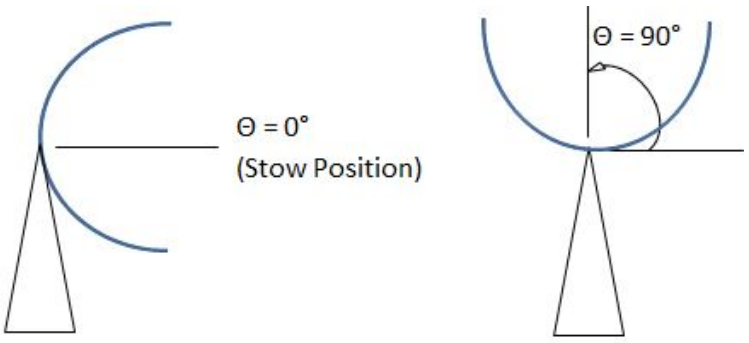


Figure 3.3: Stow Position

Figure 3.4 shows that the wind threshold limits decrease along the day as the sun angle increases. The reason for this occurrence is because the further the collectors are from the stow position (0°), the longer it takes to move back to the stow position. Therefore the collectors can withstand the greatest wind loads at stow position (0°) as the threshold value is greatest at this position. This allows the plant to always operate in a conservative manner, without the risk of damage to the collectors. Also from Figure 3.4, it is noticeable that the wind threshold depends on the sun angle, and not on the collector position. This is to avoid a situation where some collectors move to the stow position, but others do not due to the small positioning differences among them (Cabrerizo, 2017).

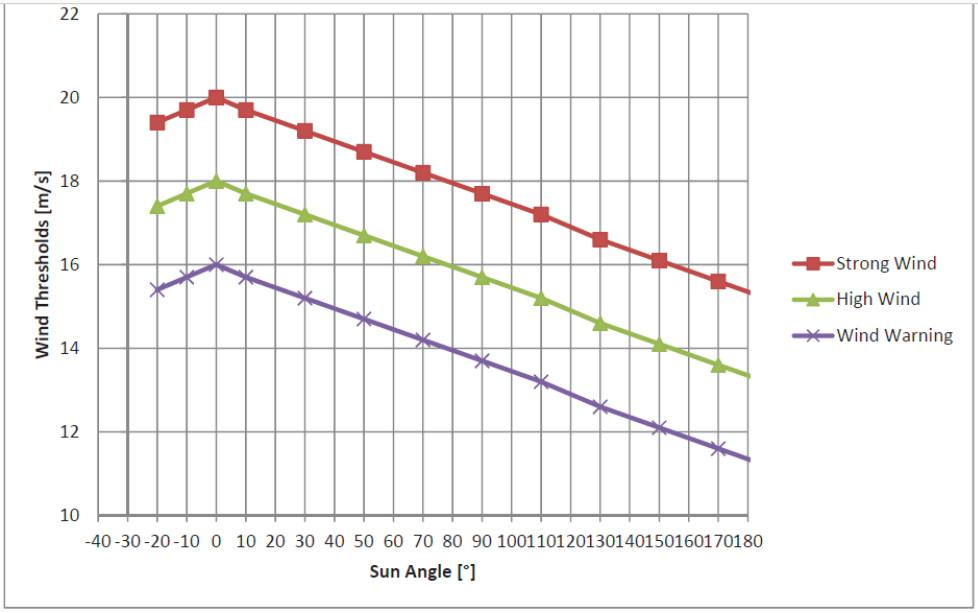


Figure 3.4: Wind Alarm Conditions (Cabrerizo, 2017)

### 3.3.1 Solar Field Sizing

Solar field sizing is usually determined during the design phase of a power plant in order to achieve the best possible output, while still abiding to regulations, policies and limitations. Solar field sizing adjustments are usually manipulated with the aid of a solar multiple (SM) and the 95th percentile of the DNI values to find the optimum solution. This percentile excludes the DNI values equal to zero, in order to account for small solar field areas in locations that experience high DNI levels, the opposite is also true. This simulation model however, is based on an existing power plant and the solar field sizing is therefore fixed and not designed. Table 3.1 summarises the sizing of the Andasol 3 solar field modelled. Further solar field parameters are represented in Appendix A, which is the Andasol 3 data sheet summary.

Table 3.1: Solar Field Sizing

| **Solar Field Sizing** | **Value** | **Unit** |
|---|---|---|
| Total Effective Aperture Area | 497 040 | $m^2$ |
| Collector Length | 148.4 | m |
| Collector Aperture | 5.77 | m |
| Collectors per Loop | 4 | - |
| Number of Loops | 152 | - |
| Row Spacing | 17.2 | m |

### 3.3.2 Solar Time and Geometry

The first modelling calculations are based on the solar time ($t_s$) and solar geometry. This requires the selected site location, otherwise known as the geographical data. Solar time is calculated using the selected site's geographical data, namely, latitude and longitude values which is given as 37.21 °N and 3.07 °W respectively (global energy observatory [Online]). The method described by Stine and Geyer makes use of the Local Clock Time ($LCT$) in 24-hour format, where the Equation of Time ($EOT$), Longitude correction ($LC$) and daylight saving modifier ($DS$) is represented in the solar time function (Stine and Geyer, 2001).

$$t_s = LCT + \frac{EOT}{60} - LC - DS \tag{3.1}$$

The ($EOT$) is calculated in minutes by making use of Equation 3.2, where (n) represents the number of days into a leap year cycle and the coefficients ($A_k$) and ($B_k$) are shown in Table 3.2 (Stine and Geyer, 2001).

$$EOT = 60 \sum_{k=0}^{5} \left[ A_k cos\left(\frac{360kn}{365.25}\right) + B_k sin\left(\frac{360kn}{365.25}\right) \right] \tag{3.2}$$

Table 3.2: Coefficients for EOT

| k | $A_k$ | $B_k$ |
|---|---|---|
| 0 | $2.0870(10^{-4})$ | 0 |
| 1 | $9.2869(10^{-3})$ | $-1.2229(10^{-1})$ |
| 2 | $-5.2258(10^{-2})$ | $-1.5698(10^{-1})$ |
| 3 | $-1.3077(10^{-3})$ | $-5.1602(10^{-3})$ |
| 4 | $-2.1867(10^{-3})$ | $-2.9823(10^{-3})$ |
| 5 | $-1.5100(10^{-4})$ | $-2.3463(10^{-4})$ |

The last two solar time parameters needed are calculated using Equation 3.3 and 3.4 respectfully. $(LC)$ is shown in Equation 3.3, as a correction modifier between the site location longitude $(L)$ and the Time Zone Meridian $(TZM)$ nearest that site location.

$$LC = \frac{(L - TZM)}{15} \tag{3.3}$$

The variable $(DS)$ is a daylight saving parameter, which conditions the solar time equation in a way that adjusts for daylight savings in countries that implement such a time shift. Regarding the developed model of Andasol 3 and the input data during the 2016 year, it is noted that daylight saving was from 27 March 2016 until 30 October 2016.

$$DS = \begin{cases} 1, & \text{when Daylight savings is implemented} \\ 0, & \text{if No daylight saving is implemented} \end{cases} \tag{3.4}$$

Once the solar time is calculated, the next step is to determine the solar geometry. The solar geometry includes geometry such as the zenith angle $(\theta_z)$, azimuth angle $(Az)$ and the incidence angle $(\theta_i)$.

Firstly, the zenith angle is defined as shown in Equation 3.5,

$$\theta_z = 90 - \alpha \tag{3.5}$$

Obtaining the zenith angle requires three other angles, namely the altitude angle $(\alpha)$, hour angle $(\omega)$ and the declination angle $(\delta)$. The Altitude angle $(\alpha)$ is defined by Equation 3.6 (Stine and Geyer, 2001).

$$\alpha = sin^{-1}(sin(\delta)sin(\phi) + \cos(\delta)\cos(\omega)\cos(\phi)) \tag{3.6}$$

Equation 3.6 contains the declination angle ($\delta$), the latitude angle ($\phi$) and the hour angle ($\omega$) parameters. The declination angle ($\delta$) is described in Equation 3.7 as a function of the day number ($N$).

$$\delta = sin^{-1}(0.39795\cos(0.98563(N - 173))) \tag{3.7}$$

Where the hour angle ($\omega$) is described as a function of the solar time ($t_s$), refer to Equation 3.8.

$$\omega = 15(t_s - 12) \tag{3.8}$$

Secondly, the azimuth angle ($Az$) is defined as shown in Equation 3.9, conditioned by Equation 3.10 measured in degrees.
If:

$$\begin{cases} \cos(\omega) >= \frac{\tan(\delta)}{\tan(\phi)}, & \text{then, } Az = 180 - A' \\ \cos(\omega) < \frac{\tan(\delta)}{\tan(\phi)}, & \text{then, } Az = 360 + A' \end{cases} \tag{3.9}$$

where,

$$A' = sin^{-1}\frac{(-\cos(\delta)\sin(\omega))}{\cos(\alpha)} \tag{3.10}$$

Thirdly, the incidence angle ($\theta_i$) is defined by Equation 3.11, where the field is orientated in a North-South direction.

$$\theta_i = \arccos[\sqrt{1 - (\cos(\alpha)^2)(\cos(A)^2)}] \tag{3.11}$$

### 3.3.3 Solar Collector

The solar collector is an assembly of parabolic shaped mirrors, which has the benefit of concentrating solar energy to a receiver tube at it's focal line. Equation 3.12 defines the calculation used to determine the amount of concentrated radiation energy incident on the receiver tubes. The energy incident on the receiver tubes are dependant on the available Direct Normal Irradiance ($DNI$) at the site location, cosine of the incidence angle ($\cos\theta_i$), optical efficiency ($\eta_{optical}$) and the Incident Angel Modifier ($IAM$). These parameters are described in more detail following Equation 3.12 and are adapted from research completed by I.V. Poole during 2016 (Poole, 2016).

$$\dot{q}_{incident} = DNI\cos\theta_i\eta_{optical}IAM(\theta_i) \tag{3.12}$$

The incidence angle describes the angle between the solar collector aperture normal and the incoming solar radiation. Figure 3.5 shows the position of the incidence angle with respect to the collector and receiver tube.

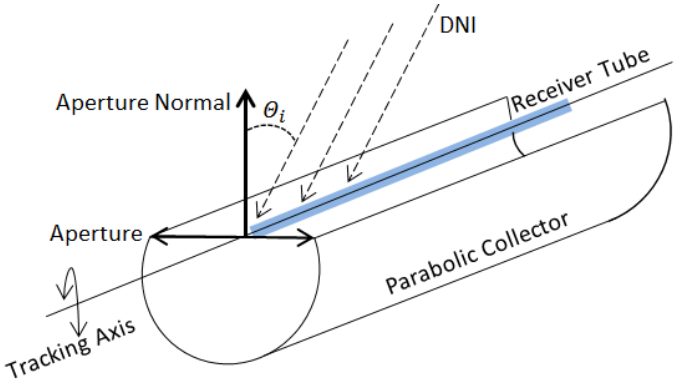


Figure 3.5: Incidence Angle

The model makes use of the Andasol 3 data sheet as seen in Appendix A, which describes the optical efficiency of the power plant to be 78 %. Equation 3.13 shows that the optical efficiency is a combination of the collector efficiency (Equation 3.14) and the receiver efficiency (Equation 3.16).

$$\eta_{optical} = (\eta_{Col})(\eta_{Rec}) \tag{3.13}$$

The optical efficiency relating to the collector ($\eta_{Col}$) is determined by multiplying each parameter given in Table 3.3 with one another:

Table 3.3: Collector Optical Efficiency

| **Collector Efficiency** | **Variable** | **Percentage Value [%]** |
|---|---|---|
| Geometry | $\gamma_0$ | 97.00 |
| Reflectance | $\rho_0$ | 94.50 |
| Cleanliness | $cf$ | 98.00 |
| Tracking | $\gamma_{Tracking}$ | 99.00 |

This results in the following equation:

$$\eta_{Col} = (\gamma_0)(\rho_0)(cf)(\gamma_{Tracking}) \tag{3.14}$$

The Indecent Angle Modifier (IAM) is calculated using Equation 3.15 (Padilla, 2011) and is a necessary parameter when considering PTPP modelling. This factor accounts for losses associated with the solar position. This includes

collector aperture foreshortening, glass envelope transmittance and selective surface absorption.

$$IAM = 1 - 5.25097(10)^{-4}\frac{(\theta_i)}{\cos(\theta_i)} - 2.859621(10)^{-5}\frac{(\theta_i)^2}{\cos(\theta_i)} \tag{3.15}$$

### 3.3.4 Receiver Tube

The receiver tube is made up of an evacuated glass tube encasing a stainless steel absorber tube. The absorber tube is the piping tube that allows thermal radiation to be transferred to the HTF (synthetic VP-1 thermal oil). The stainless steel absorber tube is coated with a spectrally selective material that increases absorptivity and reduces the amount of radiation energy emitted. Figure 3.6 is a simplified one-dimensional steady-state energy flow schematic, that summarises the energy flow at the receiver tube.

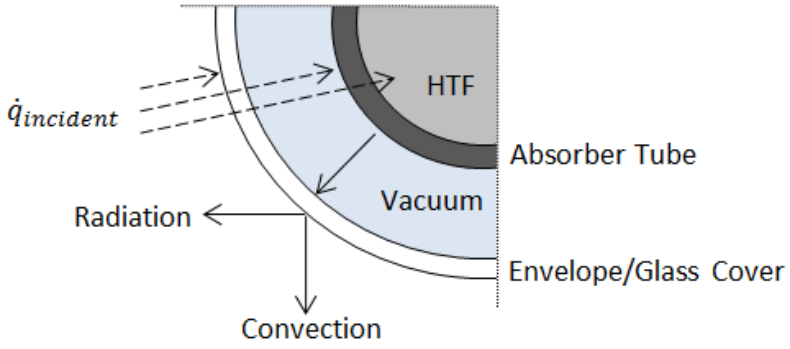


Figure 3.6: Energy Diagram of the Receiver Tube

The total receiver efficiency as shown in Equation 3.16 is a product of the receiver optical efficiencies described in Table 3.4. The Schott receiver tube is the tube of choice at Andasol 3 and has the following properties.

Table 3.4: Receiver Optical Efficiency

| **Receiver Efficiency** | **Variable** | **Percentage Value [%]** |
|---|---|---|
| Bellow | $\eta_{Bellow}$ | 98.00 |
| Clean factor | $cf_{rec}$ | 98.00 |
| Transmissivity | $\tau_{glass}$ | 96.00 |
| Absorptivity | $\alpha_{rec}$ | 95.00 |

$$\eta_{Rec} = (\eta_{Bellow})(cf_{rec})(\tau_{glass})(\alpha_{rec}) \tag{3.16}$$

Equation 3.16 is an adapted formula obtained from Wagner and Gilman (2011), which includes the assumption that the stainless steel absorber has a high level of conductivity, as well as a large heat convection coefficient, which ensures that all the solar radiation is absorbed. It is essential to consider the losses associated with the receiver tube and this is accomplished by taking into account the manufacturer's heat loss curve where the heat loss in these evacuated receivers is radiation dominant and therefore more dependent on the absolute absorber temperature than the difference between absorber and ambient temperatures. In brief, the uncertainty relating to heat loss associated with Equation 3.17 is $\pm 10$ W/m (Burkholder and Kutscher, 2009).

$$\dot{q}_{Rec,Loss} = (0.141)T_{abs} + (6.48(10^{-9}))T_{abs}^4 \tag{3.17}$$

The receiver tube heat loss is mainly dependant on the absorber tube temperature, not losses relating to wind and ambient temperature. Equation 3.17 defines the heat loss curve for the Andasol 3 receiver tubes.

### 3.3.5 Nodal Energy Balance

Each Solar Collector Assembly (SCA) consists of a single, common tracking system that drives a number of parabolic collectors and their receivers in series. Each SCA is used to incrementally heat the HTF to the design temperature and is therefore used as the lowest level of discretisation in this model. Each individual SCA is treated as an independent node within the loop. This allows for each of the SCA's to impact performance separately.

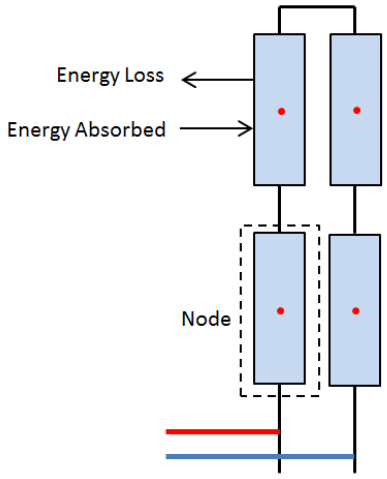


Figure 3.7: SCA node

Typically, when modelling a receiver in steady-state, the temperature rise across the node is determined and this is done by considering the absorbed energy, mass flow rate of the HTF through the receiver and the specific heat of the HTF. This is generally expressed as an energy balance for a specific node (i) as presented in Equation 3.18.

$$\Delta T_i = T_{out,i} - T_{in,i} = \frac{\dot{q}_{abs}}{\dot{m}_{htf} c_{htf}} \tag{3.18}$$

This is not the case for PTPP's as thermal inertia can impact the performance of the model to the extent that the steady-state model is insufficient. It is essential to include the thermal mass of the HTF in the headers and receiver pipes, as this will include transient terms. Thus, the energy balance for a single SCA is represented in Figure 3.8, where ($\dot{q}_{abs}$) includes the thermal losses as described in Equation 3.17.

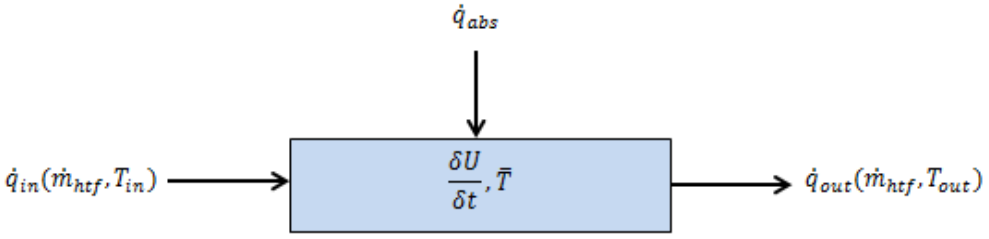


Figure 3.8: Energy Balance for a SCA Node

This energy balance is described by an inlet flow, internal energy, absorbed energy and outlet flow. The mass flow rate ($\dot{m}_{htf}$) across the closed volume boundary is constant, therefore the ($T_{in}$) and ($T_{out}$) values give the nodal average temperature ($\bar{T}$). This is assumed to be linear.

To represent the internal energy change of the node as a function of time, the term ($\frac{\partial U}{\partial t}$) is used and further defined as:

$$\frac{\partial U}{\partial t} = (mc_{htf} + (mc)_{bal,SCA} L) \frac{\partial T}{\partial t} \tag{3.19}$$

Referring to Equation 3.19, ($m$) is the mass of the HTF in the node, ($c_{htf}$) is the specific heat of the HTF and the ($L$) represents the length of the SCA. The HTF is a eutectic mixture of 73.5 % Diphenyl and 26.5 % Diphenyl Oxide, otherwise known as Therminol VP-1. The properties and equations associated with this medium are described in Appendix B.1 (Solutia, 2016).

In order to account for thermal mass in the piping, insulation and other SCA

components that thermally cycle with the HTF, an additional term is introduced namely the thermal inertia term ($(mc)_{bal,SCA}$). This term is diverse in that it eliminates the need for specific knowledge of either the exact specific heat or mass, but it still allows the user/operator to account for the inertia effect. Additionally, the ($(mc)_{bal,SCA}L$) term models the thermal inertia per meter of collector length required to raise the node temperature one degree Kelvin.

When considering a mathematical formulation, both the material properties and the HTF are assumed to be constant. However, this is not the case when system performance is evaluated. These parameters are evaluated as a function of temperature and pressure. The total energy balance in the control volume is defined as seen in Equation 3.20:

$$\dot{q}_{in} + \dot{q}_{abs} = \frac{\partial U}{\partial t} + \dot{q}_{out} \tag{3.20}$$

Consider the inlet and outlet heat flow without the addition of heat ($\dot{q}_{abs}$):

$$\dot{q}_{in} - \dot{q}_{out} = \dot{m}_{htf} c_{htf}(T_{in} - T_{out}) = 2\dot{m}_{htf} c_{htf}(T_{in} - \overline{T}) \tag{3.21}$$

Making use of Equation 3.21, Equation 3.19 and solving for the first differential, results in:

$$\frac{\partial \overline{T}}{\partial t} = \frac{2\dot{m}_{htf} c_{htf}(T_{in} - \overline{T}) + \dot{q}_{abs}}{mc_{htf} + (mc)_{bal,SCA}} \tag{3.22}$$

Equation 3.22 is a linear first order differential equation having the general solution described in Equation 3.23. This assumes constant properties.

$$\overline{T} = \frac{\dot{q}_{abs}}{2\dot{m}_{htf} c_{htf}} + C_1 \exp\left[-\frac{2\dot{m}_{htf} c_{htf}}{mc_{htf} + (mc)_{bal,SCA}}\Delta t\right] + T_{in} \tag{3.23}$$

With an unknown constant value ($C_1$), which can be determined using a known boundary condition. This boundary condition is defined as the average nodal temperature value ($\overline{T} = \overline{T}_0$) at t=0. ($\overline{T}_0$) is the temperature at the end of the previous time step. The average temperature is described assuming a linear temperature profile ($\overline{T} = \frac{T_{out}+T_{in}}{2}$). Therefore, solving for ($C_1$):

$$\overline{T} = \overline{T}|_{t=0} = \frac{\dot{q}_{abs}}{2\dot{m}_{htf} c_{htf}} + C_1 \exp(0) + T_{in} \tag{3.24}$$

$$C_1 = \overline{T}_0 - \frac{\dot{q}_{abs}}{2\dot{m}_{htf} c_{htf}} - T_{in} \tag{3.25}$$

In order to find the outlet temperature ($T_{out,i}$) for each SCA, the constant ($C_1$) is substituted into the general solution which gives:

$$T_{out,i} = \frac{\dot{q}_{abs,i}}{\dot{m}_{htf} c_{htf,i}} + T_{in,i} + 2\left(\overline{T}_{0,i} - \frac{\dot{q}_{abs,i}}{2\dot{m}_{htf} c_{htf,i}} - T_{in,i}\right) \exp\left[-\frac{2\dot{m}_{htf} c_{htf,i} \Delta t}{m_i c_{htf} + (mc)_{i,bal,SCA} L_i}\right] \tag{3.26}$$

Note that Equation 3.26 is the equation used in the simulation model which determines the temperature increase in the solar field and is applied to each control volume node (i) in the loop. This outlet temperature is determined from the net energy absorbed by the receiver tube ($\dot{q}_{abs}$), mass flow rate of the HTF ($m_{htf}$), thermal capacity of the HTF ($c_{htf}$), time step ($\Delta t$), outlet temperature of the previous node ($T_{in,i}$) and the mass of the HTF ($m$).

The mass of the HTF in each SCA is a function of the average temperature ($\overline{T}_0$), volume of the receiver tube ($V_{rec,i}$) and the HTF density ($\rho$).

$$m = (\overline{T}_0)(V_{rec,i})(\rho) \tag{3.27}$$

Equation 3.26 determines the outlet temperature for each node and is dependent on the node temperature from the previous time step as well as the inlet temperature of the previous node. The temperature of the node at the previous time step is stored and the inlet temperature is set equal to the outlet temperature of the previous node for each SCA node. However, this is not true for the very first SCA node and therefore steps are put into place to account for the first node not having any previous values to work from. The model is initialised with an estimate of the first inlet temperature and thereafter allows the rest of the simulation to run though each loop.

In addition to each SCA being modelled as a separate control volume to determine the output temperature of the solar field, there are two other piping components (the hot and cold header pipes) that are modelled using a similar logic as explained previously.

$$T_{header,out} = T_{h,0} \exp\left[-\frac{\dot{m}\Delta t}{\overline{V}_h \rho_h}\right] + T_{in} \tag{3.28}$$

Equation 3.28 describes the outlet temperature for both the cold and hot header pipes. In the case of the cold tank, ($T_{in}$) represents the temperature entering into the solar field and ($T_{out}$) represents the temperature that enters

the first SCA in the loop. In the case of the hot tank, ($T_{in}$) represents the temperature from the last SCA in the loop and ($T_{out}$) is the temperature that either flows to the storage system or is used directly in the power block.

The HTF mass of each node is calculated and controlled by making use of a Proportional, Integral and Differential (PID) control system. The PID controller forces the mass flow rate to change in response to the previous outlet temperature of the last SCA in the loop. This allows for a change in mass flow rate, which aims to achieve the desired temperature of 393 ℃ in the fastest possible time without overshooting the desired temperature.

## 3.4 Thermal Energy Storage System

The thermal energy storage system is designed to be a control system and does not rely on many equations. Rather, it relies on logic, set-point conditions and operational strategy that matches the strategy implemented by Andasol 3. Energy is either stored or discharged from the storage tanks depending on the operating philosophy of the power plant. Chapter 3.6.2 refers to the logic implemented in the simulation model. Also, refer to Appendix C.2 for the flow diagram describing the logic. The fluid used in the two-tank indirect storage tanks is molten salt, otherwise known as solar salt and has the properties described in Appendix B.2. (SerranoLopeza *et al.*, 2013). There are associated losses incurred during storage, but due to the high thermal capacity of the molten salt, these losses are kept to a minimum.

## 3.5 Power Block

The electrical power generated is calculated by making use of the thermal energy sent to the power block from the solar field and/or storage system and the power cycle efficiency. The power is modified according to a HTF temperature modification parameter ($\lambda_{T,HTF}$), refer to Equation 3.29 (Wagner and Gilman, 2011).

$$P_{el,Gross} = P_{th,HTFin}(\eta_{th-el})(\lambda_{T,HTF}) \tag{3.29}$$

Thermal energy ($P_{th,HTFin}$) is sent to the power block either directly from the solar field or from the thermal storage system. The control system determines how much energy is available from the thermal storage and solar field and makes adjustments in order to provide the power block with the required thermal energy. The thermal-to-electrical efficiency ($\eta_{th-el}$), as well as the efficiency modifier, ($\lambda_{T,HTF}$) are adjusted from performance data. The thermal-

to-electrical efficiency is represented in Figure 3.9 and changes depending on the HTF mass flow rate in the power block.

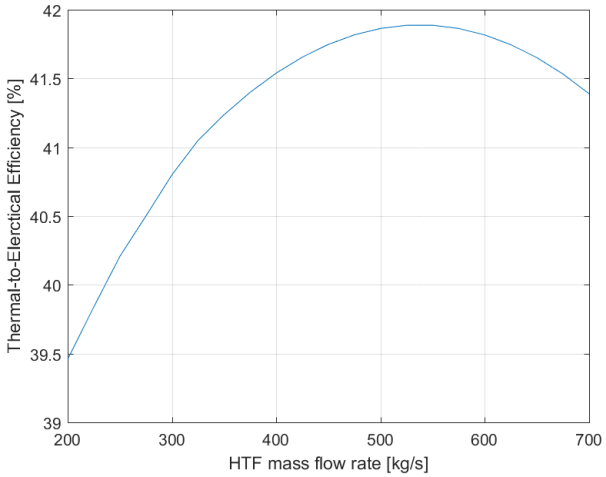


Figure 3.9: Thermal-to-Electrical Efficiency

During power cycle start-up (approximately 30 minutes), the mass flow rate to the power block steam cycle is reduced. Therefore reducing the power block efficiency by $\pm 2$ %. The HTF inlet temperature efficiency modifier ($\lambda_{T,HTF}$) has a near linear effect on the power block efficiency, refer to Figure 3.10. The relationship shows that with a low temperature entering the power cycle, the steam cycle has a low efficiency.

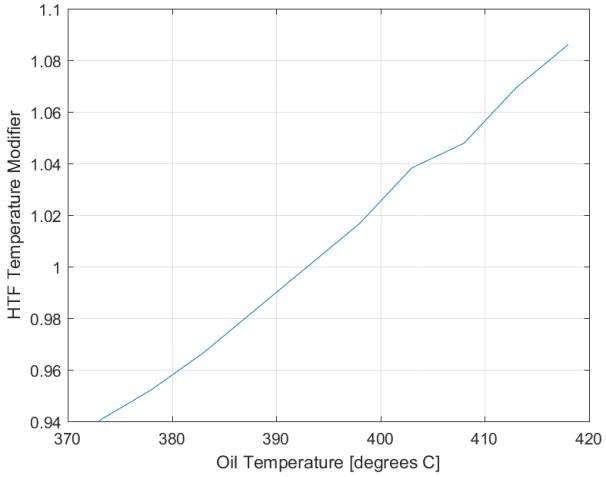


Figure 3.10: HTF Temperature Modifier

The net electricity generation is defined as the gross electric generation less the parasitic losses, refer to Equation 3.30.

$$P_{el,Net} = P_{el,Gross} - P_{Parasitics} \tag{3.30}$$

The Rankine cycle represents the steam cycle in the power block and thus stipulates that the power block efficiency increases with a high inlet temperature and lower outlet temperature. This temperature difference is between the steam condensate temperature and the wet bulb temperature, as the power plant makes use of a wet cooling systems to remove heat through evaporation. Thus the cold reservoir temperature is driven by the wet-bulb temperature. The wet cooled effect is described and accounted for in the parasitic losses, shown in Equation 3.48.

### 3.5.1 Parasitic Consumption

Generally, PTPP's experience a substantial amount of parasitic losses. The model accounts for these parasitic losses in the form of solar field HTF pump losses, steam cycle HTF pump losses, wet cooled tower, feed water pumps for the steam cycle, trace heating in piping as well as a fixed auxiliary load to run the remainder of the power plant (such as office computers and lighting).

The solar field HTF pump pressure drop makes up a large portion of the parasitic consumption and is therefore modelled in detail. The pressure required by the main HTF pumps in the solar field has a direct translation to the auxiliary consumption of the power plant. The pressure drop through the solar field piping is determined by making use of Equation 3.31.

$$\Delta P_{SF} = \Delta P_{Loop} + \Delta P_{Runner} + \sum_{k=1}^{n} \Delta P_{Header}(i) + \Delta P_{Other,Components} \tag{3.31}$$

Each pressure drop term in Equation 3.31 is calculated using the pressure drop equation for a round pipe, Equation 3.32. Hence, Equation 3.32 to Equation 3.37 is used as the generic calculations in determining influence of each pipe component in terms of their respective pressure drop over the solar field. The piping components considered for the calculations are the runners, headers and receiver tube piping in each loop.

$$\Delta P_{Pipe} = \frac{f_{Pipe} V_{Pipe}^2 \rho_{Pipe} L_{Pipe}}{2 D_{Pipe}} \tag{3.32}$$

The flow through the solar field piping is fully developed turbulent flow as the Reynolds number is within the range $3(10)^4 < \mathrm{Re} < 2(10)^6$.

$$RE_{Pipe} = \frac{\rho_{Pipe} V_{Pipe} D_{Pipe}}{\mu_{HTF}} \tag{3.33}$$

McAdams recommends the following friction factor for fully developed turbulent flow in a smooth pipe (Massoud, 2005):

$$f_{Pipe} = 0.184 Re_{Pipe}^{-0.2} \tag{3.34}$$

The remaining variables and parameters contained in Equation 3.32 are determined as follows:

$$V_{Pipe} = \frac{Q_{Pipe}}{A_{Pipe}} \tag{3.35}$$

$$A_{Pipe} = \frac{\Pi D_{Pipe}}{4} \tag{3.36}$$

$$Q_{Pipe} = \frac{\dot{m}_{Pipe}}{\rho_{HTF}} \tag{3.37}$$

**Loop Pipes:**
The design mass flow rate through each loop is described using Equation 3.38.

$$\dot{m}_{Loop} = \frac{\dot{m}_{Dp}}{N_{Loops}} \tag{3.38}$$

Where design point thermal power is used to determine the mass flow rate required by the main HTF pumps. Also, the average heat capacity of the VP-1 oil and the total temperature change over the solar field influences the design point mass flow rate.

$$\dot{m}_{Dp} = \frac{P_{th,SF}}{c_p(\bar{T})(T_{Out} - T_{In})} \tag{3.39}$$

The loop diameter in the solar field are 70 mm pipes.

$$D_{Loops} = 70\ mm \tag{3.40}$$

**Runner Pipes:**
The solar field piping layout consists of two runner pipes. One runner pipe running North and the other running South. The mass flow rate in the runner pipe is calculated as given in Equation

$$\dot{m}_{Runner} = \frac{\dot{m}_{Dp}}{2} \tag{3.41}$$

With the use of 3.41, the runner diameter is determined.

$$D_{Runner} = \sqrt{\frac{4\dot{m}_{Runner}}{\rho_{HTF} V_{Max} \Pi}} \tag{3.42}$$

**Header Pipes:**
Four header pipes, running from East to West, are represented in the solar field. The header pipes transfer the thermal oil to each loop. At each loop stemming from the header pipes, the header pipe diameter is re-calculated in order to maintain the maximum HTF velocity. Therefore, the header pipe has a reducing diameter along its length. Each header pipe distributes the fluid to a quarter of the solar field (North-East, South-East, South-West, North-West).

The initial flow rate in the header pipe is one quarter of the design mass flow rate and subsequently reduces in the remaining header sections. The number of header sections is determined using Equation 3.43.

$$N_{Header,Sections} = \frac{N_{Loops}}{8} \tag{3.43}$$

Therefore, the mass flow rate in each header section is:

$$\dot{m}_{Header,Sections}(i) = \frac{\dot{m}_{Dp}}{4} - \left[ \sum_{k=1}^{N_{Header,Sections}} \frac{\dot{m}_{Dp} k}{4 N_{Header,Sections}} \right] \tag{3.44}$$

The header diameter for each section is then computed as:

$$D_{Header,Sections}(i) = \sqrt{\frac{4\dot{m}_{Header,Sections}(i)}{\rho_{HTF} V_{Max} \Pi}} \tag{3.45}$$

**Other Components**:
The other pressure drops occur in the flexible hosing and valves. The same method is used to determine the pressure drop, Equation 3.32 to Equation 3.37. Therefore, the energy used to pump the fluid through the solar field is determined with Equation 3.46 by making use of look-up tables at each time step.

$$P_{e-Pump} = \frac{\Delta P}{\eta_p} \frac{\dot{m}_{SF}}{\rho_{HTF}} \tag{3.46}$$

The balance of the parasitic losses are constants, assumptions and coefficients developed by NREL SAM methodology (Wagner and Gilman, 2011). The energy used to power the HTF pumps to the power block is calculated using the mass flow rate and a pump cycling coefficient ($\lambda_{CyclingPumps} = 1.15\ kJ/kg$).

$$P_{el,CyclingPumps} = (\dot{m}_{HTF})(\lambda_{CyclingPumps}) \tag{3.47}$$

The parasitic consumption relating to the feed water pumps and the wet cooled tower is also adjusted due to the mass flow rate to the power block and a wet cooled tower coefficient ($\lambda_{WetCooled} = 4.2\ kJ/kg$). This is done as it gives an indication of the power cycle's level of operation.

$$P_{el,WetCooled} = (\dot{m}_{HTF})(\lambda_{WetCooled}) \tag{3.48}$$

Other miscellaneous equipment such as lighting, powering of offices and worker facilities result in a fixed parasitic load of $\pm 0.55$ $MW_{el}$.

## 3.6 Control Systems

The power plant control system is developed using the built-in finite state machine tool contained in the MATLAB/Simulink software. This tool represents an event-driven system, allowing logical decisions to be implemented in response to certain conditions or limitations. The state-flow chart graphically represents the previously mentioned finite state machine in the Simulink environment. It operates by performing the action until a parameter defining change is set true, then a transition occurs between one state and another. The parameters defining these transitions are *time of day* and *conditional set-points* related to either the solar field temperature output, energy values or limitations such as boundary conditions. The operating modes are predefined states correlating to real modes of operation in a PTPP (Silva, 2013).

### 3.6.1 Solar Field Control System

There are three main modes of operation related to the solar field operation.

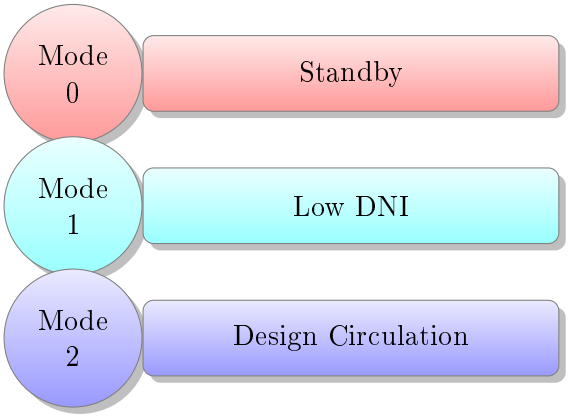


Figure 3.11: Control Modes for Solar Field Operation

Appendix C.1 describes the logic implemented, where Figure 3.11 defines the control modes for solar field operation.

- **Solar Field Mode 0: Standby**
  This mode becomes operational during night time and other times during no DNI. It is a minimum mass flow rate mode, which maintains circulation in the solar field. In addition, during cases where the overnight temperature drop forces the start-up in the power block to be longer than usual, a Liquefied Natural Gas (LNG) heater is implemented ensuring that the solar field temperature remains above its minimum temperature. This prevents lengthy start-ups allowing the power plant the opportunity to start electricity production as soon as possible without many losses. This mode of using external gas heaters usually occurs during the winter months. In order to start operation, a set condition is used to determine the time of day according to the zenith angle. A controller then signals the next operation mode (Mode 1: Low DNI) and the plant begins to run.

- **Solar Field Mode 1: Low DNI**
  Operations are initialised, which enables preheating and preparation of electricity generation within the power block. The solar field mass flow rate increases in order to achieve the desired 393 ℃ solar field output temperature. During this mode there is insufficient DNI to meet solar field design output temperature. However, the model does attempt to reach the temperature during this mode and if the design temperature is reached then the next mode (Mode 2: Design Circulation) is activated. Alternatively, If the time of day reaches such a time that the elevation angle is not sufficient for the solar field to operate in it's current mode, then the previous mode (Mode 0: Standby) is activated.

- **Solar Field Mode 2: Design Circulation**
  This is the desired operation of the power plant. The HTF is transferred through each SCA loop to reach the desired solar field outlet temperature of 393 ℃ and maintain that design temperature by means of a proportional control feedback system. The mass flow rate is adjusted in order to achieve this design temperature and is limited by approximately 20 % more mass flow rate than the design HTF mass flow rate. The controller limits the HTF form reaching 400 ℃. This is due to the changes in the thermal oil properties and molecular degradation. In the case of low DNI input to the power plant, the control system responds by reducing the mass flow rate when the design temperature is not being met and if the time of day still allows for operation, (mode 1: Low DNI) is then activated.

### 3.6.2 Thermal Energy Storage Control System

Molten salt is the storage HTF and is pumped from the one storage tank to the other. This is dependant on the operations implemented and described in Appendix C.2. These operations are summarised in Figure 3.12, which represent the four main thermal storage operations (Stine and Geyer, 2001). In this model, the thermal losses during the heating of an empty storage tank are neglected and the minimum temperature for the salt is 260 ℃. It is necessary to determine the full capacity of the storage system and this is done by first calculating the operating point of the power block as shown in Equation 3.49. The variable ($Pe_{PB}$) is the plant size in terms of its electrical generation. This model makes use of a 50 MW plant size with a turbine design point efficiency ($\eta_{PB}$) of 41.5 %.

$$Pth_{PB,dp} = \frac{Pe_{PB}}{\eta_{PB}} \tag{3.49}$$

Equation 3.50 describes the calculation used to determine the full capacity of the storage system.

$$E_{Capacity,Full} = (3600)(FLH)(Pth_{PB,dp}) \tag{3.50}$$

The full capacity of the storage system is used as a restricting condition, which limits the amount of heat energy allowed to be stored at any given time. In this calculation, the Full Load Hours ($FLH$) for the Andasol 3 power plant is 7.5 hours.

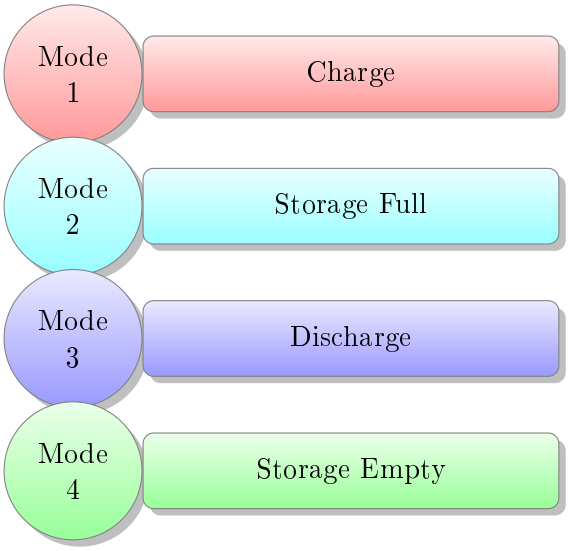


Figure 3.12: Control Modes for Thermal Storage Operations

- **Storage Mode 1 (Charge):**
  The conditions for this storage operation mode includes excess energy (more energy than the design point energy value) being captured by the solar field and the energy capacity of the thermal storage system being less than full capacity. Thermal energy is stored during this mode of operation. The VP-1 thermal oil flows through the salt-to-oil heat exchanger and heats up the molten salt flowing from the cold tank to the hot tank. This process charges the TESS with the excess solar field heat. The amount of energy stored is determined through the energy equation for the molten salt medium.

$$\dot{q}_{Stored} = (\dot{m}_{salt})(C_{p,salt})(\Delta T) \tag{3.51}$$

  The mass flow rate of the salt ($\dot{m}_{salt}$) is calculated by means of a PID control system dependant on the energy difference between the solar field and the design point energy level. The heat capacity of the molten salt ($C_{p,salt}$) is determined from Equation B.5. The temperature difference ($\Delta T$), is the molten salt temperature increase due heat exchanged from the high temperature VP-1.

- **Storage Mode 2 (Storage Full):**
  The conditions for this storage operation mode includes excess energy (more energy than the design point energy value) being captured by the solar field and the energy capacity of the thermal storage system being equal than full capacity. The thermal storage system at full capacity encounters a heat loss factor of 0.1 %/hour and no additional heat being stored. It is from a full tank that the only next operational step is to discharge the energy when desired by the power plant or on demand.

- **Storage Mode 3 (Discharge):**
  The conditions for this storage operation mode includes less energy being captured by the solar field than the design point energy level. In addition, the stored energy capacity of the thermal energy storage system must be greater than an empty storage tank capacity level and limited to a full thermal storage capacity. This mode of operation is activated when the amount of energy from the solar field does not reach the desired operating energy levels to run the power plant. During this mode the thermal oil flows in the opposite direction through the salt-to-oil heat exchanger and is heated by the molten salt. In this case the molten salt is flowing from the hot tank to the cold tank. The heat from hot storage tank is combined with the energy from the thermal oil from the solar field. This combination of energy when discharging gives the advantage of providing energy on demand or when desired. The discharge of the stored energy is adjusted to being either a full discharge operation or a

partial discharge operation. A full discharge operation is where there is no additional thermal energy from the solar field and the power plant is able to operate at its full 7.5 hour full load capacity without sunshine. During a partial discharge operation, the power plant can operate for a duration longer than the full load capacity, just at a lower electricity generation rate. This discharge rate is decided by the operators of the power plant. The discharge energy is calculated using the same principle as 3.51, except the energy is leaving the storage tanks.

$$\dot{q}_{Discharge} = (f_{Partial,Operation})(\dot{m}_{salt})(C_{p,salt})(\Delta T) \tag{3.52}$$

Equation 3.52 has an additional parameter ($f_{partial,operation}$), which adjusts for the partial discharge capabilities of the power plant.

- **Storage Mode 4 (Storage Empty):**
  The conditions for this storage operation mode includes less energy being captured by the solar field than the design point level and the energy capacity of the thermal storage system is equal to zero, which is an empty storage tank. No thermal energy is stored during this mode and the energy capacity remains at zero until the charging cycle begins again.

### 3.6.3 Power Block Control System

The power block control system defines the steam cycle operational strategy for the PTPP. There are four modes of operation describing the steam cycle.

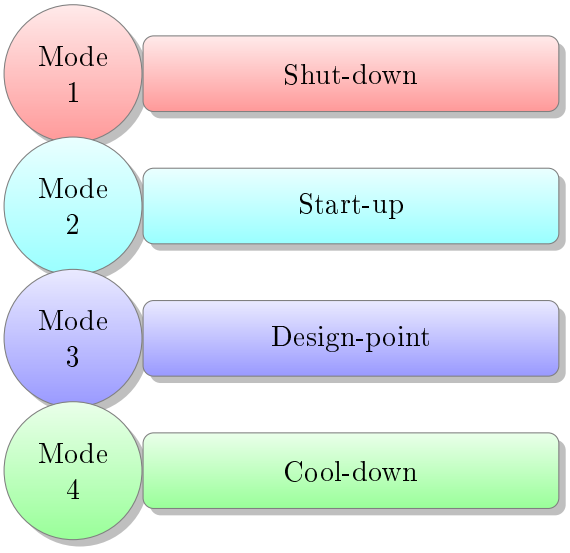


Figure 3.13: Control Modes for Power Block Operations

These modes ar are conditioned by the time of day and solar resource available during that time period. Appendix C.3 shows a flow diagram of the logic described in Figure 3.13.

- **Power Block Mode 1: Shut-down**
  This is a state where no electricity is produced and where the steam cycle is in a complete shut-down operation mode. There is no steam mass flow rate allowing the turbine to rotate and generate electricity. A steam cycle minimum mass flow rate and the set-point depicting the time of day, are the conditions needed to be satisfied in order to enter into the next power block control mode, (Mode 2: Start-up).

- **Power Block Mode 2: Start-up**
  To resemble the start-up process experienced, the turbine is switched to half of the design capacity. In reality the turbine experiences thermal losses during a restart and is compensated for by setting the turbine to 50 % operation which accounts for the reheating of components, mass flow rate ramp-up and temperature increase in the solar field in order to operate at design point. A one hour start-up is implemented, thereafter the control logic enables the next mode (Power Block Mode 3). Alternatively, if the mass flow rate in the power block drops below the start-up mass flow rate then the previous mode (Power Block Mode 1) is enabled.

- **Power Block Mode 3: Design-point**
  The HTF is transferred at the design point mass flow rate ensuring a turbine operation of $\pm$100 %. The turbine is able to vary approximately 5 % to 10 % of it's design point capacity in order to meet the thermal design point. If there is insufficient energy to meet design point operations in the power block or the time of day exceeds the set-point criteria for that specific operation day, then Power Block Mode 4 is entered.

- **Power Block Mode 4: Cool-down**
  This operating mode begins ensuring the cool-down of the entire steam generating system. The cool-down period is set prior to the simulation run and is an estimate of the average time for a typical day experiencing a similar solar resource. The turbine is turned off during this operating mode. If the solar resource increases and the turbine has the capacity to restart, then the operation mode returns to Power Block Mode 3. If this is not the case, the operation mode that entered is Power Block Mode 1, where the operations are in shut-down mode.

The development of this control logic and strategy is driven by revenue and in turn power plant performance. The power block modes therefore describe efficiencies which allow for performance outputs that match the strategies defined by Andasol 3.

# Chapter 4

# Plant Model Validation

Validation of a simulation model gives credibility to the work done and assures that the model is functional and valid for design, evaluations, refinements, feasibility and optimisation. This chapter verifies the methodology and techniques used in the PTPP simulation and shows that the assumptions made are reasonable and applicable.

The model allows for any number of days to be simulated at the resolution desired by the user (but dependant on the available input data resolution). The resolution and time-step set by the user will determine the overall run time and resolution accuracy of the simulation output results. This study makes use of a 10 second time-step, which allows for a fast simulation run time with high resolution results for analysis and evaluation. Figures 4.1 to Figure 4.4 show the selected simulation days and therefore the x-axis shows the time in days and not in 10 second intervals which would make the x-axis difficult to read. The reason for this is to show how the model operates for consecutive days and not just one specific day. The simulation dates chosen are from 11 April 2016 to 16 April 2016, thus a six day simulation period. Additionally, data for a longer duration (01 June 2016 to 23 June 2016), thus a 23 day simulation period was also simulated in order to validate the model. These dates where chosen due to data availability from Andasol 3, during the development time of the model. The data represents good DNI days, average DNI days and volatile DNI days. This therefore shows how the model performs and functions under various weather conditions in order to achieve an accepted modelling error of below 10 % for monthly yield according to Guédez (Guédez, 2017). The 10 % modelling accuracy margin was chosen with reference to other parabolic trough simulation programs, such as a TRNSYS simulation for the SEGS VI power plant (Jones *et al.*, 2001). The simulation model generates performance plots and saves these results in separate files, making it convenient for the operator to find, identify and evaluate.

## 4.1 Simulation Model Operation

An investigation into the operation of the model indicates the performance of the model and what it is capable of achieving/calculating. Additionally, the level of detail and accuracy is investigated in this section. The simulation model operation will be shown in three sections, namely: *Solar Field - Energy to the HTF*, *Solar Field Outlet Temperature* and the *Storage Level*. These graphical representations are analysed and described to ensure a reliable and functional model.

### 4.1.1 Solar Field - Energy to the HTF:

The Direct Normal Irradiance (DNI) from the sun is converted into thermal energy in the HTF. Figure 4.1 shows how the DNI (blue graph) experiences losses from the mirror collector (orange graph) and then further at the receiver tube (yellow graph). The final loss in the solar field occurs from the receiver tube to the HTF (purple graph). This is approximately 5 ℃ loss due to the receiver tubes at the Andasol 3 power plant.

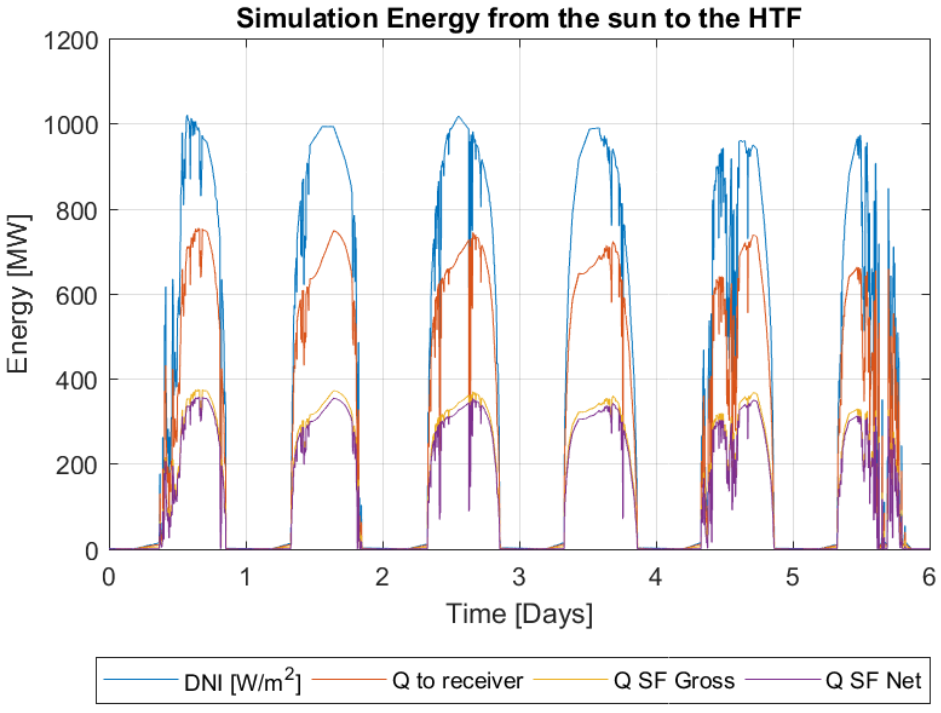


Figure 4.1: Simulation: Energy to the HTF (11-16 April 2016)

### 4.1.2 Solar Field Outlet Temperature:

Once the thermal energy is determined in the HTF, the temperature increase in each SCA is calculated by making use of the same methodology outlined in the System Advisor Model (SAM). This method is outlined in Chapter 3.3.5, which describes a nodal analysis. The initial solar field inlet temperature (±293 ℃) is adjusted to reach and maintain the desired solar field outlet temperature (±393 ℃). After the fluid has been transferred through the cold header pipe it flows through each SCA and the temperature gradually increases until the desired outlet temperature is reached.

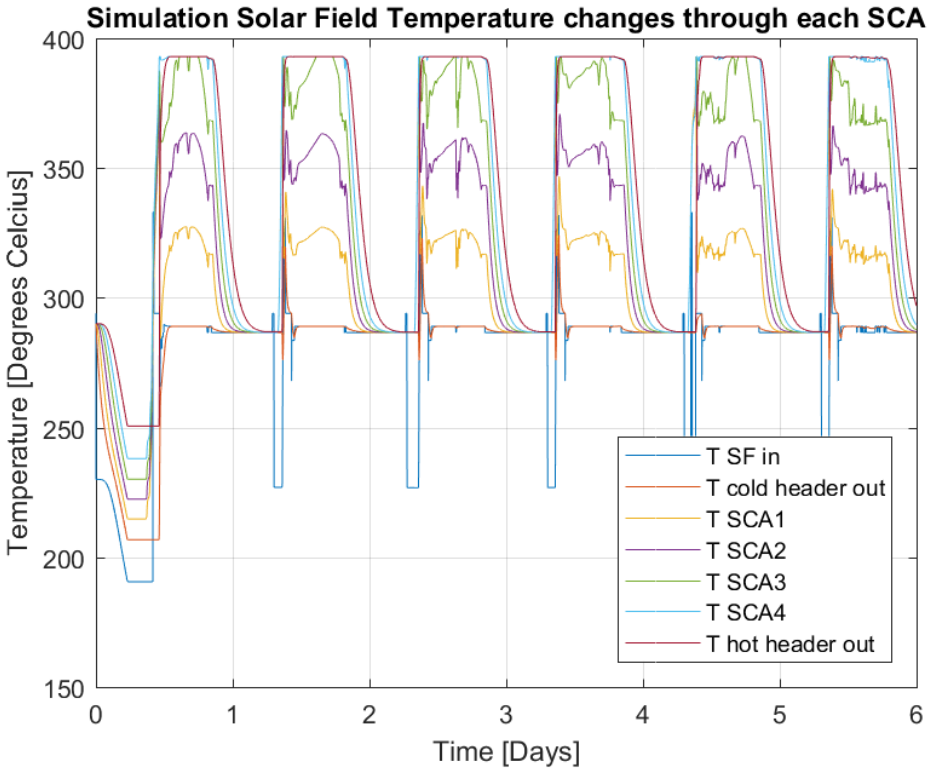


Figure 4.2: Simulation: Solar Field Temperature (11-16 April 2016)

Figure 4.2 shows how the temperature increases through each SCA and changes due to DNI and thermal inertia. The temperature mainly increases proportionally due to the DNI values as this is the variable increasing the temperature in each loop. The PID control system implemented is a closed loop feedback controller which receives a new feedback temperature after each time step. Once the temperature being fed back into the nodal model is near the desired outlet temperature of 393 ℃, the controller attempts to maintain this desired outlet temperature without exceeding the 400 ℃. This is done by adjusting the HTF mass flow rate in order to meet the desired outlet temperature. At this time the outlet temperature reaches a stable and almost constant desired solar field

outlet temperature of 393 ℃ as seen with the *T hot header out* (red graph) in Figure 4.2. The reason for a drop in solar field inlet temperature before the beginning of each day is due to the lack of heat in the solar field and storage system for these consecutive days. The plant does not produce electricity during this time and therefore it is in a standby operation mode where the HTF in the solar field has no choice, but to drop until the sun begins to shine the following day and give new DNI input into the power plant.

### 4.1.3 Storage Level:

The tank level changes throughout each day of operation. These changes are dependant on the amount of energy received from the solar resource for that particular day, which in turn influences the output temperature of the solar field. Figure 4.3 shows the DNI (green graph) and the energy being stored and released from storage (blue graph). The right hand side y-axis represents the hot tank storage level in a percentage format, where 100 % represents a full hot storage tank.

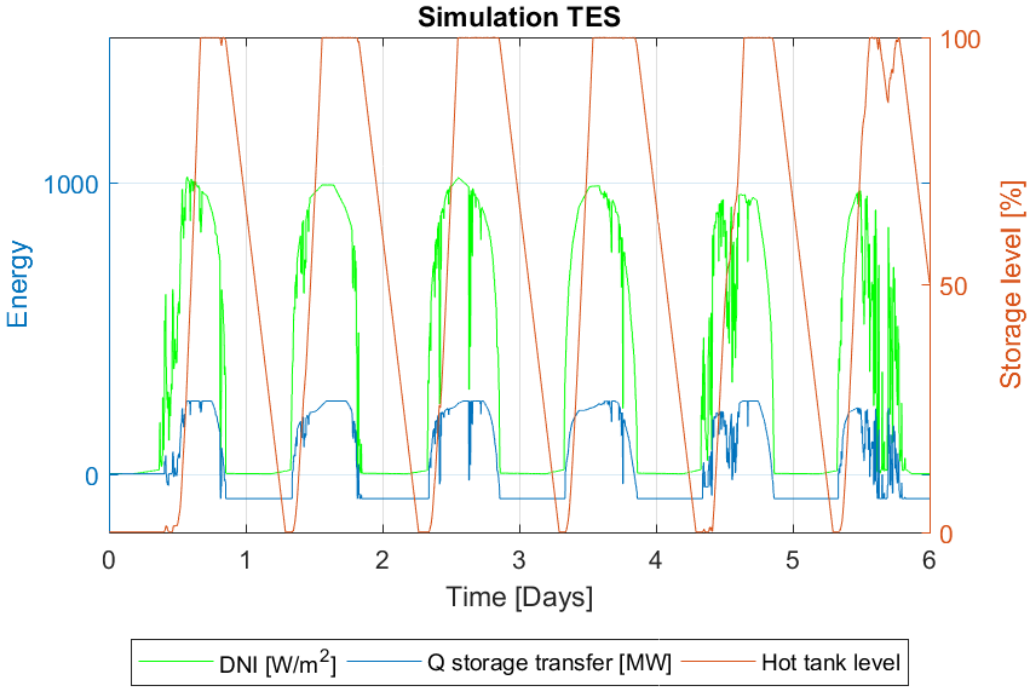


Figure 4.3: Simulation: Thermal Energy Storage (TES) (11-16 April 2016)

Once the storage is fully charged, it enters a different mode of operation, where a small thermal loss of $\pm 0.1$ % per hour occurs. During the next time step the charging condition is met and executed which drives the storage into a storage full mode and the cycle continues until the storage is discharged. During each of these six simulation days, the hot tank level is at approximately 60 % full during midnights. The hot level then drops steadily as the demand for the hot thermal oil remains constant. The hot tank level then reaches it's empty state and the storage system enters the storage empty mode (Storage Mode 4). Once the storage system goes into this mode of operation, the power plant shuts down because there is no solar resource or thermal storage energy available for energy production.

As each day progresses to approximately 06:30 am (depending on the day), the solar field has the capability of heating the thermal oil to temperatures exceeding design point and is therefore used to store excess energy. This can be seen with an increase of the *Q Energy transfer* (blue graph). This is achieved with the charging mode of the thermal storage operation and correlating to the rising level in the hot tank (red graph). The rate at which the hot tank level rises is initially at the same rate as the DNI level, but this changes to a constant rate as it hits the charging limit, which is applied by a maximum salt mass flowrate from one tank the other. Depending on the day, but generally just before 03:00PM the hot tank reaches it's full capacity and the storage tank is not able to absorb more heat. If the storage system is full and the solar field is able to meet the desired thermal energy from the power block, then some of the mirrors are defocused in order to eliminate excess energy being fed through the system. Later in the day, approximately 05:30PM the thermal storage system changes into discharge mode and the storage level begins to decrease as the solar field is not able to produce enough hot thermal oil on it's own to satisfy the demand. The discharged energy can be seen as represented on the plot as *Q Energy transfer* (blue graph), which is below zero, representing the discharge of energy. This therefore concludes that the blue graph in Figure 4.3 shows all the storage operation modes, where the charging and full values are positive and the discharging of energy is shown as negative values. Therefore, describing the thermal energy transfer towards and from the hot storage tank.

## 4.2 Simulation Results vs Measured Results

In order to validate and evaluate the accuracy of the model and it's performance, a comparison between the actual output from the power plant and the simulation model is necessary. This gives credibility to the simulation model, techniques and the methodology implemented. The comparison relates the output electricity generation from the power plant to the simulation model.

The comparison graphs, Figure 4.4 and Figure 4.6, are plots from 06:00 am to 06:00 am the following day. The reason that this is shown from 06:00 am to 06:00 am is because the simulation model begins from a shut-down operation mode, where this is not the actual case. The power plant is operational prior to these simulation days and therefore generates electricity during the previous night, prior to the first simulation day.

### 4.2.1 Generated Electricity Comparison:

Figure 4.4 is a graphical representation showing the comparison of the generated electrical output from the simulation compared to the actual output from the Andasol 3 power plant for the six operation days. The reason that the electricity generation drops from ±53 MW to ±40 MW is because of the partial discharge operation. This occurs during the discharge mode of the storage system (Storage Mode 3) and is approximately operating at a 65 % discharge rate. According to Andasol 3, the strategy is to operate in this manner because it is possible to keep the turbines warm for the last hour before start-up. The plant also wanted to empty the storage tanks and produce the most electricity possible in order to receive the highest return for their electricity production to the grid for those days.

Initially the plot shows that the power plant produces energy from the previous day (orange graph), where the simulation begins from zero (blue graph). This is an initial starting point used in the simulation model and was chosen in order to prevent any estimations of the amount of previously stored energy, mass flow rates and solar field temperatures from the previous day. The model operates in a similar manner for the chosen simulation days. The reason for this is because the operational strategy for these days are almost identical. The power plant desired a similar performance output for the various input DNI values. Also, the discharge rate was maintained similar for these days.

It is essential to note that the simulation days match the energy generation well during times without discharging of the stored energy. Once the power plant and simulation model move into a discharge operation to produce ±40 MW, there is a slight discrepancy. The discrepancy occurs because the simulation model discharges at a constant rate where the actual power plant has a variable discharge rate. The simulation therefore either marginally exceeds or marginally underestimates the actual operation chosen by the operator, but still maintains a good correlation. Also, during the last day (16 April 2017), the simulation model attempts to account for volatile DNI and manages to operate in a similar fashion to that of the actual power plant. The power plant does not produce as much energy as the simulation model and this is attributed a large number of maintenance operation and hot salts being saved in order to support operation for the next day.

Figure 4.4 is an important validation aspect of this study as it compares the generated output of the simulation model to that of the actual power plant. The simulation model (blue graph) includes all the modelling, techniques, methodology, operations and strategy implemented to achieve a result that has the same trends and similar performance results to that of the actual power plant (orange graph). The precise similarity will be discussed further in Chapter 4.2.3

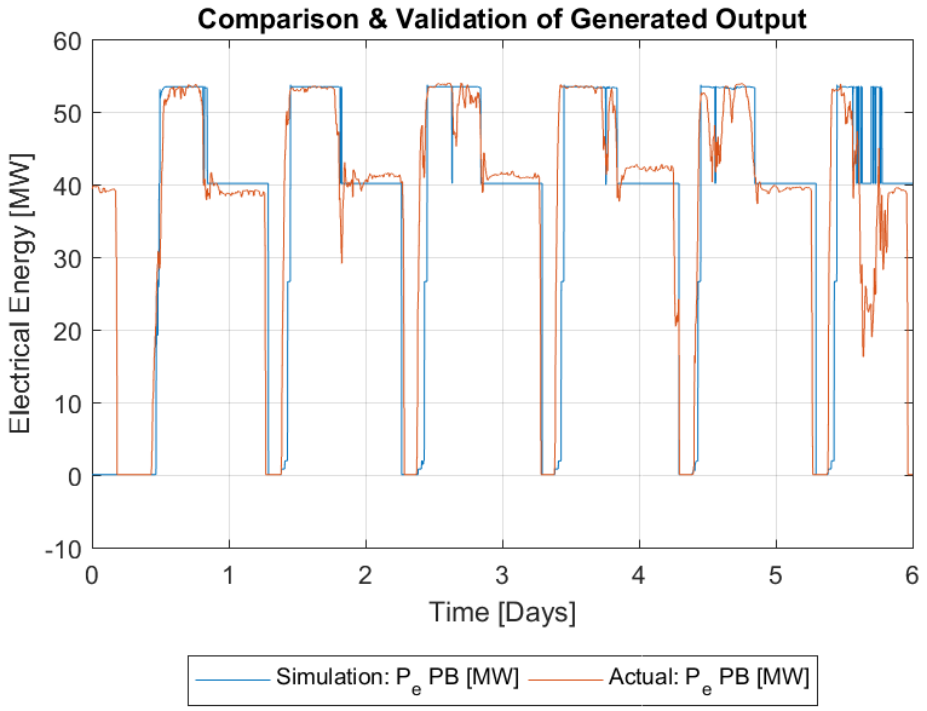


Figure 4.4: Comparison and Validation of Generated Output (11-16 April 2016)

Analysing the first day (11 April 2016) of Figure 4.4 provides validation to the model. Figure 4.5 is a plot generated by means of the same 10 second simulation increment as Figures 4.1 to Figure 4.4, but the x-axis is represented in seconds for a more in-depth analysis. Comparing the simulation (blue graph) to that of the actual output (orange graph) shows that the simulation start-up takes approximately 30 minutes longer to begin generating energy, but then manages to reach the design circulation mode faster than the actual power plant. This inconsistency can be attributed to the control system attempting to reach the design circulation operation mode as soon as possible according to the PID parameters selected, which regulate the solar field mass flow rate.

The model generates the same amount of energy during the design circulation mode and charging mode. It then begins to discharge at the same time as the actual power plant, approximately 08:45 pm. The simulation and the actual power plant attempt to adjust when discharging as a specific rate and therefore initially need to compensate for different mass flow rates and addition of heat from the hot storage tank. Once the model and actual plant reach a flow equilibrium when discharging, they both discharge at the same rate achieving a 40 MW output. The simulation discharges at a constant rate until the hot tank is empty and takes approximately 15 minutes longer to cool-down than the actual power plant. This is due to the model having an increased production during the discharge operation.

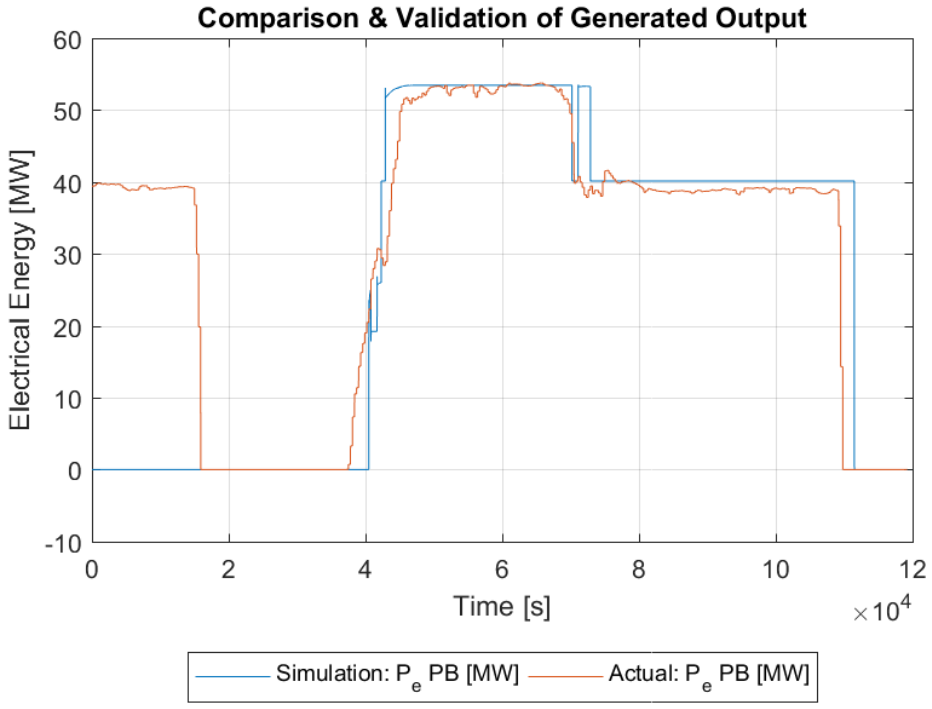


Figure 4.5: Comparison and Validation of Generated Output (11 April 2016)

### 4.2.2 Cumulative Energy Comparison:

A cumulative energy generation comparison, see Figure 4.6, shows that the simulation model has a similar trend to that of the actual output of the power plant for the full duration of the chosen simulation days in April 2016. Figure 4.6 is a plot which is derived from the cumulative energy generation starting

at 06:00 am. The blue graph represents the simulation result, where the orange graph represents the actual output from the power plant. Therefore, this plot shows a good correlation between the simulation model and the actual power plant and how they relate in terms of cumulative energy production for the April simulation days. Both graphs following the same trend and aid in concluding that the simulation has a similar operational strategy.

Although Figure 4.4 shows that the Andasol 3 power plant initially produces electricity (from time zero until all the energy was discharged from the storage tank) and the model does not account for the energy carried over from the previous day. The simulation (blue graph at time zero) begins from an initial production value of zero. Therefore in Figure 4.6, that initial energy carried over from the previous day was set to zero in order to have a fair comparison between the model and the actual power plant electricity production. It is for this reason that Figure 4.6 shows both graphs beginning at zero energy production and as the first day of production begins the graphs increase.

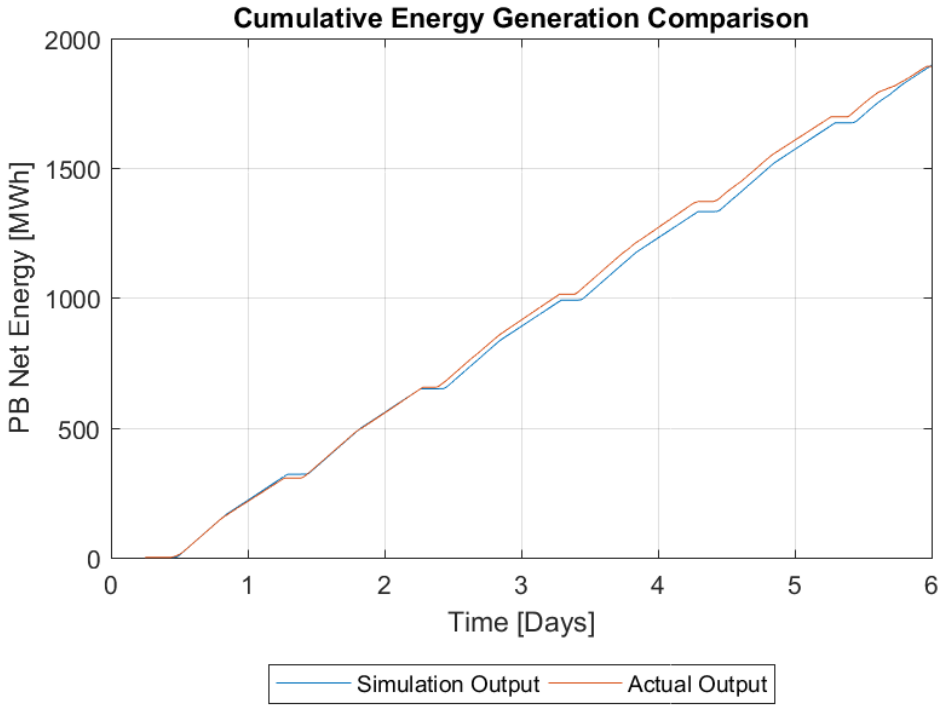


Figure 4.6: Cumulative Energy Generation Comparison (11-16 April 2016)

### 4.2.3 April Bar Chart - Mean Absolute Percentage Error (MAPE):

The mean absolute percentage error (MAPE) is determined by calculating the absolute percentage error for each day of the simulation and then calculating the average/mean over the simulation duration selected. This is achieved by making use of Equation 4.1.

$$MAPE = \frac{100}{n} \sum_{k=1}^{n} \left| \frac{(Actual_k - Forecast_k)}{Actual_k} \right| \tag{4.1}$$

Where (n) is the number of simulation days, (k) represents each specific day and the multiplication by 100 makes the result appear as a percentage.

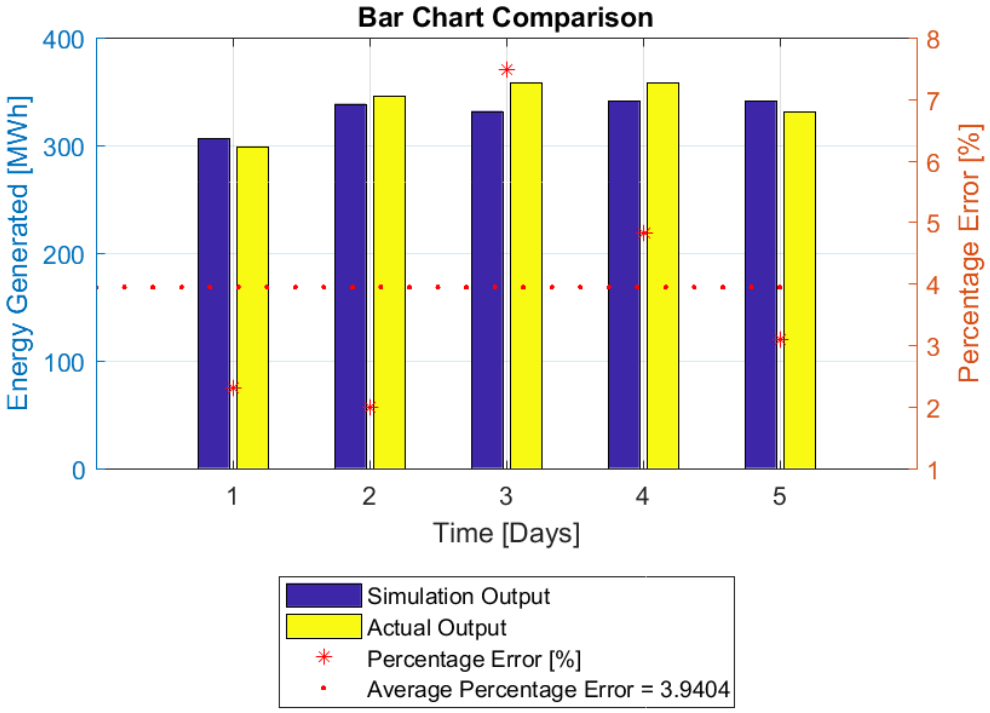


Figure 4.7: Bar Chart Comparison (11-16 April 2016)

Figure 4.7 is a bar graph representing the daily energy production from the power plant (Yellow graph) and from the simulation (blue graph). The percentage error is shown on the right hand side y-axis and is represented as a percentage. The red stars represent the percentage error for each day and the red dots show the mean absolute percentage error for the simulation duration. Although, this is only a six day simulation, the MAPE is calculated to be

±3.94 %, which is below the modelling error limit of 10 % for monthly yield. Section 4.2.4 is therefore needed to better show that the model remains below the 10 % modelling error limit. The section focuses on a longer simulation duration almost a month of data which allows for a better analysis.

### 4.2.4 June Bar Chart - Mean Absolute Percentage Error (MAPE):

An additional simulation was run where similar graphs were plotted for a different time and duration in the same year. Figure 4.8 shows a 23 day simulation during June 2016. Figure 4.8 is set out in the same manner as Figure 4.7, however, the MAPE is ±10.48 %. This is bordering on the acceptable limit when modelling power plant performance output.

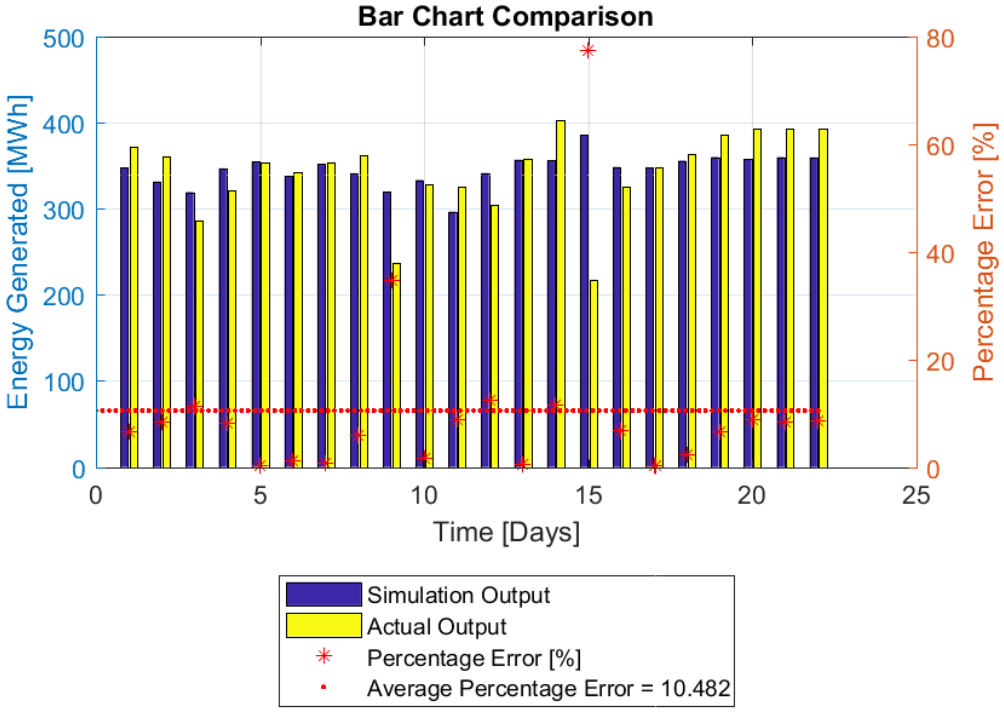


Figure 4.8: Bar Chart Comparison (01-23 June 2016)

Notably, there are some outliers within this data set (01 June 2016 - 23 June 2016). Focusing on the two days (9th June 2016 and 15 June 2016) where the performance of the simulation model exceeds that of the actual data by approximately 36 % and 79 % respectfully, it is found from the daily reports that the reasons for such inconsistencies are that the actual power plant had specific issues on those days. These issues restrict the actual performance,

where the model was not able to take into consideration such unforeseen outcomes. In the case of the 9th June 2016, it was a hazy day and dusty winds. In addition, the plant was in a normal operation mode, but there were pipe blockages and damages, as well as 5 loops were out of order. This explains the model over predicting the generated energy by ±36 %. In the case of the 15th June 2016, it was a sunny day and the plant was in a normal operation mode. There was however, failure in the high pressure turbine seal system, where a valve leading to the low pressure turbine did not open. This caused a drastic drop in energy production which relates to the 79 % error that day. With these two outlying days eliminated from the mean absolute percentage error calculation, the error is reduced to below the acceptable limit defined for power plant modelling and therefore restores credibility to the model.

In order to obtain a more accurate MAPE value for this same simulation, the outlying data points which occur on the 9th June 2016 and 15th June 2016 are excluded. This results in a 20 day simulation that gives a 5.93 % MAPE, see Figure 4.9.

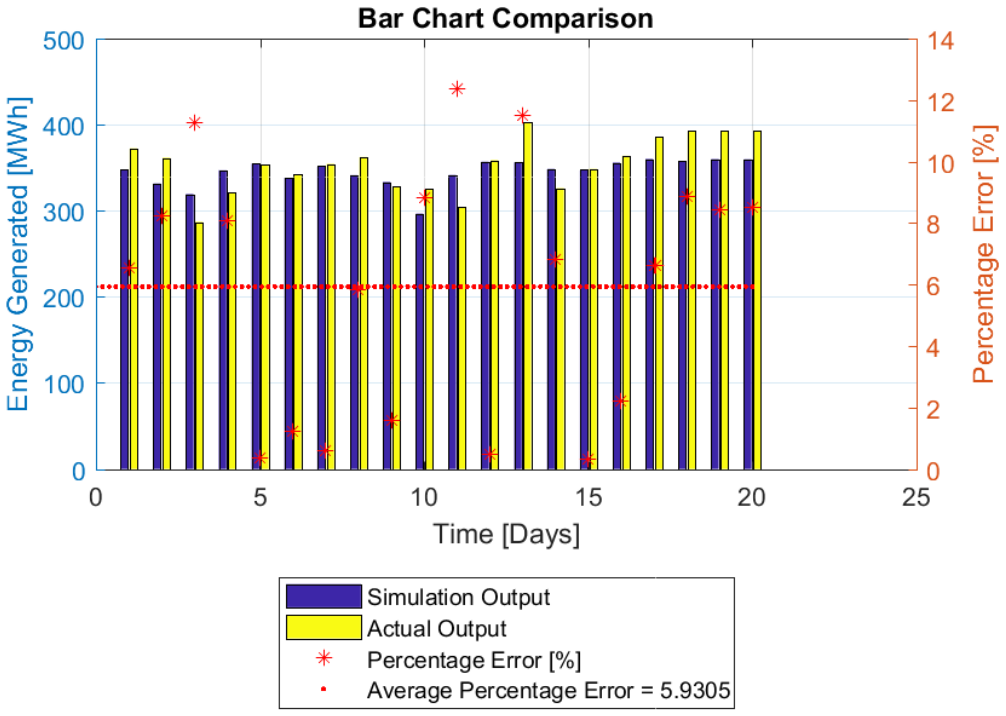


Figure 4.9: Bar Chart Comparison without Outliers (01-20 June 2016)

# Chapter 5

# Operational Feasibility

The purpose of this chapter is to be an example of how the simulation tool is to be used or implemented in a real application. It will attempt to describe possible outcomes and options available to the operator. The decisions made by the operators are based on multiple conditions and limitations which vary each day. These decisions are related to a host of different aspects/factors. This tool allows the operator to focus on power plant performance, while still focusing on the proposed strategy to reach the desired output and optimise production.

## 5.1 Operational Feasibility Aspects

The operational strategy aspects are related to the storage, amount of energy available at any given time and the management of distributing the available solar resource and stored thermal energy. This simulation tool will assist the operator to evaluate the following aspects:

1. Performance
2. Efficiency
3. Operational Mode
4. Thermal Energy Stored/Available
5. Thermal Storage Discharge Rate
6. Cycle Mass Flow Rates
7. Operational Strategy
8. Cool-down Time
9. Heat-up Time
10. Maintenance areas
11. Components in operation and their capacity
12. Payments and Shareholder Interests
13. Closed Cycle System Operations
14. Solar Resource Input Compared to the Available Stored Energy
15. Energy Discharged Compared to the Tariff Structure

The discharge rate of the stored thermal energy is a key factor as many of the other listed aspects rely on the discharge rate. It also determines the operational modes and overall efficiency that the power plant will experience. For example it could influence whether the power plant enters a 24-hour operation mode or not. In addition, the cool-down period, heat-up the next morning and tariff structure creates a diverse set of parameters, which the operator is to analyse and make operational decisions which will benefit the plant. It should allow for the largest possible monetary return from delivering electricity to the grid without hindering maintenance or components. The advantage of such a tool is that it allows the operator the ability to make comparisons between various operational strategies based on performance output plots.

## 5.2 Operational Feasibility and Comparison

Three feasibility studies are carried out in this section, which resemble examples of how the performance output is able to be analysed by the plant operators. Thus, these feasibility studies are only used as examples. The first feasibility scenario focuses on a simulation during the Summer/high DNI period, the second scenario focuses on a simulation during the Winter/low DNI period and the third scenario focusses on limiting the LNG use. The application of this simulation tool remains the same for any day during the course of the year, however, the considerations and limitations differ. In turn, this affects the decisions that are to be made by the plant operators.

**High DNI Feasibility Analysis:**
A randomly selected simulation period was chosen for the high DNI feasibility study (1 June 2016 and 2 June 2016). In order to show the application of this tool, an investigation and analysis is shown while referring to Figure 5.1. Figure 5.1 depicts a two day simulation period (blue graph), which resembles the actual performance output of the Andasol 3 power plant (orange graph). Investigating the start-up and cool-down periods for each day, shows that the start-up is slightly slower than the actual start-up time for both simulation days. However, the cool-down time during the first day is accurate, but cools down rapidly at the end of day two where it should have discharged energy at a slower rate in order to better depict the actual output. Analysing the discharge rate shows that it is approximately 60 % when the model reaches the discharge mode (storage Mode 3). This is slightly lower than the actual power plant discharge rate during the first day. This can be seen where the actual output result (orange graph) is above the simulation graph (blue graph). Day 2 matches the discharge value that the power plant actually experiences, however, it is not maintained for the same duration as the actual value.

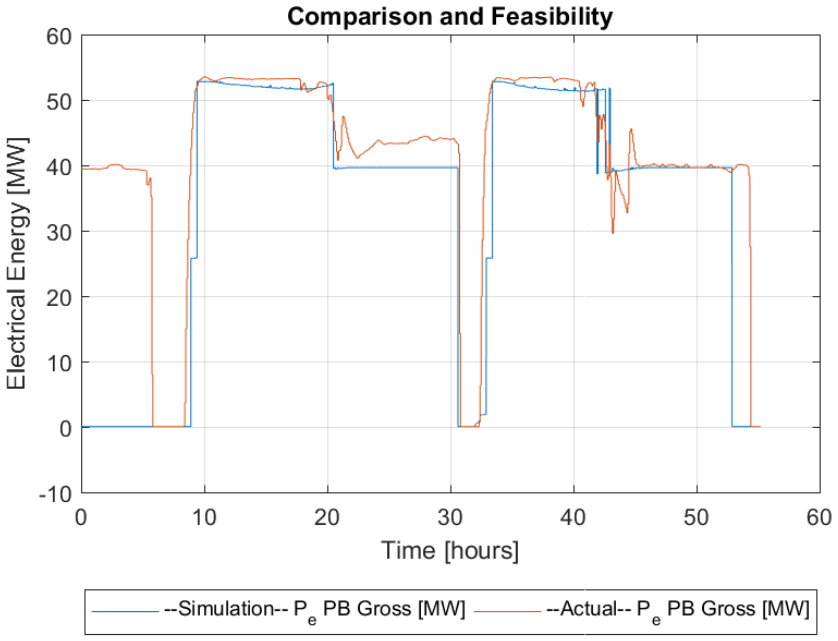


Figure 5.1: Feasibility (1-2 June 2016)

The operator has two main options when deciding how to operate the power plant in order to obtain the best performance result. This includes a discharge rate which produces less energy for a longer duration or to discharge the stored energy slightly faster by either enabling a full discharge rate or an almost full discharge rate, see Figure 5.2a and Figure 5.2b respectfully. Figure 5.2a shows that the power plant is able to enter into a 24-hour operation mode with this approach, see the purple graph. Thus, the partial discharge rate promotes a longer operating duration for the power plant. The power plant operators might not want to shut down the turbines or even enter them into a standby mode and therefore could continue producing electricity for as long as there is solar resource, sufficient thermal energy stored and a partial discharge rate enabled. Figure 5.2b shows the influence on performance, if the operator were to choose to discharge the stored energy at an increased rate (see the green graph). This would be a viable option if the plant is planning on doing maintenance, then there is time at the end of the day when this is possible. Alternatively, the power plant would like to receive the maximum amount of money for the electricity they deliver to the grid and would therefore be interested in increasing the production for that day to it's maximum. The operator is to run various simulation scenarios and evaluate and analyse the best operation option. This would give rise to optimised operations at the power plant as the operator is able to make decisions dependant on the amount of stored energy available and relate other operating conditions.

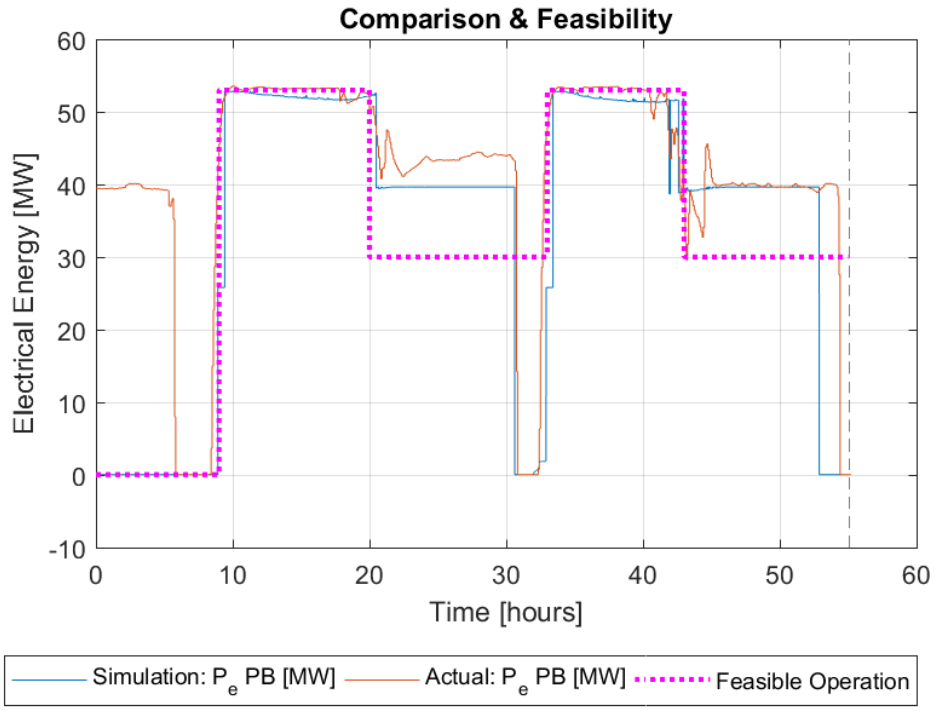


(a) Slow Discharge Rate

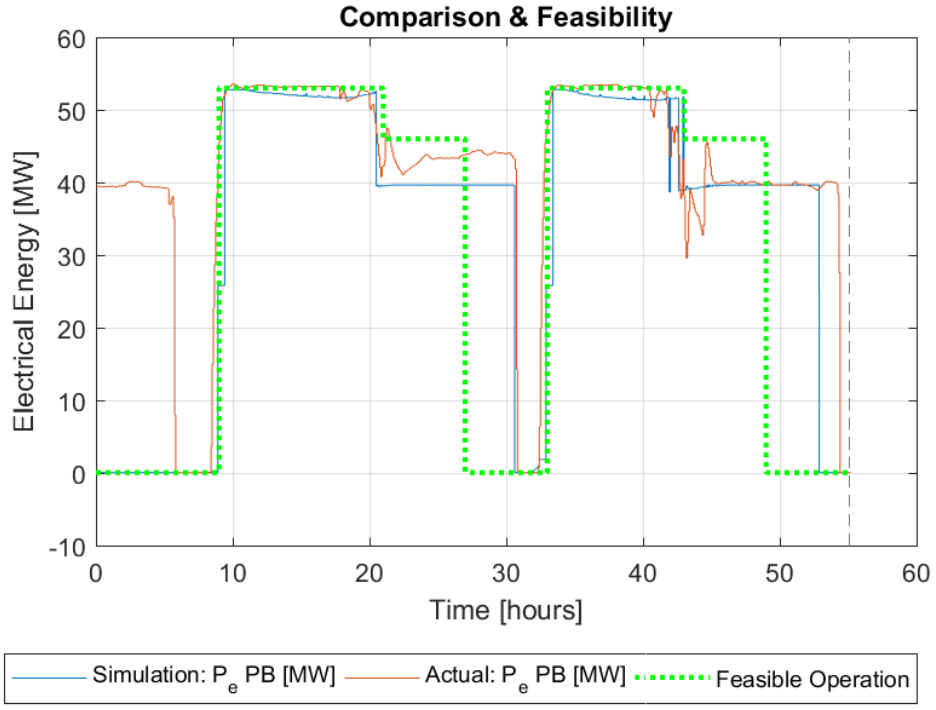


(b) Fast Discharge Rate

Figure 5.2: Operational Feasibility Discharge Options

**Low DNI Feasibility Analysis:**
A randomly selected simulation period was chosen for the low DNI feasibility study (1 January 2016 and 2 January 2016), refer to Figure 5.1. When analysing Figure 5.1, there is a major difference between the operational strategy during the low DNI period and the previously described high DNI period. This difference is in the amount of stored thermal energy available. During the winter/ low DNI days, there is insufficient energy to store large amounts of energy for production during the night time or overcast times. This drastically limits the flexibility/dispatch-ability of the power plant during low DNI days.

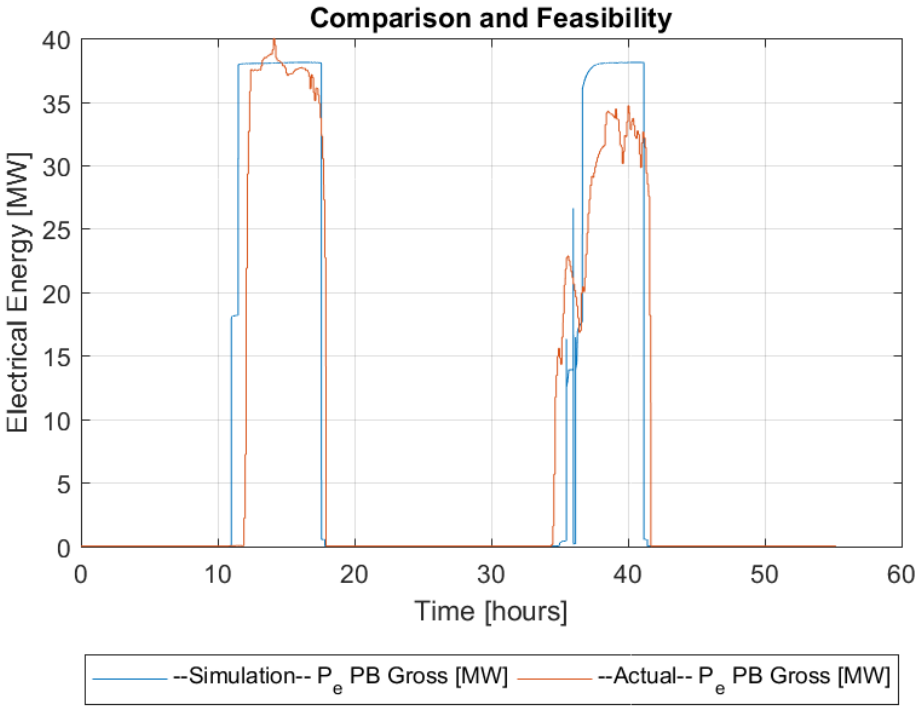


Figure 5.3: Feasibility (1-2 January 2016)

Figure 5.3 depicts a two day simulation period (blue graph), which resembles the actual performance output of the Andasol 3 power plant (orange graph). The power generation produced by the simulation over estimates the actual electricity generated by approximately 7.90 %. The error between the simulation and the actual power plant values increases when highly volatile DNI values are used as an input. Analysing the start-up and cool-down periods for each simulation day, indicates that the start-up is faster than the actual start-up time. However, the second simulation start-up time is slower than the actual start-up experienced by the power plant. The cool-down times for both days are accurate, but occur a few minutes prior to the actual cool-down

time of the power plant. During this two day period the power plant managed to store only a small amount of energy in the hot storage tank. This effects the energy production of the power plant as the strategy implemented is to enable a full discharge rate and dispatch all the stored energy as soon as the energy from the solar field does not meet the energy values desired in the power block. The power plant is able to vary the dispatch-ability in the same way as described for the high DNI simulation, refer to Figure 5.2. The only difference is that 24-hour operation is not attainable and that there is a very small influence on the electrical output generated. During the low DNI days the power plant will generally dispatch all the energy produced in order to obtain the maximum return on a low energy production day.

**Gas (LNG) Feasibility Analysis:**
This feasibility analysis investigates the use of Liquefied Natural Gas (LNG) heaters, refer to Figure 5.4. The use of these heaters usually occurs during the winter time or days of low DNI. The reason is to reduce the time it takes to heat the solar field to the desired operating temperature, therefore giving a more efficient start-up. This allows the power plant to reach the specified pressures. This way the power plant is able to produce electricity sooner in the day and therefore deliver electricity to the grid and receive a return for production. This analysis considers the second day in January 2016, which is the second day plotted in Figure 5.3 (between 24 and 48 hours). The reason this day was chosen is because the Andasol 3 power plant made use of the LNG heaters (unlike days of high DNI such as during Summer) and allowed for a comparison with the simulation model. Figure 5.4a displays a blue graph, which resembles the electrical energy generated by the simulation and an orange graph that shows the actual output of Andasol 3 for the $2^{nd}$ January 2016. In addition to the electrical energy generated, it shows that the model slightly over estimates the actual LNG used. The energy generated by the gas heaters from the simulation are shown as the black graph and the actual LNG energy is shown by the purple graph. This can be seen just after hour 30 of Figure 5.4a. The power plant operators are able to adjust the use of the gas heaters and assess the influence of potentially eliminating the use of gas heaters for this day. The result is shown in Figure 5.4b where the purple dotted line indicates the new electrical energy produced by the simulation. It can be identified that without the use of the gas, the plant produces less electrical energy as the start-up of the plant is influenced. The power plant takes longer to warm up the solar field without the use of the gas heaters and therefore does not produce the initial energy shown by the blue graph at approximately hour 35. The plant operators are able to assess the difference in electricity production and whether it is plausible to eliminate the use of gas heaters for the specific day and run the plant in a more environmentally friendly manner.

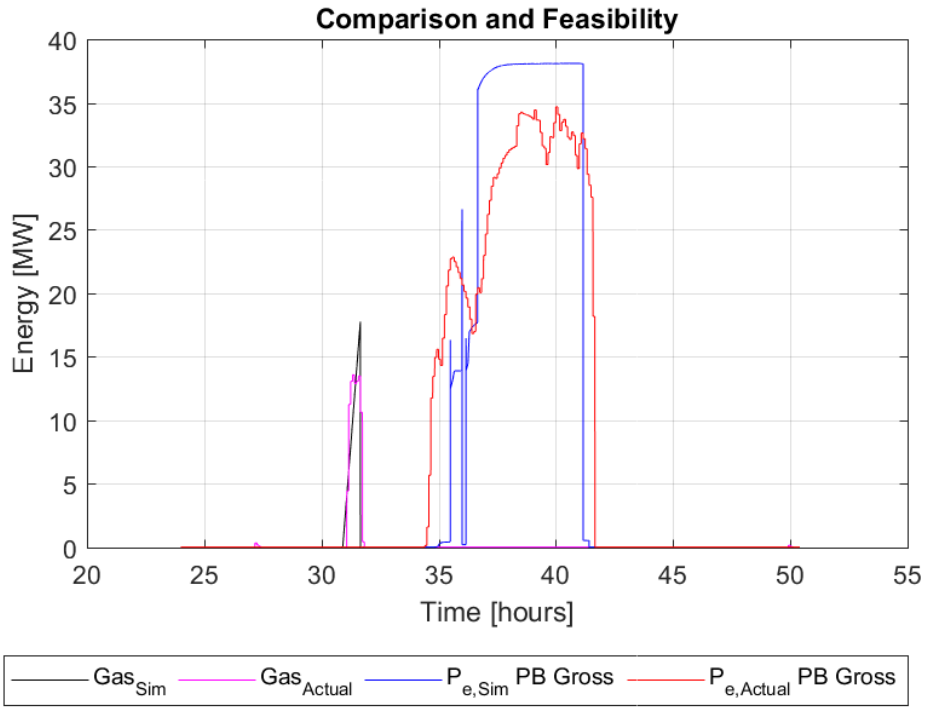


(a) Feasibility with LNG Heaters

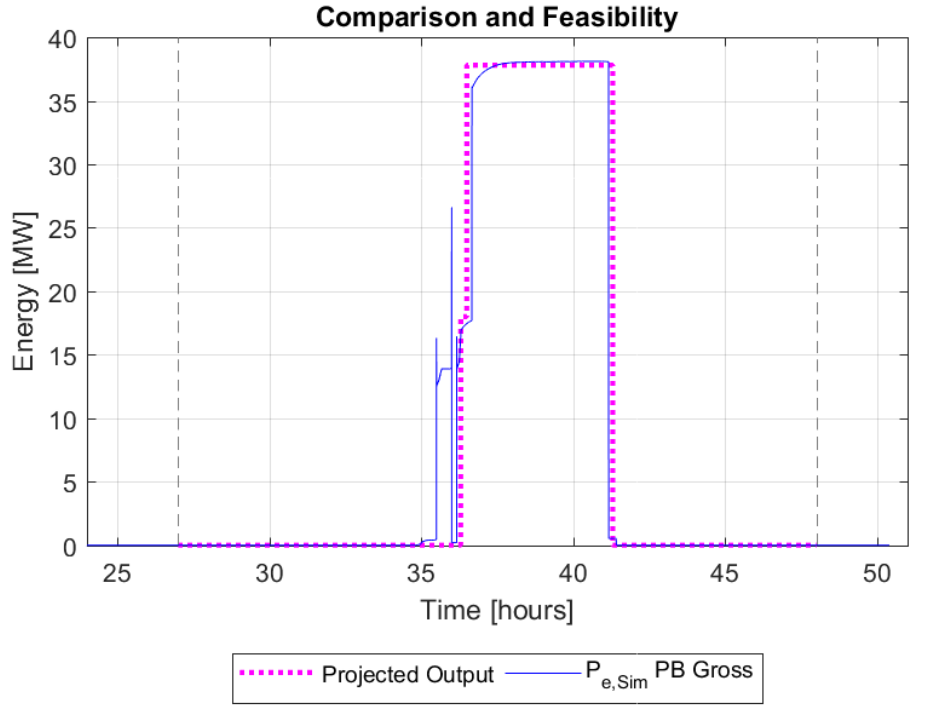


(b) Proposed Output without LNG

Figure 5.4: Feasibility (2 January 2016)

# Chapter 6

# Conclusion

To conclude the work presented in this study, the findings will be discussed along with recommendations for PTPP's and the possibility of a continuation/advancement of this simulation tool or similar work.

## 6.1 Summary of Findings

The results obtained from the simulation model give credibility to the methodology used. This is due to the model being verified through a comparison with the actual power plant, Andasol 3, performance and what is generated by the simulation. The implementation of the operational modes and different control systems allow for a similar daily electricity yield to be obtained, which proves that the operational modes implemented are a replication of the Andasol 3 modes of operation. A mean absolute percentage error (MAPE) is calculated to identify the error with the simulation program results. The percentage error is less than 10 % for this PTPP simulation models. The calculated errors, for the two simulation periods expressed in this document, provided positive results in the range of 3.94 % and 5.93 %, which highlights the accuracy of the model. The modelling techniques also allow for a functional model to be produced, which generates performance output graphs useful to the power plant operators. Power plant operators are able to make use of this simulation tool to optimise the plants performance outcome. Currently the model resembles the Andasol 3 power plant and simulates the performance of the plant, but is capable of being adjusted to suit any PTPP. The developed model is a functional dynamic simulation tool for PTPP operators, where the it will assist plant operators with the daily decision making process regarding operational strategy and performance.

## 6.2 Research Contributions

This research is a contribution to optimise PTPP's. The work done is directly related to PTPP modelling and simulations. The tool contributes by means of it's application. The tool is to assist PTPP operators in the decision making process on a day-to-day basis. Operational strategies outlined by the operators can be simulated, where the performance output is evaluated in order to give insight into various scenarios desired by the power plant managers/operators. The research also contributes to the in-house software available at the Solar Thermal Energy Research Group (STERG) at Stellenbosch University. Additionally, the methodologies, techniques and strategies can be used to assist fellow Engineering students, colleagues and professionals with design, modelling and simulations of similar power plants. The model has been coded and modelled in order to accommodate similar power plants being modelled. This gives the model the capacity to be adjusted to replicate/resemble power plants in the South African market as well as those in the European market place for example.

## 6.3 Recommendations

The simulation comes with the added benefit that it is adaptable to similar PTPP's. Along with the accuracy of the model, this also promotes the simulation tool and encourages PTPP's to implement such a tool. The simulation run time is short, only a few minutes, depending on the simulation duration and input resolution chosen for simulation. This allows time for analysis and evaluation of the results, while still having sufficient time for plant operators to make changes to the operational strategy of the power plant.

### 6.3.1 Recommendations for Andasol 3

The use of this tool will increase electricity production and power plant performance, while giving the plant operators confidence in operational decision making. This confidence will come from the credibility and accuracy of the model and the output results produced relating to performance. The decisions being made are based on alternative operational strategy scenarios that ensure the most feasible solution, where the daily electricity yield is optimised.

### 6.3.2 Recommendations for Further Work

Optimisation of any power plant is usually carried out during the design phase of a power plant model. However, Andasol 3 is an existing power plant and was modelled as such. Therefore, it is noted that the model is drawn up in such a way that it can be used during the design phase of future power plants

and aid in the design phase if necessary. The model is well commented, easy to understand and promotes further research into PTPP's. Some considerations with PTPP design is the sizing of the solar field and storage sizing, which is easily adjusted in the simulation code if this model were to be used for design purposes. The model is less accurate for simulations with highly volatile DNI inputs and therefore further work could improve the accuracy under these conditions. In addition to the model being able to be modified and used to assist the design phase, there is also an option to add a financial aspect to the dynamic performance model developed. The financial aspect could calculate the monetary return that the power plant would see if they produced a certain amount of electricity to the grid. This would apply for the various scenarios that the operator would simulate, analyse and evaluate. The last recommendation would be to add a predictive component to the model, where the simulation model would adjust it's operational mode dependent on the amount of solar resource predicted. The prediction could make use of accurate weather forecasts for the specific site location of the power plant and would have to be studied to identify a sufficient prediction period, maybe 24 hours or less.

# Appendices

# Appendix A

# Andasol 3: Data Sheet

Appendix A describes the Andasol 3 power plant and acts as a summary of the actual data sheet. The points highlighted below describe the tables that follow in this Appendix.

- Table A.1: Describes the location of the Andasol 3 power plant which is situated in the South of Spain (Guadix).
- Table A.2: Describes the solar field and the SKAL-ET 150 collectors.
- Table A.3: Refers to the HTF, which is a Eutectic Mixture of 73.5% Diphenyl and 26.5 Diphenyl Oxide.
- Table A.4: Describes the 2-tank molten salt (Nitrate salt mixture containing 60% $NaNO_3$ and 40% $KNO_3$) storage system.
- Table A.5: Refers to the power block parameters of the power plant. It is important to note that the turbine type is a condensing turbine with a single reheat and six extractions.
- Table A.6: Describes the power plant performance.

Table A.1: Andasol 3: Site

| **Site** | | |
|---|---|---|
| **Parameter** | **Value** | **Unit** |
| Longitude | 3.07 | °W |
| Latitude | 37.21 | °N |
| Annual DNI | 2 136 | $kWh/m^2$ |
| Field Length (N-S) | 1 400 | m |
| Field Length (E-W) | 1 500 | m |

Table A.2: Andasol 3: Solar Field

| **Solar Field** | | |
|---|---|---|
| **Parameter** | **Value** | **Unit** |
| Collector: Length | 148.4 | m |
| Collector: Aperture | 5.77 | m |
| Number of Mirror Segments per Collector | 366 | - |
| Collectors per loop | 4 | - |
| Number of Loops | 152 | - |
| Number of Collectors | 608 | - |
| Total Effective Mirror Area | 497 040 | $m^2$ |
| Row Spacing | 17.2 | m |
| Design Solar Field Inlet Temperature | 294 | ℃ |
| Design Solar Field Outlet Temperature | 393 | ℃ |
| Automatic Defocus Temperature | 398 | ℃ |
| Nominal Design Thermal Output | 243.8 | MW |
| Design Pressure Drop on Solar Field | 10.4 | bar |

Table A.3: Andasol 3: HTF System

| **HTF System** | | |
|---|---|---|
| **Parameter** | **Value** | **Unit** |
| Complete HTF Volume at 30 ℃ | 2 154 | $m^3$ |
| HTF Main Pumps no. in operation/for spare | 3/1 | - |
| Mass Flow Rate at 100/105% load | 1 011/1 061 | kg/s |
| Variable Loads(Controlled by Frequency Converter) | 30-105 | % |
| Motor Rated Power | 1.35 | MW |
| Nominal Operating Temperature | 294 | ℃ |
| Expansion Vessel Total Volume | 1 000 | $m^3$ |
| HTF Auxiliary Heaters Net Thermal Output Capacity | 30 | MW |

Table A.4: Andasol 3: Thermal Storage

| **Thermal Storage** | | |
|---|---|---|
| **Parameter** | **Value** | **Unit** |
| Storage Capacity (with Cold Tank Temp. 275℃) | 1 218 | MWh |
| Storage Tank Size: Height | 14.25 | m |
| Storage Tank Size: Diameter | 38 | m |
| Heat Exchanger Capacity | 122 | $MW_{th}$ |
| Salt Mass | 29 000 | tons |
| Total Salt Flow Rate during Charge (Design) | 814 | kg/s |
| Total HTF Flow Rate during Charge (Design) | 499 | kg/s |
| Cold Tank Temperature (during winter) | 275 | ℃ |
| Design Cold Tank Temperature | 286 | ℃ |
| Design Hot Tank Temperature | 386 | ℃ |

Table A.5: Andasol 3: Power Block

| **Power Block** | | |
|---|---|---|
| **Parameter** | **Value** | **Unit** |
| Gross Capacity | 49.9 | MW |
| Total parasitics | 6.54 | MW |
| Plant Efficiency | 41.02 | % |
| Generator: Voltage | 10.5 ±10% | kV |
| Generator: Frequency | 50 | Hz |
| Generator: Nominal Nameplate Power | 49.9 | MW |
| Turbine Inlet Steam Conditions: Pressure | 102.4 | bara |
| Turbine Inlet Steam Conditions: Superheated Temp | 383 | ℃ |
| Turbine Inlet Steam Conditions: Reheated | 383 | ℃ |
| Turbine Inlet Steam Conditions: Nominal Steam Flow | 53.1 | kg/s |
| Turbine Inlet Steam Conditions: Design Back Pressure | 0.042 | bara |
| Cooling Water: Nominal Rated Flow | 8 110 | $m^3/h$ |
| Cooling Water: Nominal Temp Rise | 7.6 | K |
| Cooling Water: Supply/Return Temp | 19.4/27 | ℃ |
| Water Consumption at Full Load | 163 | $m^3/h$ |

Table A.6: Andasol 3: Performance

| **Performance** | | |
|---|---|---|
| **Parameter** | **Value** | **Unit** |
| Optical Efficiency | 78 | % |
| Thermal Efficiency: Peak | 68 | % |
| Thermal Efficiency: Annual | 41.3 | % |
| Total Heat from Solar Field at Measuring Point | 419 783 | MWh/a |
| Annual Gross Output | 187 756 | MWh/a |
| Annual Electricity Supplied to Grid | 169 228 | MWh/a |
| Annual Auxiliary Consumption | 22 753 | MWh/a |
| Solar to Electric Efficiency: Peak | 27.9 | % |
| Solar to Electric Efficiency: Annual | 17 | % |
| Estimated Annual Water Consumption | 784 884 | $m^3$/a |
| $CO_2$ Savings Compared to Caol Fired Power Plant | 140 618 990 | kg/a |
| Gas Consumption (LHV) | 81 561 | MWh/a |

# Appendix B

# Fluid Properties

## B.1 VP-1 Properties

The VP-1 thermal oil properties are described Equation B.1 to Equation B.4 and represented in Figure B.1 to Figure B.4 (Solutia, 2016).

Heat Capacity $[kJ/kg \cdot K]$:

$$C_p = 1.498 + 0.002414(T) + 5.9591e{-}6(T)^2 - 2.9879e{-}8(T)^3 + 4.4172e{-}11(T)^4 \tag{B.1}$$

Density $[kg/m^3]$:

$$\rho = 1098.5 - 0.9729(T) \tag{B.2}$$

Enthalpy $[kJ/kg]$:

$$h = -18.175 + 1.4968(T) + 0.0014(T)^2 \tag{B.3}$$

Viscosity $[m \cdot Pa \cdot s]$:

$$\mu = 179.43(T)^{-1.167} \tag{B.4}$$

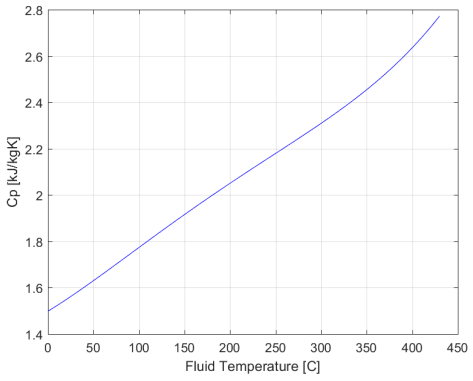


Figure B.1: Heat Capacity

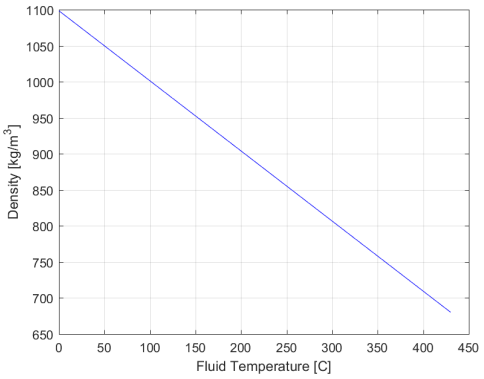


Figure B.2: Density

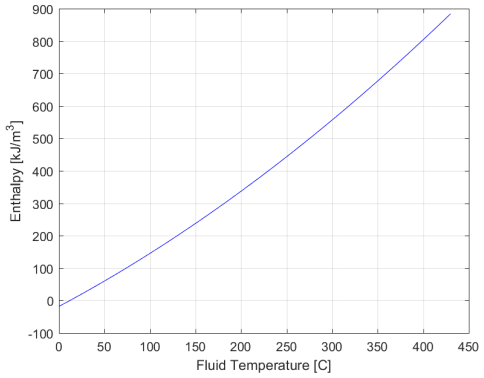


Figure B.3: Enthalpy

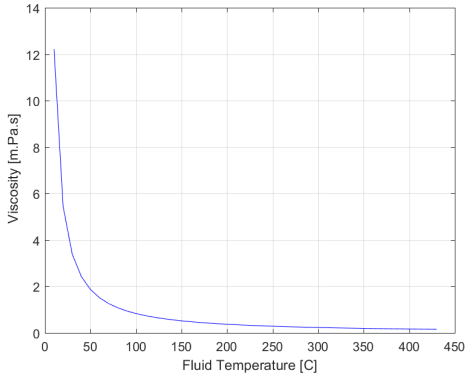


Figure B.4: Viscosity

## B.2 Molten Salt Properties

Heat Capacity $[J/kg \cdot K]$:

$$C_p = 1396.044 + 0.0172(T) \tag{B.5}$$

Density $[kg/m^3]$:

$$\rho = 2090 - 0.636(T) \tag{B.6}$$

Enthalpy $[kJ/kg]$:

$$h = -15.068 + 1.15172(T) \tag{B.7}$$

# Appendix C

# Flow Diagrams

## C.1 Solar Field Operation

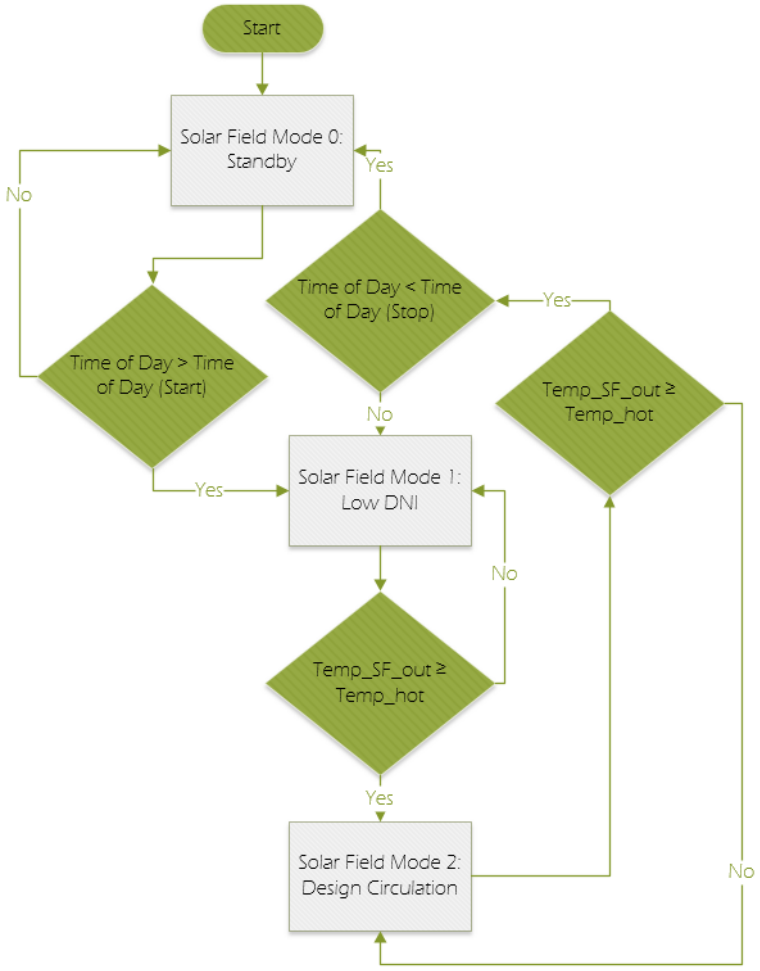

## C.2 Thermal Energy Storage Operation

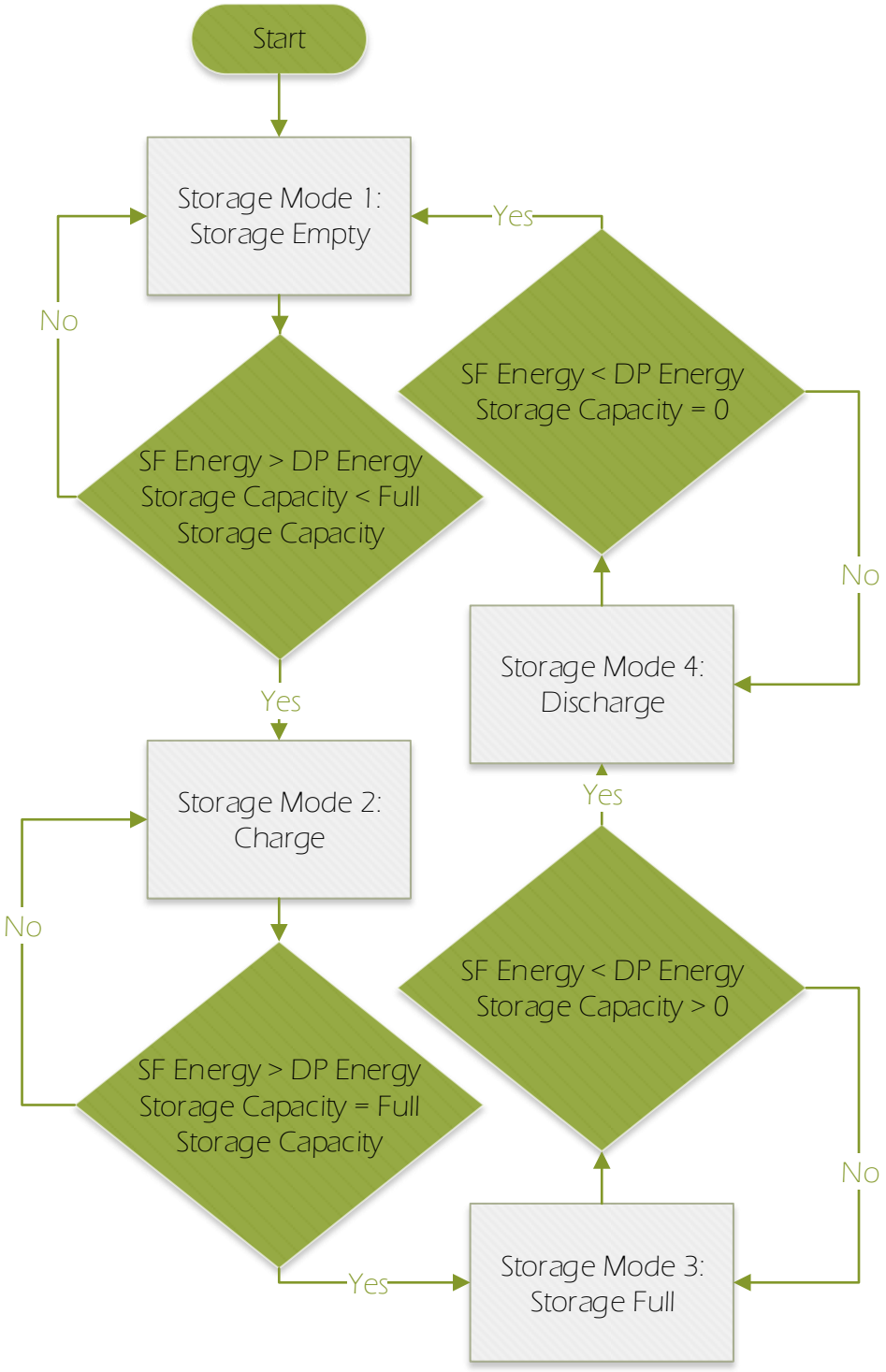

## C.3 Power Block Operation

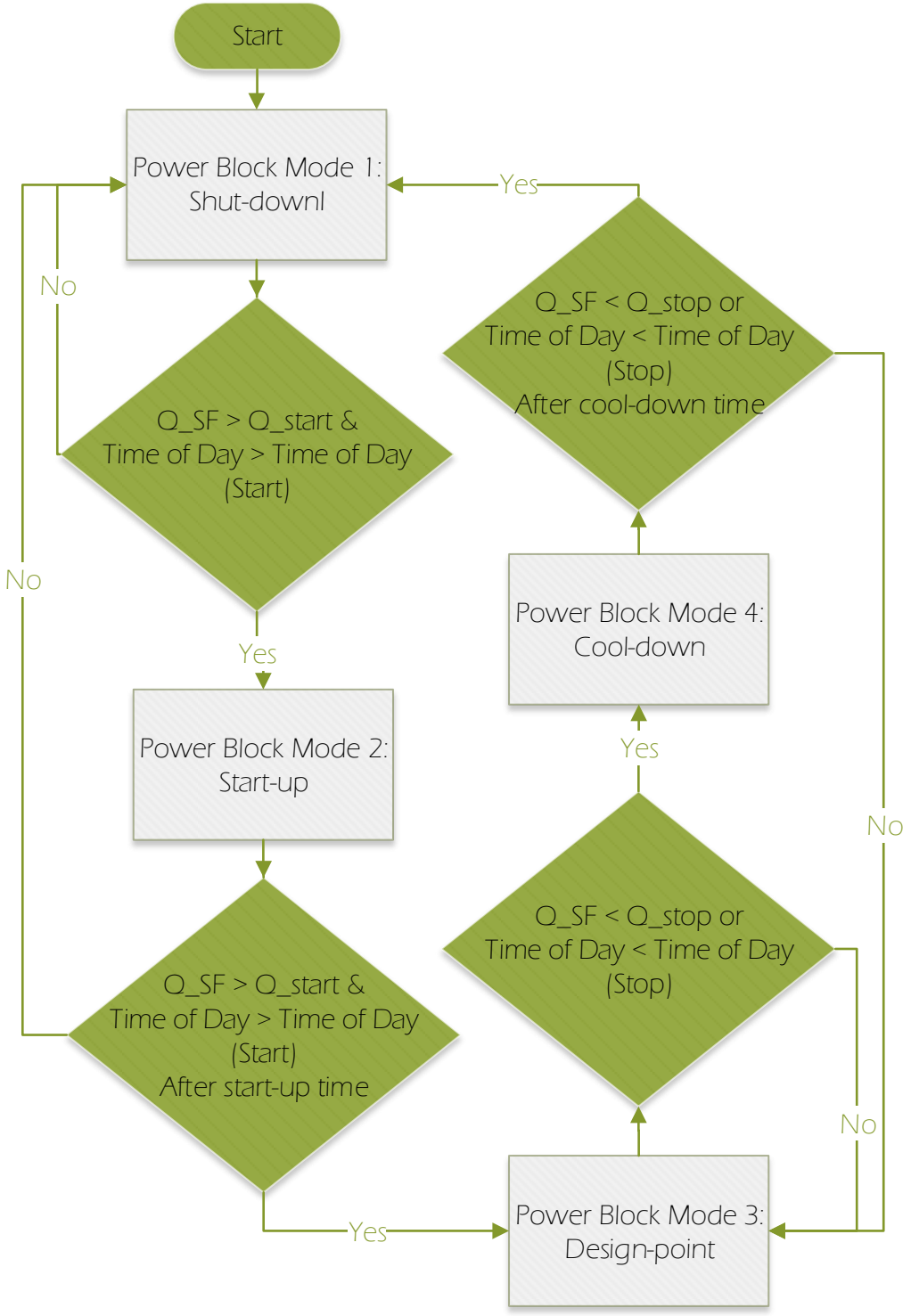

# List of References

Amin, A.Z. (2016). The power to change: Solar and wind cost reduction potential to 2025. Paper 1, IRENA.

Askarov, D.[Online] (2010). Available at: `http://large.stanford.edu/courses/2010/ph240/askarov2/`, [2010].

Blair, N., Dobos, A.P., Freeman, J., Neises, T. and Wagner, M. (2014). System advisor model, sam 2014.1.14: General description. Paper 1, National Renewable Energy Laboratory (NREL).

BrightSourceLimitless (2015). Ivanpah a brightsource energy concentrating solar power project. Paper 1, Bright Source Energy.

Burkholder, F. and Kutscher, C. (2009). Heat loss testing of schott's 2008 ptr70 parabolic trough receiver. Paper NREL/TP-550-45633, National Renewable Energy Laboratory (NREL).

Cabrerizo, J.A.R. (2017). Personal Interview.

Conti, J. (2016). International energy outlook 2016. *U.S. Energy Information Administration*, vol. 1, no. 1, p. 9.

CSPplaza[Online] (2017). Available at: `http://en.cspplaza.com/csp-prices-have-dropped-50-to-under-5centskwh-since-may.html`, [2017].

Deign, J. (2012). *CSP Today, The trouble with dish stirling CSP*. 1st edn.

Dinter, F. (2014). Operation experience of a 50 MW solar thermal parabolic trough plant in spain. *SASEC*, vol. 1, no. 1, p. 3.

EBSILONProfessional (2014). Ebsilonprofessional. Paper 1, steag.

Energy Next Solar [Online] (2013). Available at: `http://www.energynext.in/indias-first-csp-plant-commissioned-under-jnnsm/`, [2013].

Flownex[Online] (2017). Available at: `https://www.flownex.com`, [2017].

GearSolar [Online] (2017). Available at: `http://www.gearsolar.com/MetaGglassTubeReceivers.aspx`, [2017].

Geuder, N., Trieb, F., Schillings, C., Meyer, R. and Quaschning, V. (eds.) (2003). *COMPARISON OF DIFFERENT METHODS FOR MEASURING SOLAR IRRADIATION DATA*. Deutsches Zentrum fur Luft und Raumfahrt e.V. (DLR) and Plataforma Solar de Almeria, Spain.

Gladen, H. and Mayer, T. (2008). The parabolic trough power plants andasol 1 to 3. Paper 1, Solar Millennium.

global energy observatory [Online] (2012). Available at: `http://globalenergyobservatory.org/geoid/42924`, [2012].

GrandViewResearch (2017). Concentrating solar power market analysis, by technology (parabolic trough, linear fresnel, dish, power tower), by region (North America, Europe, Asia Pacific, South and Central America, MEA), and segment forecast, 2014 - 2025. Paper GVR-1-68038-996-8, Market Research Report.

Guédez, R. (2017). Personal Interview.

Gunther, M., Joemann, M. and Csambor, S. (2016). Chapter 5 parabolic trough technology. In: Guizani, A., K.D. and Hirsch, T. (eds.), *Advanced CSP Teaching Materials*, pp. 11, 73, 80, 88. enerMENA - DLR, Germany.

HELISCSP[Online] (2016). Available at: `http://helioscsp.com/concentrated-solar-power-csp-cost-forecasts-undervalue-benefit-to-future-grid-balancing/`, [2016].

IndustriaDevelopmentCorporation (2012). The cost evolution of renewable energies. Paper 1, Department of Research and Information.

Jones, S.A., Pitz-Paal, R., Schwarzboezl, P. and Cable, R. (2001). TRNSYS modeling of the SEGS VI parabolic trough solar electric generating system. Paper 1, Solar Energy: The Power to Choose.

Kopp, J.E. (2009). *Two-tank indirect thermal storage designs for solar parabolic trough power plants*. Master's thesis, University of Nevada Las Vegas (UNLV), Las Vegas.

Kotzé, J.P., von Backström, T.W. and Erens, P.J. (2012). NaK as a primary heat transfer fluid in thermal solar power installations. *Southern African Solar Energy Conference (SASEC)*, vol. 1, no. 1, p. 3.

Massoud, M. (2005). *Engineering Thermofluids: Thermodynamics, Fluid Mechanics, and Heat Transfer*. Springer Science and Business Media, London.

McLamb, E. (2011 September). Fossil fuels vs. renewable energy resources. Ecology webinar series (Energy).
Available at: `http://www.ecology.com/2011/09/06/fossil-fuels-renewable-energy-resources/`

NREL (2013). Andasol-3. Paper, National Renewable Energy Laboratory (NREL).

Padilla, R.V. (2011). *Simplified Methodology for Designing Parabolic Trough Solar Power Plants*. Master's thesis, University of South Florida, USA, Florida.

Pitz-Paal, R. (2013). Solar thermal power plants: Utilising concentrated sunlight for generating energy. Paper 1, BINE information Service (DLR and FIZ Karlsruhe).

Pool, S. and Coggin, J.D.P. (2013). Fulfilling the promise of concentrating solar power. Paper 1, Center for American Progress.

Poole, I.V. (2016). *Concentrating solar power in South Africa - a comparison between parabolic trough and power tower technologies with molten salt as heat transfer fluid*. Master's thesis, Stellenbosch University, South Africa, Cape Town.

PowerTechnology: Andasol Solar Power Station, Spain[Online] (2017). Available at: `http://www.power-technology.com/projects/andasolsolarpower/`, [2017].

Pyrheliometer [Online] (2015). Available at: `http://sinovoltaics.com/learning-center/components/pyrheliometer-used-solar-energy-systems/`, [2015].

Quasching, V. (2003). Solar thermal power plants (technology fundamentals ). *Renewable Energy World*, vol. 6, no. 1, pp. 109–113.

Quaschning, V., Ortmanns, W., Kistner, R. and Geyer, M. (2001). greenius - a new simulation environment for technical and economical analysis of renewable independent power projects. Paper 39, Deutsches Zentrum fur Luft- und Raumfahrt e.V. (DLR). Plataforma Solar de Almeria (PSA).

Roos, T. (ed.) (2012). *Thermal storage options for CSP*. SolarENERGY AFRICA, CSIR, Cape Town, South Africa.

Schiffer, H., Van der Westhuizen, Z., Radu, C. and Ibeanu, N. (2016). World energy resource, solar 2016. Paper 1, World Energy Council.

SEIA (2014). Concentrating solar power. Paper 1, Solar Energy Industries Association (SEIA).

SerranoLopeza, R., Fraderaa, J. and CuestaLopez, S. (2013). Molten salts database for energy applications. Paper 1, Universidad de Burgos.

SiemensAGEnergySector (2011). Steam turbines for csp plants (industrial steam turbines). Paper 1, Siemens.

Silva, J.P. (2013 September). Modelling and simulation of parabolic trough power plant. Technical University of Lisbon.
Available at: `https://fenix.tecnico.ulisboa.pt/downloadFile/395142728356/ModellingandSimulationofParabolicTroughPowerPlant.pdfl`

Sioshansi, R. and Denholm, P. (2010). The value of concentrating solar power and thermal energy storage. Paper 1, Ohio State University and National Renewable Energy Laboratory.

Solargis DNI Maps 2015 [Online] (2015). Available at: `http://solargis.com/products/maps-and-gis-data/free/download/spain`, [2015].

Solutia (2016). Themino.l vp-1. Paper 1, Solutia (Applied Chemistry, Creative Solutions).

Stine, W.B. and Geyer, M. (2001). *Power From The Sun*. 1st edn.

SunLab (1998). Solar trough systems. *Concentrating Solar Power Program (U.S. Department of Energy)*, vol. 1, no. 1, pp. 1–2.

Tawney, L. (2017 January). The buyers principles collaborating to deliver more affordable, clean energy today.

THERMOFLOW (2015). Thermoflow software. Paper 1, THERMOFLOW Inc.

Torresol Energy [Online] (2010). Available at: `http://www.torresolenergy.com/TORRESOL/gemasolar-plant/en`, [2010].

Transient System Simulation Tool (TRNSYS) [Online] (2017). Available at: `http://www.trnsys.com/`, [2017].

Valenzuela, L. (ed.) (2012). *STE plants with parabolic trough collectors*. CIEMAT, Plataforma Solar de AlmerÃa (PSA), SFERA Summer School, Spain.

Wagner, W.J. and Gilman, P. (2011). Technical manual for the SAM physical trough model. Paper NREL/TP-5500-51825, National Renewable Energy Laboratory (NREL).

Wang, Y. (2008 September). Parabolic trough power plants. Summary (How The Sun Gets Into The Power Plant).
Available at: `https://www.mtholyoke.edu/ wang30y/csp/PTPP.html`

Zervos, A. (2016). Renewables 2016 global status report. Paper 1, Renewable Energy Policy Network.

Zervos, A. (2017). Renewables 2017 global status report. Paper, number = ISBN 978-3-9818107-6-9, Renewable Energy Policy Network.